# Politecnico di Torino

Nanotechnologies for ICTs
A.a. 2020/2021
Sessione di Laurea Luglio 2021

# 2D MXENE MEMBRANES

## Synthesis, materials and design for fast water purification, gas separation and solvent filtration.

Relatori:
Elena Maria Tresso

Candidati:
Giacomo Savio

# TABLE OF CONTENTS

# PART 1 - Introduction to MXenes

## 1.1.1 - 2D Materials

Two-dimensional (2D) materials are characterized by very high aspect ratios and nearly atomic layer thickness. In general, these materials are mechanically exfoliated or chemically exfoliated from bulk 3D precursors, or deposited by nano CVD, having a layered structure where layers are usually bonded together by weak van der Waals forces [1]. The reduced dimensionality and quantum confinement renders them excellent from the chemical, electronic, mechanical, thermal and optical point of view with respect to the bulk 3D counterpart [2]. In addition to, their properties can be further adjusted to a desired optimum level, opening a wide range of possible application in the field of energy storage, electronics, biotechnology and photovoltaics. Among this, graphene and TMDs appear to be the two most predominant 2D materials in the field of research.

Since the discovery of graphene in 2004 [3], new class of 2D materials have been introduced in literature which include transition metal oxides and dichalcogenides (TMDs)[4], hexagonal boron nitrides (h-BN) [5], transition metal carbides or nitrides (called MXenes) which are layers composed by a transition metal M element and carbon or nitrogen X element, obtained from bulk precursor the MAX phase, by etching out the A element, and other single element 2D materials such as silicene [6], borophene [7], phosphorene [8], ect. Graphene which is an atom thick layer of graphite, has been raising heights in the field of research each year with its unique properties of ultrahigh carrier mobility (2.5 x 10^5 $cm^2V^{-1}s^{-1}$) [9], superior mechanical strength with a Young modulus of 1.0 TPa [10], high surface area (ca. 3000 $m^2g^{-1}$) [11], and very high thermal conductivity (ca. 3000 $Wm^{-1}K^{-1}$) [12]. It is also stable in harsh chemical environment and has a great versatility, making it suitable for use in broad range applications such as nanoelectronics, photocatalysts, biomaterials, ect. [13,14]. It can also be obtained in the form of membranes for gas separation and water purification or in the form of a hydrogels and aerogels for energy storage, dye absorption, ect [15, 16, 17].

MXenes are a novel class of two-dimensional inorganic compounds that consist in few atoms layer of transition metal carbides, nitrides or carbonitrides.

## 1.1.2 - 2D MXenes

Theoretically described in 2011, MXenes combine metallic behavior, as conductivity, of transition metal carbide/nitride with high hydrophilic nature of their oxygen or hydroxyl terminated surfaces (-O, -F and -OH). MXenes combine other unique characteristics, such as stiffness and high strength. In

2011, the exfoliation of 2D transition metal carbides have been studied by Naguib et al. at Drexel University [21] via the selective etching of ‘A’ elements from the so-called MAX phases, which consist in the 3D bulk precursor of the 2D MXene. These 2D layered MXenes have the suffix -ene to indicate the similarity to the graphene [22].

The precursor, MAX phases, are orderly aligned carbides and nitrides of ternary metals which are usually represented as $M_{n+1}AX_n$ (MAX), where n differs from 1 to 3, M is a transition metal such as Zr, Cr, Mo, Ti, etc., A can be a group 13 to 16 element such as Ge, Si, Al, Ga, etc., and X can be either carbon C, nitrogen N, or a mixture of them as reported in Figure 1 [20].

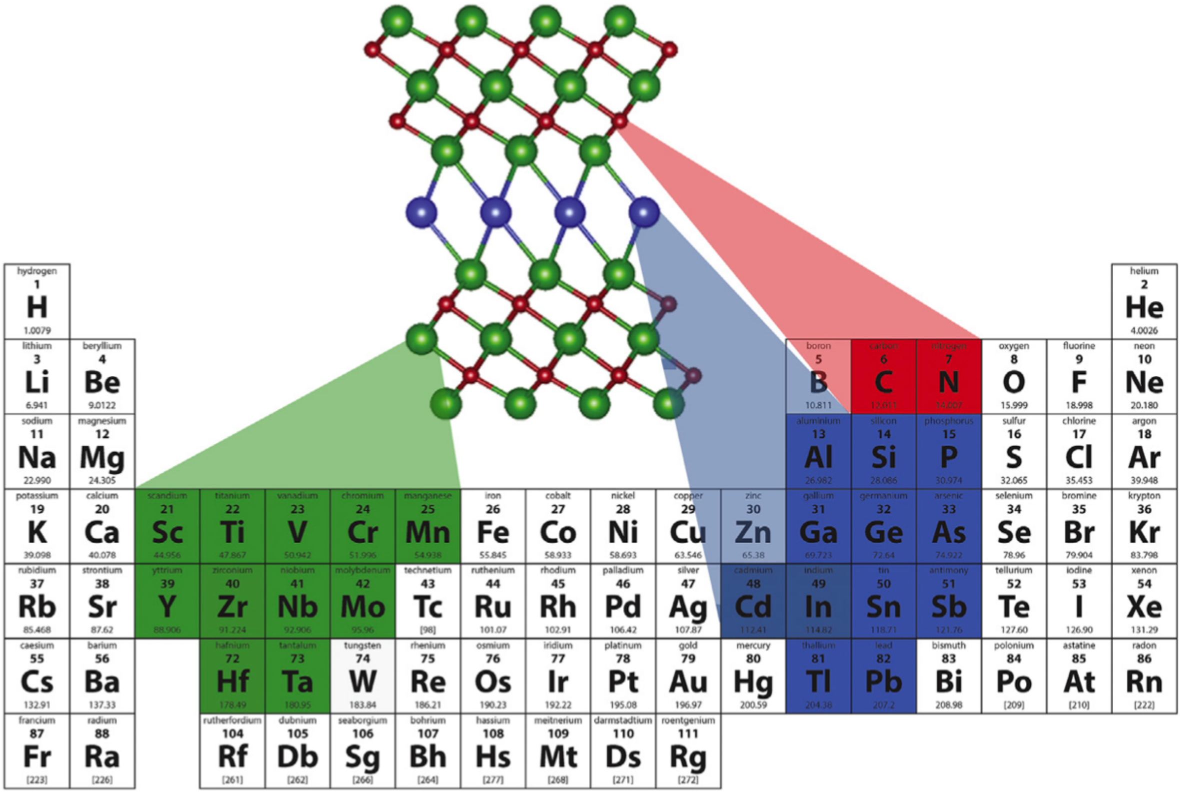

*Figure 1: $M_{n+1}AX_n$ phases MAX forming elements [20].*

The layered hexagonal MAX phases comprise of M layers that are almost densely packed, and octahedral sites occupied by X atoms while the layers of M and X are bonded together by A atoms (see Figure 2) [24].

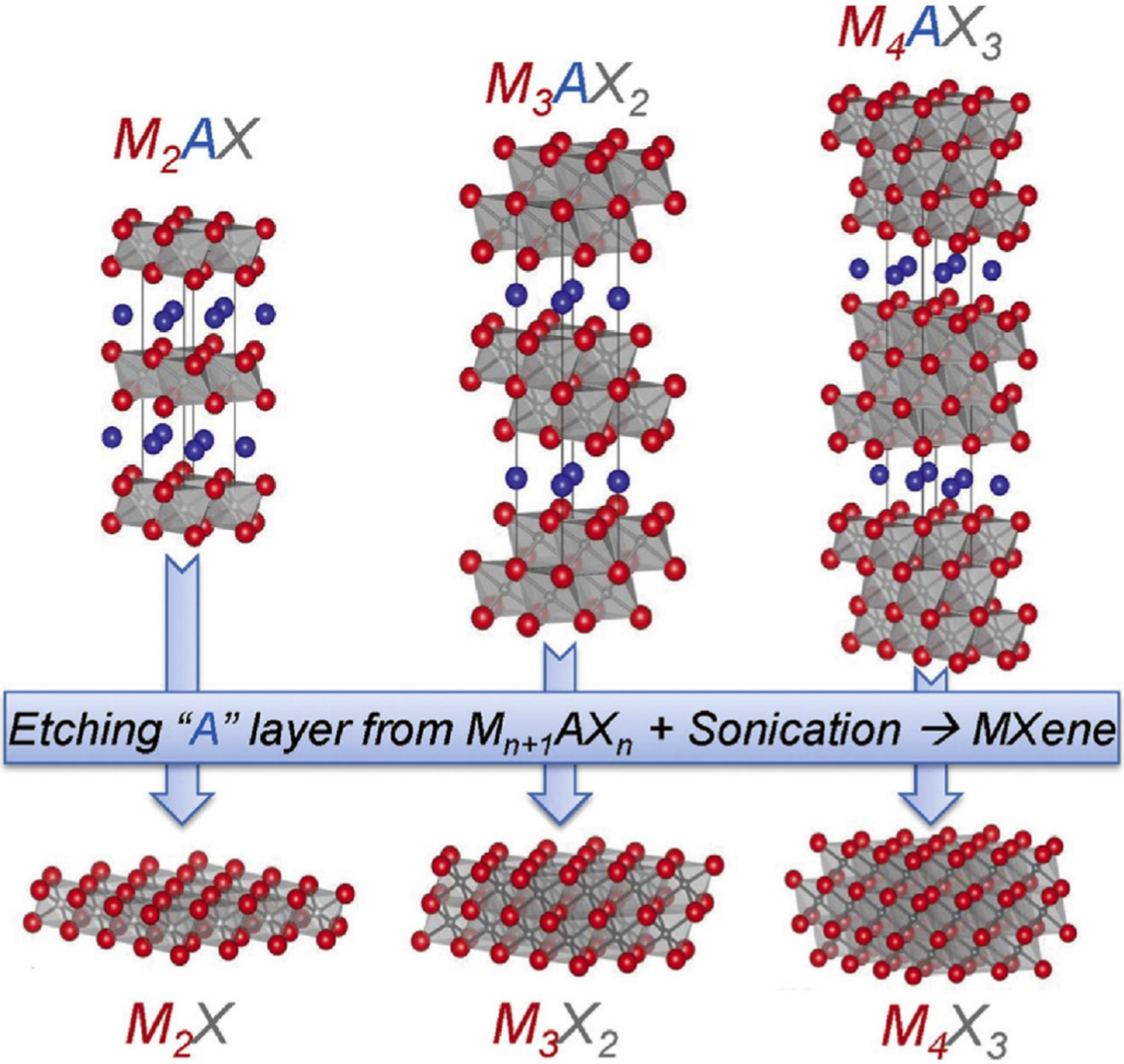

*Figure 2: Structure of MAX phases and their derivative MXenes [23].*

In the MAX phase, the M-X bond displays a mix of ionic/metallic/covalent nature while the M-A bond, usually, display a metallic behavior [25]. Thus, because of the strong interlayer bonding in the MAX phases, shearing or mechanical exfoliation of these bond has not been possible unlike in graphite and TMDs where weak van der Waals forces grips the layers together. To delaminate these layers, the idea is to work on the relatively higher reactivity of M-A bonds, compared to M-X bonds, so its reacts with the etchants and selectively removal the A atoms, thus exfoliation process becomes much easier. As the metallic M-A bonds are strong, the selective etching is commonly made by strong etchants under well-controlled conditions without drastically jeopardizing the 2D structure yet formed [119].

MAX phases exhibit an unusual mix of properties that belong to ceramics and metals: alike ceramics they have good brittleness, stiffness, strength and thermal stability while they as well conduct heat and electricity like metals [26,27].

MXenes formed by selectively etching of A layers from the MAX phases, are three or more atomic layer thick 2D materials which have different properties compared to the 3D counterpart.

In general, MXenes are represented as $M_{n+1}X_nT_x$ where n ranges from 1 to 3 and T is the functional groups (-O, -F and/or -OH) resulting from the interaction with acids during the etching step. As the n values range from 1 to 3 in the MAX phases, the resulting MXenes exists in three possible lattice structures: $M_2X$ , $M_3X_2$ , $M_4X_3$ (3, 5 or 7 atomic layers) as shown in Figure 2 [23]. It is also possible to have more than one M element in MXene, this structure can be obtained in two forms: ordered phases and solid solutions. In ordered phases mono or bi layer of one transition metal is sandwiched between another transition metal layer (eg. $(Mo_2Ti)C_2$ and $(Ti_2Ta_2)C_3$), whereas in solid solutions, two different transition metal elements are randomly distributed in the M layers (eg. $(Ti,V)_2C$ and $(Ti,Nb)_4C_3$) [29].

### 1.1.3 - Structure of MXenes

The MXene surface, because of the etching with acid during the synthesis, gets grafted with oxygen, hydroxyl and fluorine-based functional groups.

The first structure of multilayer (ML)-MXene ($Ti_3C_2T_x$) was proposed based on density functional theory (DFT) calculations [21]. The XRD patterns from these simulated models contrast with the experimental XRD pattern reported for $Ti_3C_2T_x$ (figure 3) [21].

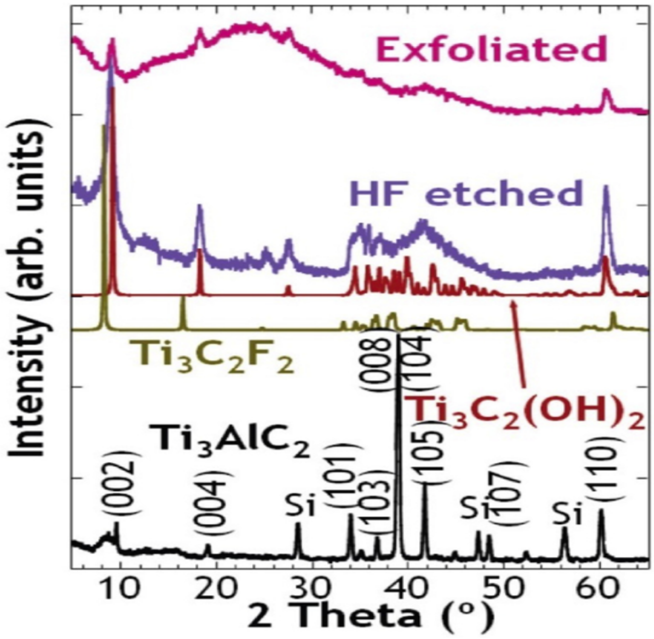

*Figure 3: XRD analysis of MAX and MXenes [21].*

The pattern confirms the disappearance of sharp peak of $Ti_3AlC_2$ MAX phase after etching with hydrofluoric (HF) acid. The final structure also loses its crystalline order after sonication resulting in weakening of peak intensity. XPS analysis confirms the occurrence of OH, F, and O terminating functional groups, the c-lattice parameter from the experimental data shows a closest match to a fully hydroxylated MXene ($Ti_3C_2(OH)_2$) [30].

MXenes obtained via HF etching can show different morphology depending on numbers of layers: multi- layers (ML) for more than five layers or few-layers (FL) when there are less than five layers [23].

MXenes are typically in hexagonal close-packed (HCP) crystal structure. However, it is reported that M atoms in $M_3X_2$ and $M_4X_3$ favors face centered cubic (FCC) crystal structure sequence (ABCABC) while $M_2X$ exhibit HCP sequence (ABABAB) [28]. This atomic arrangement is of importance when it comes to the synthesis of MXenes involving M elements with HCP ordering in bulk state, such as carbides of chromium (Cr) or molybdenum (Mo). An example comes from DFT simulations in which reveal the major stability of hexagonal molybdenum carbides in respect the FCC counterparts [31]. It is also found from the formation energies that MXenes such as $Mo_3C_2T_x$ and $Mo_4C_3T_x$ are unstable as the M atoms follows rock salt arrangement [29], while it is stable in the case of $Mo_2CT_x$ [32,33]. To stabilize them, another transition metal, Ti, is inserted into the structure so that it bond with C and prevents the unstable Mo-C bonds, therefore forming an ordered double-M element 2D carbides such as $(Mo_2Ti_2)C_3T_x$ and $(Mo_2Ti)C_2T_x$ [29].

In 2012, Enyashin et al. [34] analyzed and compared the atomic structure and stability of $Ti_2C(OH)_2$. Figure 4 shows the atomic structures of free standing $Ti_2C$ (fig. 4a) and their hydroxylated forms with three different configurations (fig. 4b-d,f.-h). Configuration A (fig.4 b and f) has OH groups placed in the hollow space in different atomic sites respect to C and M. In configuration B (fig. 4c and g) the OH terminals are located on top of C atoms on either side of the MXene layer, while configuration C (fig. 4d and h) has a mixture of configuration A and B such that each half of MXene layer is occupied by A and B. Comparing their relative total energies, it was found that configuration A have the highest structural stability followed by C and then B for both F and OH terminated $TiC_x$ [23]. Thus, both functional groups prefers configuration A, this maximum stability of A arise probably from the formation of ABCABC ordering because of different atomic positions of MX and T. The steric repulsion between the T and C atoms underneath is the likely cause of lack of stability in B [35]. MXenes terminated by methoxy groups ($-OCH_3$) were also found to be stable by means of DFTB (density-functional tight-binding) calculations besides

-O, -F, -OH groups, suggesting a high surface/catalytic activity for MXenes [23,26].

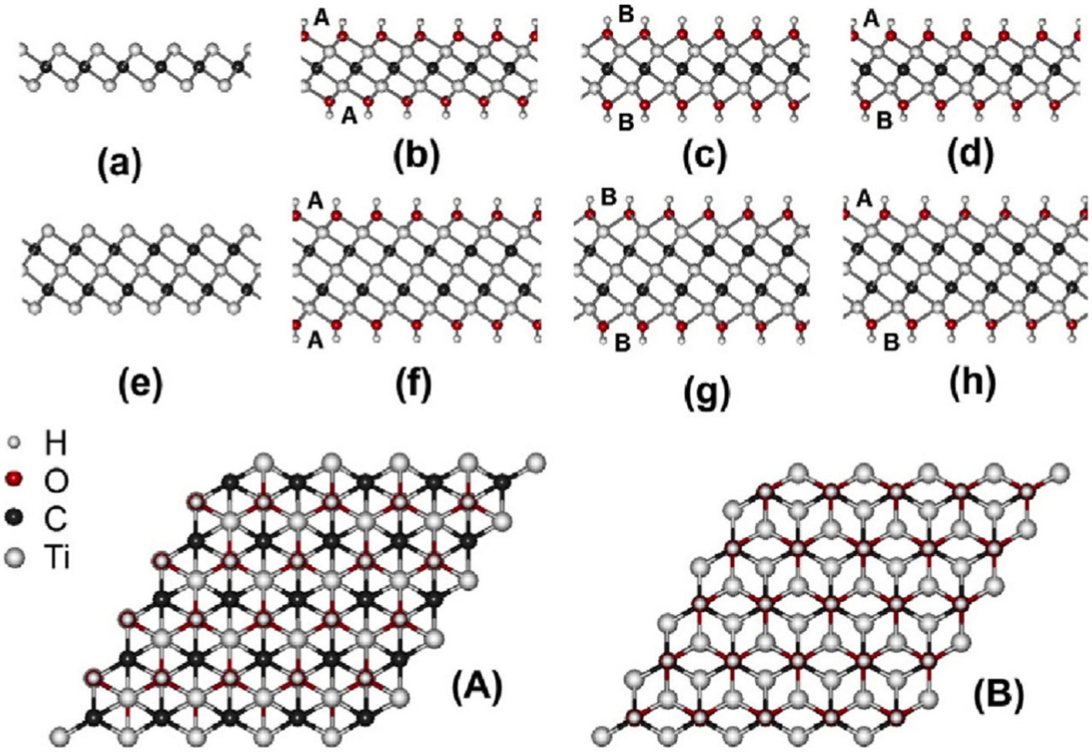

*Figure 4: Atomic ordering of TiC2 (a) and Ti2C3 (b) and their hydroxylated forms Ti2C(OH)2 (b-d) and Ti3C2(OH)2 (f-h), with three configurations according to the placement of (OH) groups. (A) and (B) are the top views configuration a and b respectively [34].*

## 1.2 - Synthesis methods of MXenes

### 1.2.1 - Top-Down approach from MAX phase

MXenes are typically synthesized by a top-down selective etching process. Producing a MXene by etching a MAX phase occurs mainly by using strong etching solutions that contain fluoride ion $F^-$ such as ammonium bifluoride, and hydrofluoric acid, and a mixture of hydrochloric acid and lithium fluoride. A schematic of synthesis of MXenes from MAX phases is illustrated in Figure 5 [35]. In this process, layered MAX phase powders are stirred with aqueous HF acid at room temperature for a given time. As a result, the A layers of MAX phase gets selectively etched, and the metallic bonds between the MX layers gets replaced with weak bonds of surface terminations such as fluoride or oxygen or hydroxyl, on the surface of ML-MXene. Then to obtain FL-MXene, the solution is further centrifuged and filtered so that the supernatant gets isolated from solid followed by washing with deionized water until pH pf the mixture maintained in the range of 4 and 6. It is to be noted that a further decrease in the pH of MXene solution, for instance, 1 in the case of $Ti_3C_2T_x$, can lead to crumpling of MXene flakes [38].

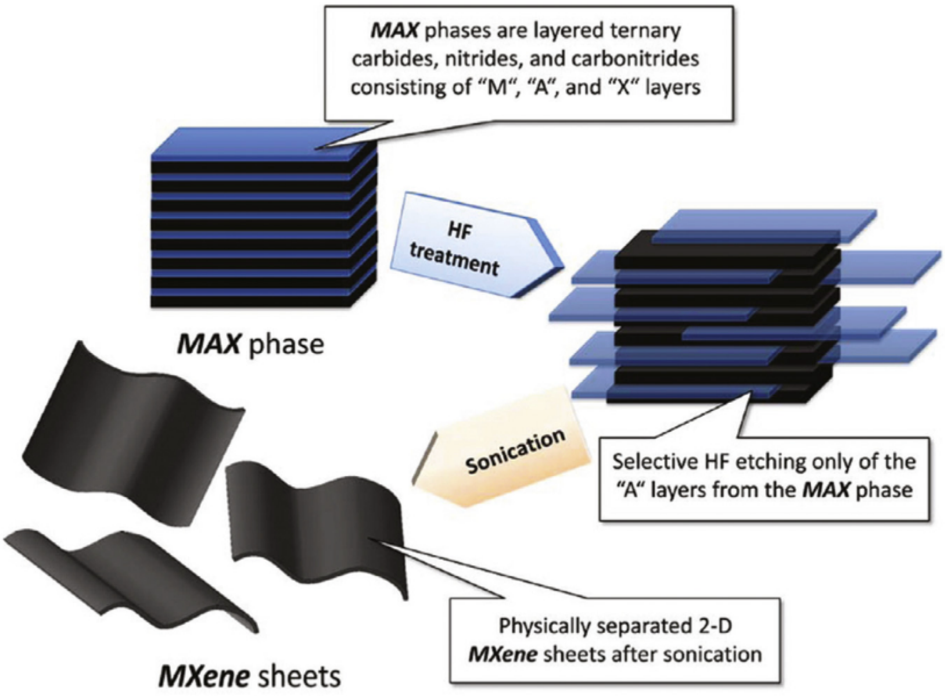

*Figure 5: Schematic of MXene synthesis [22].*

For the case of $Ti_3C_2T_X$ and $Ti_2CT_X$ etching with concentrated HF acid and LiF as a fluoride source, morphology is more compact with a larger inter-layer spacing. The material has been found to be clay-like: $Ti_3C_2T_X$ demonstrated the ability to expand its interlayer distance hydration and can reversibly exchange charge-balancing Group 1 and Group 2 cations. When hydrated, the MXene clay becomes pliable and can be molded into desired shapes becoming hard solid upon drying. MXene clay shows high electrical conductivity upon drying unlike most clays, and is hydrophilic, being easily dispersed into single layer two-dimensional sheets in water without surfactants. Due to this property, it can be quickly rolled into freestanding, additive-free electrodes for energy storage.

### 1.2.2 - MXene from non-MAX phase

MXene synthesis from non-MAX phase precursors were also reported with $Mo_2Ga_2C$ being the first of this kind, where Ga layers are etched to produce $Mo_2CT_x$ MXenes [32,33]. It differs from MAX phase because there are two A layers of Ga in $Mo_2Ga_2C$ with respect to one found in MAX phase. The $Zr_3C_2T_x$ MXene derives from $Zr_3Al_3C_5$ [39] is another example where aluminum carbide

($Al_3C_3$) layer was etched rather than just aluminum (Al) layer in the typical method

### 1.2.3 - Nitrides MXenes and high temperature etching

MXenes have also been synthesized from MAX phase by etching at high temperatures. Nitrides MXenes are produced by a different procedure than those used for carbide MXenes: the MAX phase is mixed with eutectic fluoride salt mixture and treated at elevated temperatures. The first nitride-based MXene was experimentally synthesized by this method in 2016, wherein molten fluoride salt mixture (59%KF, 29%LiF, 12% NaF) was employed in an inert atmosphere of argon gas at 550°C to etch the Al layer part from $Ti_4AlN_3$ powder which was further delaminated by tetrabutylammonium hydroxide (TBAOH) to produce monolayers of $Ti_4N_3T_x$ MXene as shows in Figure 6 [40].

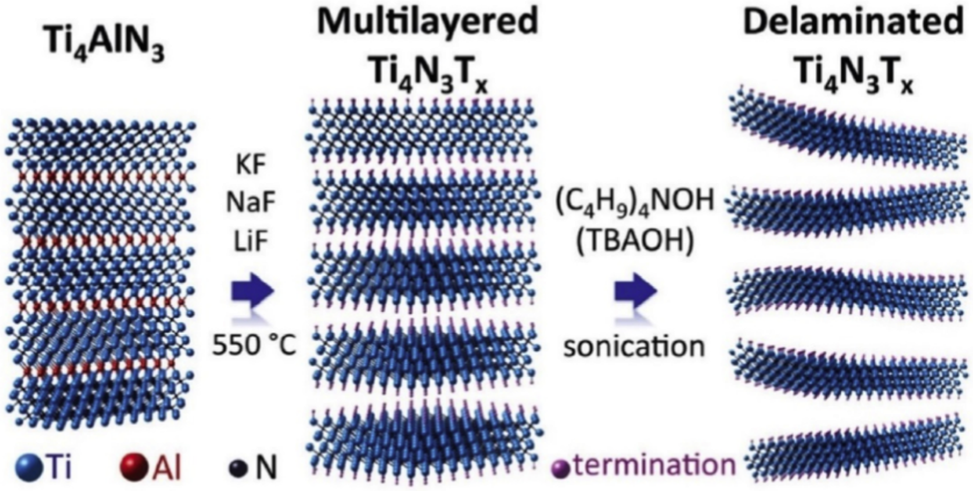

*Figure 6: Schematic synthesis of first nitride MXene by molten salt approach [24].*

There are also some reports involving elimination of Si layers from $Ti_3SiC_2$ at temperature of 960°C by using molten cryolite [42] and sublimation of In layers from $Ti_2InC$ at 800°C to form $TiC_x$ in vacuum [41]. However, ordered non-stoichiometric transition metal carbides were found to be stable only below 800°C which is in accordance with their phase diagram [43], thus, the resulting carbides were found to be 3D structure rather than 2D because of certain treatment conditions like gas and temperature. Therefore, all the treatment and synthesis procedures of MXenes must be performed below such temperatures otherwise the resulted structure can be composed by a mixture of 2D and 3D features. [118]

### 1.2.4 - Scalable salt-templated method

Different approaches were established to synthesized 2D metal nitride, ie. GaN, through migration-enhanced encapsulation growth method [44].

In 2017, Xu Xiao et al. [45] synthesized MoN nanosheet and other 2D nitrides by means of scalable salt-templated synthesis method by virtue of lattice match between the salt-template surface and crystals [46], that serves as precursors for synthesis of 2D metal nitrides via ammoniation, demonstrating that this method is an efficient way to fabricate 2D transition-metal oxides. In their work they first obtained 2D hexagonal $MoO_3^-$ coated NaCl (2D h-$MoO_3$@NaCl) by annealing the Mo precursor in NaCl powders in Ar atmosphere at 280°C. Then 2D h-$MoO_3$@NaCl powders were slowly ammoniated in a $NH_3$ atmosphere at 650°C. Here, the presence of salts may act as stabilizer to avoid the morphology change during transformation from h-$MoO_3$ to MoN [47]. Finally, 2D h-MoN@NaCl were washed in deionized water with further filtration to remove the salts, resulting in MoN nanosheets (Figure 7a).

Other 2D nitrides such as $V_2N$ and $W_2N$ were fabricated utilizing last procedure where 2D hexagonal oxides were ammoniated to form 2D nitrides.

One of the features of this salt-templated method is a large yield because the synthesis can be easily scaled up by adjusting the amount of salt, and the salt could be recycled for further usage. In addition, negatively charged 2D MoN nanosheets would be beneficial for cation intercalation [47]. The X-ray diffraction (XRD) pattern shown in Figure 7b reveals the crystal structure of hexagonal MoN, and in Figure 7c a detailed analysis is depicted to show the presence of Mo-N bond centered at around 393,7 eV that confirms the formation of MoN. Here, another peak assigned to Mo-O bonding, which should be attributed to a surface termination similar to the case of MXene [48]. The morphology of 2D MoN nanosheets was verified by scanning electron microscopy (SEM) and transmission electron microscopy (TEM). In Figure 7d the 2D nanosheets were observed in SEM. The lateral size of some flakes exceed 20 $\mu m$, owing the templating effect of the salt crystals which were larger than 50 $\mu m$. [45]

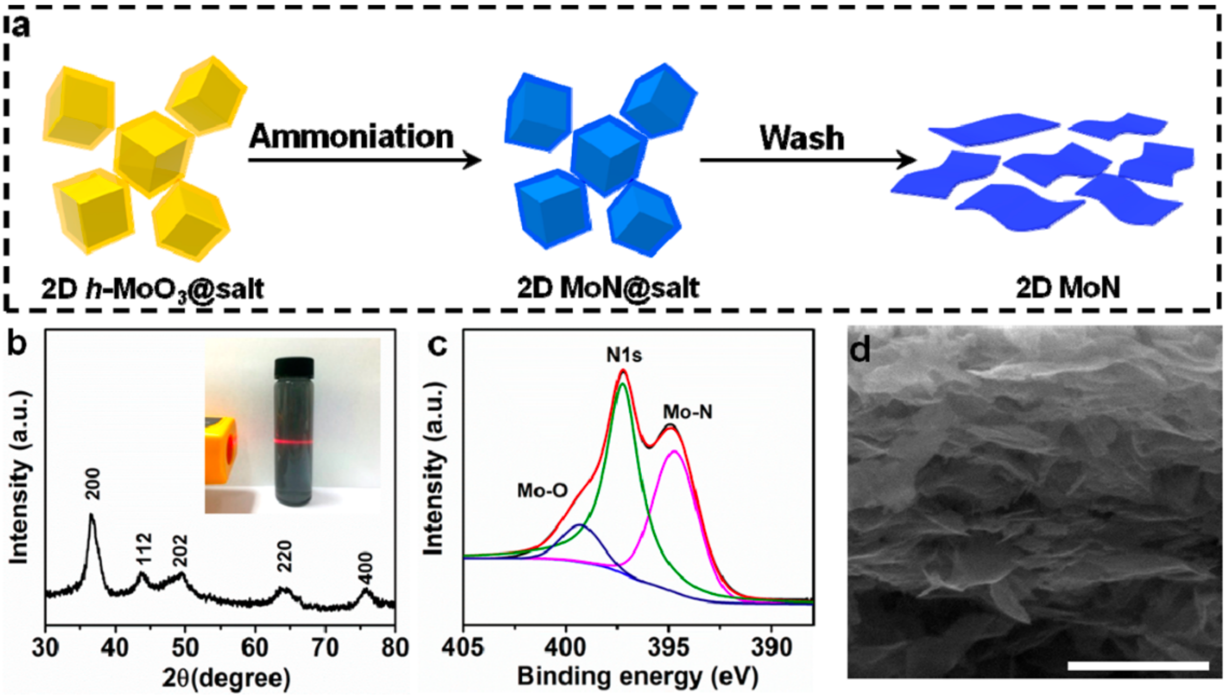

*Figure 7: Synthesis process and characterization. (a) Schematic synthesis of 2D MoN. (b) XRD pattern of 2D MoN powder. The insets show the Tyndall effect of the 2D MoN colloidal solution in water, demonstrating the good dispersity in water. (c) N 1s and Mo 3p XPS spectrrum of 2D MoN. (d) SEM image shows the 2D morphology of MoN, scale bar 500nm [45].*

### 1.2.5 - Nitrides via Ammoniation

Same year, Urbankowski et al. reported on the synthesis of 2D $V_2N$ and $Mo_2N$ from their respective 2D carbide MXenes $V_2CT_x$ and $Mo_2CT_x$ via ammoniation at 600°C so that the C atoms get replaced by N atoms [49]. Although the 2D nitrides were obtained through ammoniation in both cases, the resulting crystal structure varied from each other: in the latter method, $Mo_2N$ sustained the carbon MXene structure and the $V_2CT_x$ Mxene changed into a mixed phase of cubic VN and trigonal $V_2N$ [49].

### 1.2.6 - CVD synthesis approach

The 2D MXenes obtained with these methods have some defects with surface terminated functional groups and can have lateral size of maximum $\sim 10\ \mu m$. However, in 2015, Chuan Xu et. al. [50] produced high quality and defect-free ultrathin molybdenum carbide crystals by chemical vapor deposition (CVD) process with lateral sizes up to and higher than 100 $\mu m$ that also exhibit low-temperature 2D superconductivity. This method is analogous to the CVD growth of high-quality graphene. The procedure followed involved a copper (Cu) foil substrate placed on the top of molybdenum (Mo) foil with methane gas as a source of carbon at temperature above the melting point of copper which is 1085°C. As a result, Cu dissolve into Mo foil and form Cu-Mo alloy at their interface. The Mo atoms then diffuse through the interface to subsequently react with carbon accomplished by methane gas disintegration allowing to grow ultrathin $\alpha$-Mo₂C crystals (Figure 8a). MXene products contrast in a similar way as graphene; as how pristine graphene varies from artificially functionalized and imperfect reduced graphene oxide [51-54]. The minimum thickness of $\alpha$-$Mo_2C$ crystals achieved by Chuan Xu et al. was 3nm as shown in fig. 8b (bottom), while the monolayer MXenes (top) are yet to be demonstrated. Figs. 8c and 8d show the optical micrograph and high-resolution transmission electron microscopy (HR-TEM) of tungsten carbide crystal indicating the versatility of this method to produce other 2D composition. These recent synthesis method by CVD and salt-templated synthesis lay a new foundation to produce not only novel 2D carbides but also nitrides and carbonitrides in the near future [118].

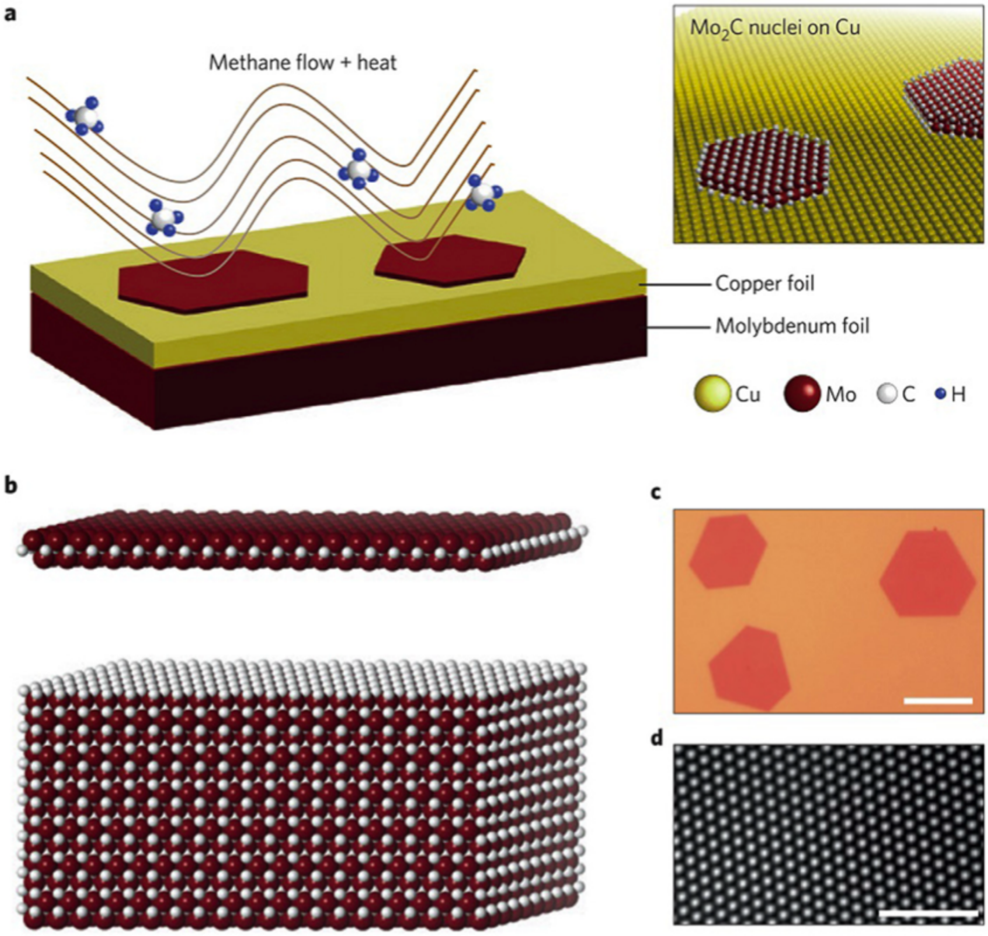

*Figure 8: 2D TMC crystals grown by CVD process. (a) Schematic fabrication of Mo2C crystal at 1085°C with Cu foil as substrate and methane gas as carbon source. (b) Monolayer Mo2 C (top) and experimental $\alpha$-Mo2C crystal of 3nm thickness (bottom). (c) optical image (10$\mu m$ scale) and (d) HR-TEM (2nm scale) of WC crystal grown by this method [51].*

## 1.3 - Intercalation and delamination of MXene

Intercalation refers to the inclusion of ions or molecules in between the layered structures of materials having weak bonds such as graphite and TMDs like

$MoS_2$ [55,56]. Because of the weak bonding between MX layers, MXenes can accommodate various ionic, organic and inorganic species intercalating between the layers thereby weakening their bond and increasing the interlayer spacing [30,57]. MXene layers can accommodate an array of multivalent cation, ie. $Na^+$, $Li^+$, $K^+$, $Mg^{2+}$, $NH_4^+$ and $Al^{3+}$, which suggests usage in metal-ion batteries [58] and supercapacitors having capacitance values over 300 F $cm^{-3}$, which is superior tan all carbon-based [15,59] electric double-layer capacitors (EDLC) and comparable with activated graphene (350 F $cm^{-3}$) [54]. Fig. 8 shows the intercalation of cations in most widely studied $Ti_3C_2T_X$ MXene [54]. Polar organic molecules, for example TBAOH, urea, hydrazine, isopropanol and dimethyl sulfoxide of ranging sizes, can also be intercalated to increase interlayer spacing of MXene. In case of $Ti_3C_2T_X$, the lattice parameter raised from 19,5Å to 25Å when intercalated with hydrazine [30]. Intercalation with such molecules is also essential in producing 'MXene paper', which involves the steps of sonication in water and filtering of supernatant colloidal solution [30].

### 1.3.1 – MXene Clay

In 2014, Ghidu et al. [60] synthesized MXene clay by using a solution of LiF and HCl instead of using the highly corrosive and harmful HF acid for etching. The HF is produced in situ by reaction of metal fluoride with the hydrogen-based acid, this process aids the selective etching of the A elements. This process is advantageous for two reason with respect the common one: involves the use of metal halide instead of the strong HF, and the $Li^+$ ions gets intercalated into the MXene along with water increasing the interlayer spacing, $c \sim 28Å$, and thus eliminating the extra step of delamination. In this work, the $Ti_3AlC_2$ MAX powders were introduce to the solution mixture of LiF and HCl so that the Al layers gets etched away to produce $Ti_3C_2T_x$. The resulting powder becomes a thick paste, after hydration, that is so pliable that it can be rolled into a film of suitable thickness or molded into preferred shape or diluted to produce conductive ink and painted on a surface to produce thin conductive coatings (fig. 9)[60].

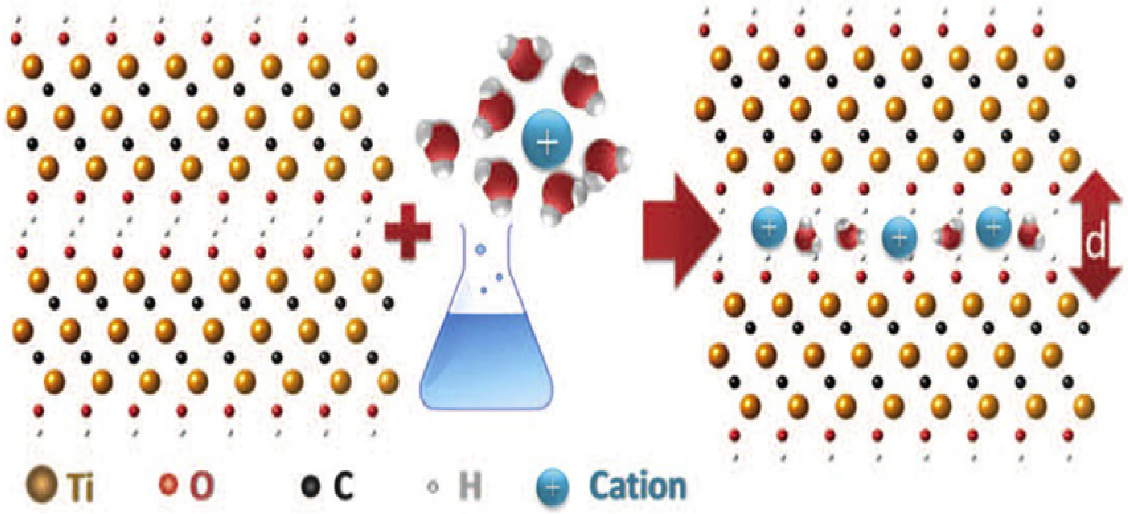

*Figure 9: Intercalation of cations in Ti3C2Tx MXene [57].*

The material behaves like a clay indicating that it can swell and shrink down in volumes reversibly when hydrated and dried but at the same time is highly conductive (1500 S cm$^{-1}$). Moreover, the volumetric capacitance exploited by MXene clay in 1M $H_2SO_4$ solution is about 900 F cm$^{-3}$ at 2mV/s (fig. 10a), which is almost two times the capacitance value of 450 F/cm$^3$ reached by MXene paper in 1M KOH electrolyte (Fig. 10b) etched from pure HF, with no assessable capacitance losses even after 10.000 cycles providing an almost 100% retention (fig. 10c)[60]

It has been proposed that such high capacitance value are partly attributed by the use of acidic electrolyte where intercalation of the smallest cations, ie. protons, take place, resulting in enhanced accessibility of the electrochemical active sites. In that report, the highest gravimetric capacitance achieved was 245 F/g.

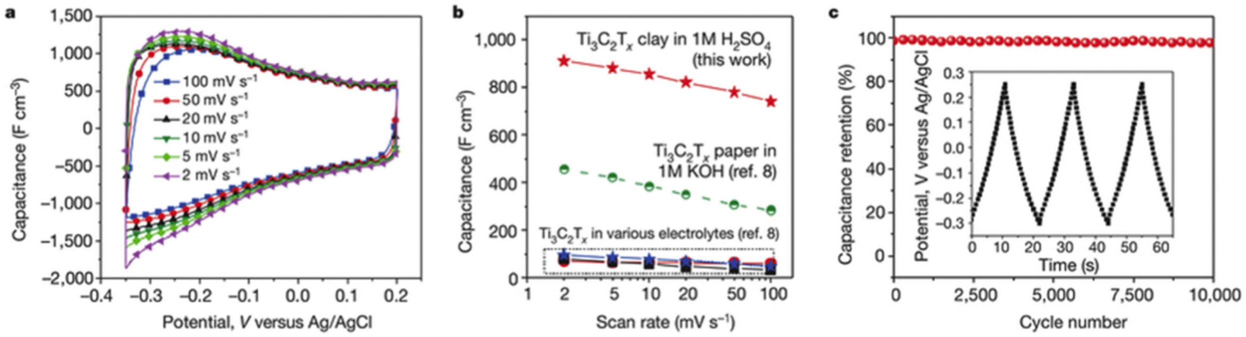

*Figure 10: Electrochemical behavior of MXene clay. (a) Cyclic Voltammetry (CV) profile of 5μm thick electrode in 1M H2S=4 at various scan rates. (b) rate performance of Ti3C2Tx 'clay' vs Ti3C2Tx 'paper'. (c) capacitive retention test of Ti3C2Tx electrode with galvanostatic cycling data in the inset [60].*

Despite that, Li et al. in 2017, showed more than doubled values of ≈517 F/g by intercalating $Ti_3CT_x$ with $K^+$ ion and calcinating to remove the -F and -OH functional groups so that the number of active sites, the Ti atoms, is increased thereby increasing redox reaction in MXene [61]. This tremendous increase in capacitance values together with high intercalation pseudocapacitance opens a pathway to its potential applicability in supercapacitors where high power and energy densities are required. [118]

## 1.4 – Properties of MXenes

### 1.4.1 – Electronic properties

With a high electron density at the Fermi level, MXene monolayers are predicted to be metallic. Due to removing the A element from the MAX phase, MXenes electron density at Fermi level, N(E), is 2.5-4.5 times higher than respective MAX phases. However, experimentally, the predicted higher N(E) has not been shown to lead to higher resistivities than the corresponding MAX phases.

DFT calculations illustrated that the bandgap of MXene can be modified by altering surface termination as shown in the dispersion diagram in fig.11 [21].

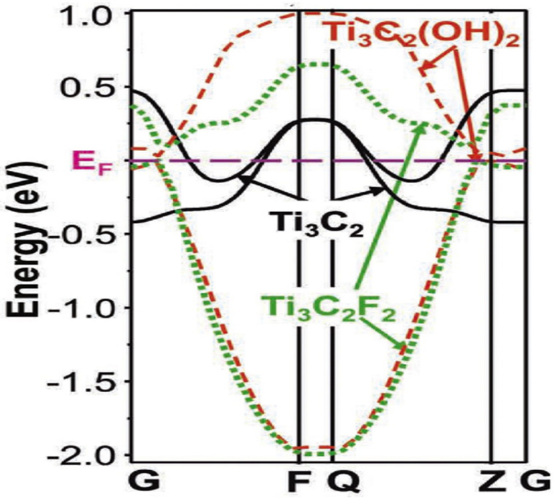

Figure 11: Electronic structure of Ti3C2 MXene with OH, F and no termination [21]

Non-terminated MXenes, $Ti_3C_2$, behave as a metallic conductor in nature, whereas the OH and F terminated ones are semiconductors with bandgap values of 0.05 eV and 0.1 eV respectively [21]: these materials can be employed in applications ranging from field-effect transistors to semiconductors depending on altering their bandgap [59,60]. Another way to change the bandgap of MXene is to alter the composition of M layers. Anasori et al. [64] demonstrated and replaced the top 2 layers of Ti in $Ti_3C_2(OH)_2$ which is metallic with Mo layers in a way that a 2D double-layer TMC of $Mo_2TiC_2(OH)_2$ is produced in which Mo atoms imparts semiconducting property to the MXene with fine bandgap of 0.05 eV. Fig 12 a-d show the atomic ordering and density of states of $Ti_3C_2(OH)_2$ and $Mo_2TiC_2(OH)_2$ illustrating this transition which is confirmed by the positive and negative magnetoresistance values of both MXenes at 10 K (fig 12e) [28,64].

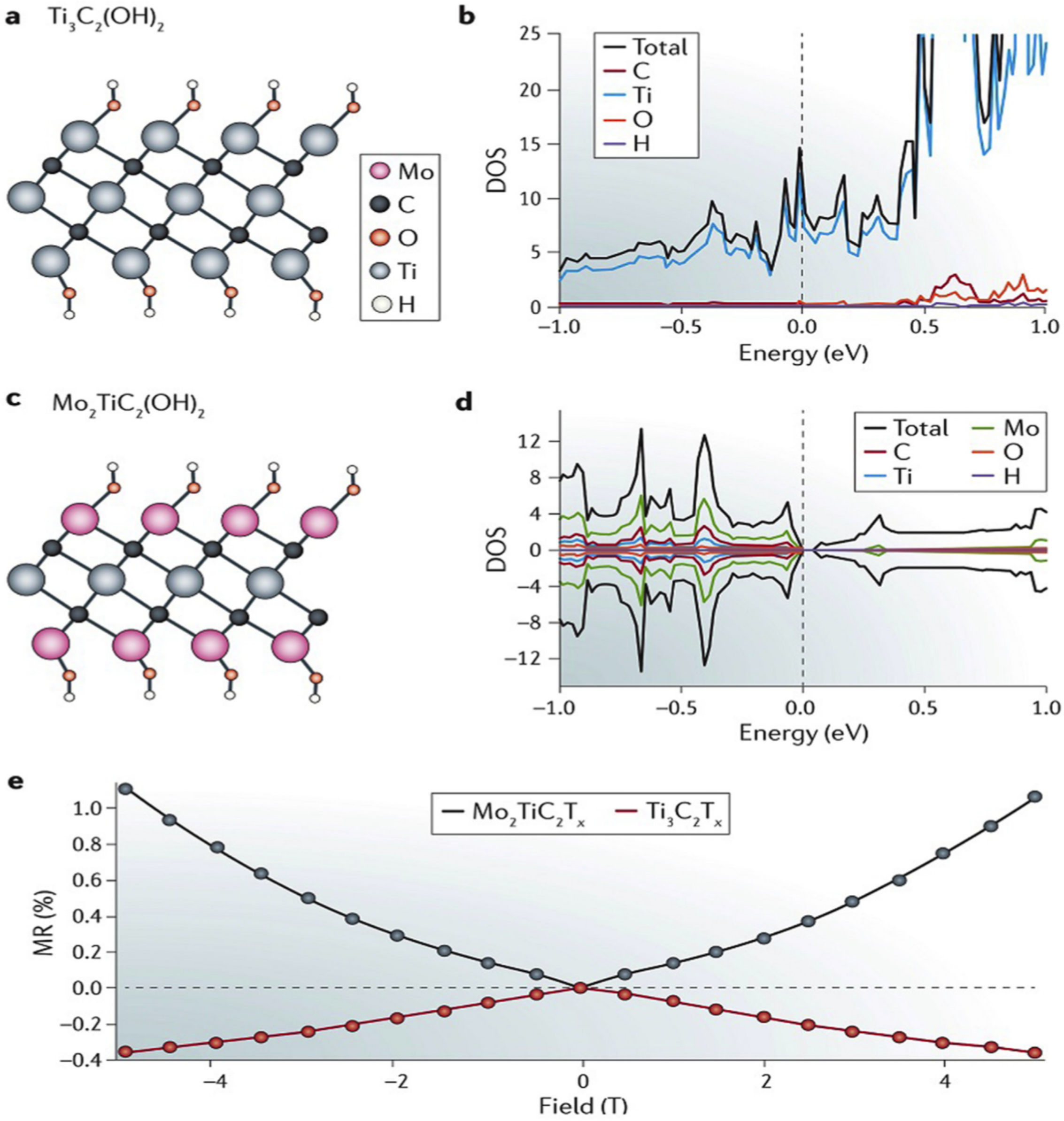

*Figure 12: Change in electronic properties by altering the external M layer of MXene. Schematic illustration of structure and DOS calculations of hydroxyl affected Ti3C2 (a,b) and Mo2TiC2. (c,d) DFT analysis of Ti3C2(OH)2 and Mo2TiC2(OH)2. (e) Magnetic field-dependent magnetoresistance of Ti3C2 and Mo2TiC2 at 10K [28].*

### 1.4.2 – Mechanical properties

MXenes offer impressively metallic conductivity and hydrophilicity along with unique mechanical properties. The electron mobilities of some MXenes have already reached as high as $10^6$ $cm^2V^{-1}s^{-1}$ which are analogous to or even higher than that of graphene (~2,5x$10^6$ $cm^2V^{-1}s^{-1}$) [65]. $Ti_3C_2T_x$ films has shown metallic conductivity values around 6500 S $cm^{-1}$, surpassing other 2D counterparts such as graphene and CNT [66,67]. Their competing 2D materials like graphene oxide [54,55], clays, or layered double hydroxides are hydrophilic but insulating [66]. In addition to their high strength, hardness and wear resistance, they have also high bending rigidity (D∼49,55 eV) [69] in contrast to graphene (D∼2.3 eV) [70,71] and $MoS_2$ (D∼9,61 eV) [69]. In particular, molecular dynamics (MD) illustrated that $M_2X$ MXenes exhibit better properties in terms of stiffness and strength compared with $M_3X_2$ and $M_4X_3$ structures as shown in stress vs. strain plot in fig. 13a [73]. A novel work [74] calculated the Young's modulus of 0.33±0.03 TPa for single layer (SL) $Ti_3C_2T_x$, recorded to be the highest value among all other solution-processed 2D counterparts including GO (∼0.21 TPa) [75] and $MoS_2$ (∼0.27 TPa) [76], but this value is only one-third of the Young's modulus of pristine graphene (∼1 TPa) [11].

Figs. 13b and 13c shows the mechanical flexibility of $Ti_3C_2T_x$ film made as a paper aircraft and wrapped on a glass rod. It is reported that a 5$\mu m$ thick and 10 mm wide cylinder made of $Ti_3C_2T_x$ can withstand 4000 times its own weight but as show in fig. 13d this value still increases to 15.000 times when 10 wt% PVA is compounded to it [66]. Ultrathin MXene films and their composites are transparent (fig. 13e) [77]. For instance, $Ti_3C_2$ has a visible light transmittance of 97% with increase of 1nm thickness [67]. Fig. 13f show the behavior between increasing thickness and overall transmittance. In 2017, monolayers of $Ti_3C_2T_x$ MXene have been rendered visible in optical microscope [78] similar to the graphene monolayers [79].

### 1.4.3 – Chemical properties

The increase in thickness as well has an adverse impact on the electrochemical performance of MXenes: it may create a barrier which makes difficult for ions to transport resulting in reduced capacitance values.

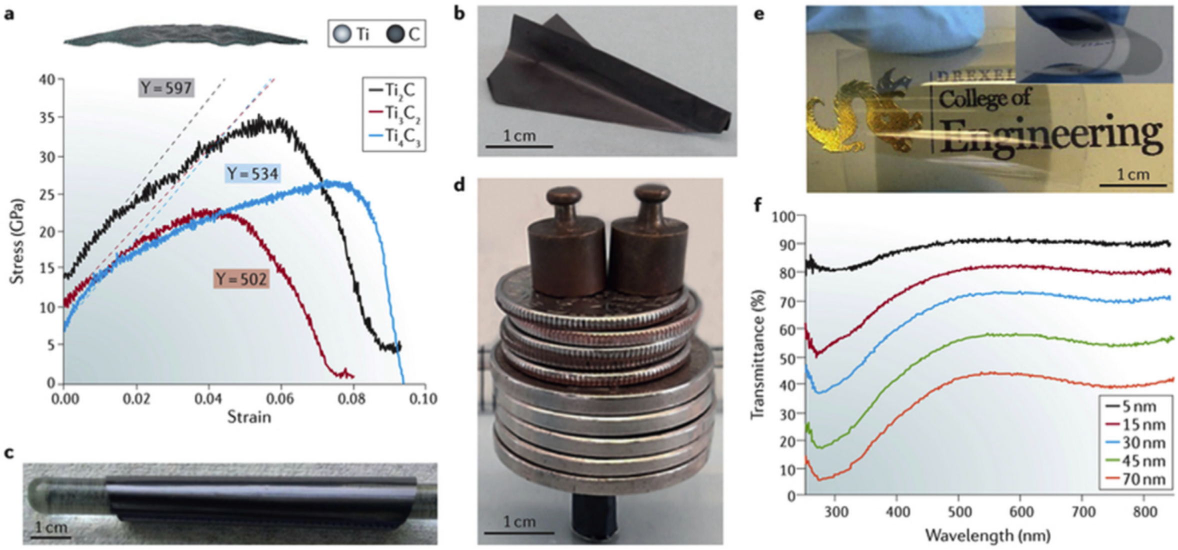

*Figure 13: Optical and mechanical properties of Ti3C2Tx MXene. (a) Stress vs Strain curves attained by tensile load testing of Ti(n+1)Cn samples along with a snapshot of Ti2Cafter equilibration at room temperature. Ti3C2Tx film shaped as a paper aircraft (b), rolled onto a glass rod (c), and made into hollow cylinder (d) by compounding 10 wt% polyvinyl alcohol withstanding a load 15000 times its own weight showing its flexibility and strength. (e) Optical image of Ti3C2Tx film demonstrating its transparency and bending capability (inset of e). (f) UV-Visible spectra of Ti3C2Tx film with different thickness [28].*

In 2018, Xia et al. [80] synthesized $Ti_3C_2T_x$ MXene liquid crystal where electrochemical performance was observed to be independent of the film for a thickness up to 200 $\mu$m by aligning the films vertically instead of stacking them horizontally. The vertical alignment of films was achieved by providing a mechanical shear to the liquid crystal mesophase of $Ti_3C_2T_x$ in way that it is stacked perpendicular to the current collector, resulting in the fast movement of ions.

### 1.4.4 – Stability

A considerable number of research were also conducted to determine the reactivity of Ti-based MXenes, especially oxidation and hydrolysis [81-83]. In 2017, Zhang et al. [84] noted that the colloidal solution of water and $Ti_3C_2T_x$ MXene tend to degrade within 5 days when stored in air at room temperature because of the dissolved oxygen formed by the interaction between air and water, but the MXene solution was found to be stable for more than 2 years when placed in Ar atmosphere at 5°C as it prevents the formation of dissolved oxygen, which is considered as the primary oxidant in this case, during the process.
Two years later, in 2019, Huang and Mochalin [85] proposed that it is indeed the water that plays a significant role in the degradation of MXene solution rather than the oxygen present. The researchers prepared colloidal solution of $Ti_2CT_x$ and $Ti_3C_2T_x$ Mxene in water and isopropanol (IPA) saturated in Ar and air atmosphere. Surprisingly, $Ti_3C_2T_x$ in water/Ar degraded in 41days, while it took around 2026 days for the same to occur in IPA/$O_2$ environment, suggesting that MXene degrade faster in the aqueous medium than the oxygen atmosphere.

MXenes, in general, exhibit lower thermal stability in comparison to the one of graphene and $MoS_2$. The atomistic simulation models suggested the melting points of graphene and single-layer (SL) $MoS_2$ to be 4500K [86] and 3700K [87], respectively. Meanwhile the melting points of Ti-based MXenes are significantly low with 1050K ($Ti_2C$), 1500K ($Ti_3C_2$) and 1700K ($Ti_4C_3$) [88]. This imply that MXenes may not be suitable in applications such as nanoelectronics where temperature is very high [118].

### 1.4.5 – Fluidic properties

Furthermore, $Ti_3C_2T_x$, has a contact angle of 21.5° when placed in contact with a water droplet, and unlike graphene oxide, it remains firm and stable even after vigorous shaking in water [60,66]. Thus, it establishes a great scope and potential use in water purification, desalination, membrane sequestration, and other water-based applications. Researchers have already demonstrated success in removal of lead [89], phosphorous [70], copper [71] and chromium [72] from water by using $Ti_3C_2T_x$ given its phenomenal antibacterial property [93].

$Ti_3C_2$ MXene shows a higher antibacterial efficiency towards both Gram-negative E. coli and Gram-positive B. subtilis. Damage to the cell membrane was observed, which resulted in release of cytoplasmic materials from bacterial cells and cell death [93]. The principal in vitro studies of cytotoxicity of 2D sheets of MXenes showed promise for applications in bioscience and biotechnology. Presented studies of anticancer activity of the $Ti_3C_2$ MXene was determined on two normal and two cancerous cell lines and cytotoxicity results indicated that the observed toxic effects were higher against cancerous cells compared to the normal ones [94]. Further studies on $Ti_3C_2$ MXene revealed potential of MXenes ad a novel ceramic photothermal agent used for cancer therapy [95].

The important results obtained in water removal can be attributed to the very small interlayer spacing in the MXene membranes ($\sim 6$Å), which are capable of adsorbing and rejecting ions/molecules with a radius larger than the interlayer spacing [96].

One-micron-thick $Ti_3C_2$ MXene membranes demonstrated ultrafast water flux (37.4 L/(Bar·h·$m^2$) and differential sieving of salts depending on both the hydration radius and charge of the ions. Cation larger than the interlayer spacing of MXene do not permeate through $Ti_3C_2$ MXene membranes. As for smaller cations, the ones with larger charge permeate an order of magnitude slower than single-charged cations [96].

With the problem of fouling and low water flux faced in commercial 2D materials, a group led by Khaled surpassed their own water flux value, reported above, to 420 L/(Bar·h·$m^2$) by grafting MXene with silver (Ag) nanoparticles [97].

In 2017, Li et al. [98] reported a phenomenal increase in water permeability of MXenes membranes with values over and above 1000 L/(Bar·h·$m^2$). The high values reported can be clarified from the following reasons: fragmented and nanosized MXene sheets were utilized instead of conventional microsized MXene sheets to get a rich pathway for water flux and a bigger interlayer spacing was obtained by creating additional nanochannels via intercalating and removing $Fe(OH)_3$ nanoparticles which in turn provide more fluid channels for water transport [98].

## 1.5 - Applications

The abovementioned properties not only qualified MXenes for use in energy storage and water purification but also in diverse range of applications, to name a few, electrochemical biosensor [99], electromagnetic absorption and shielding [100-105], structural composites [106], gas separation [107], electrocatalysts [108], transparent conductive films and coatings [109-112], hydrogen storage [113] and antibacterial membranes [114]. In 2017, Anasori et al. [28] performed an extensive review on the numerous applications of MXenes. MXenes have accumulated consideration in various new fields as of late which has been outlined in table 1. As it can be inferred from the table, the tunable and multifunctional properties of MXene demonstrated novel progress in different fields of MXene research from micro-supercapacitors to textile technology. However, among all these fields of application, MXene have been known to show significant and prominent contributions as electrodes in supercapacitors owing to their porous morphology, anodes in metal-ion batteries with due respect to their phenomenal intercalation ability and in water treatment and environmental remediation strategies such as adsorbents, membranes and biosensors [115].

**Table 1**
Recent application of MXenes.

| Application | Material | Description | Ref. |
|---|---|---|---|
| Micro supercapacitors (MSC) | $Ti_3C_2T_x$ and $Ti_3CNT_x$ | 3D printable energy storage devices from MXene aqueous inks. | [113] |
| | $Ti_3C_2T_x$ and r-GO | Flexible MSCs free from binder and current collector with MXene serving as cathode and r-GO as anode. | [114] |
| Flexible triboelectric nanogenerators (TENGs) | $Ti_3C_2T_x$ and glass | TENGs which can generate electric power from basic muscle movements such as texting and typing. | [115] |
| Selective gas separation | $Ti_3C_2T_x$ | MXene membranes with exceedingly high hydrogen permeability beneficial for $CO_2$ capture and $H_2$ production. | [102] |
| Broadband absorber | $Ti_3C_2T_x$ | Straightforward and simple to-deliver metasurface appliance created by utilizing the strong and local plasmonic resonances in MXene. | [116] |
| Photonic diodes | $Ti_3C_2T_x$ thin films | Passive photonic diodes for optical isolators by making use of the saturation absorption behavior in MXene. | [117] |
| Chemiresistive gas sensors | $Ti_3C_2T_x$ | Chemical sensors with superior signal-to-noise ratio alongside high sensitivity to gases especially $H_2$ bonded gases. | [118] |
| Sodium-ion storage | $Ti_3C_2T_x$ | Porous $Ti_3C_2T_x$ electrode created by inserting and removing sulfur into it capable of storing sodium ions. | [119] |
| HER catalyst | $MoS_2 \perp Ti_3C_2$ | The low onset potential and Tafel slope together with steady catalytic stability makes it ideal for HER catalyst. | [120] |
| Hybrid sodium-ion capacitors | $Ti_3C_2T_x$ | Binder, current collector, and additive-free MXene electrode with reversible electrochemical storage of $Na^+$ ions. | [121] |
| Textile technology | $Ti_3C_2T_x$ and liquid crystal GO (LCGO) | MXene with LCGO assisted fiber spinning for wearable gadgets. | [122] |
| | $Ti_3C_2T_x$ and carbon cloth | Flexible supercapacitors with excellent cyclability. | [123] |

## 1.6 - Challenges

MXenes are arguably the fastest-growing 2D materials in the post-graphene era, since their discovery in 2011, they have attracted widespread research interest due to their intriguing electrical, thermal, mechanical, chemical, as well as biological properties. As of January 1st of 2020, the unique term “MXene” appears in the titles, abstracts and/or keywords of >1500 publications cataloged in two major databases, with clearly exponential expansion of the field as a function of published papers per year (figure 14a). A fine collection of reviews provided insights regarding their preparation, functionalization, purification, characterization, and material properties. Several reviews also focused on the application potential of MXenes for a wide range of subject as mentioned before and shown in figure 14b, and in membrane-based separations applications (figure 14c).

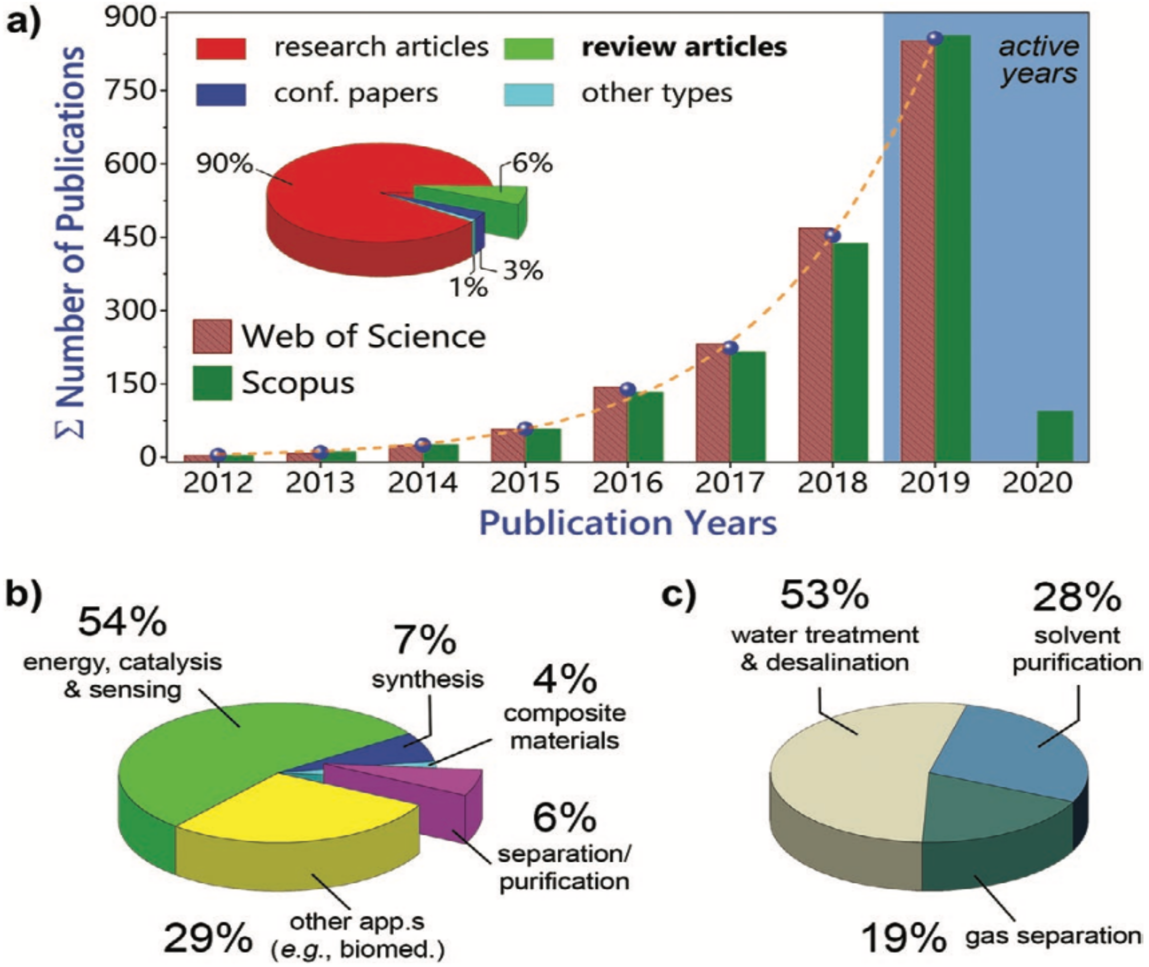

*Figure 14: The expansion and topical distribution of the MXene literature as of January 01, 2020. (a) Growth of MXenes based on Scopus and Web of Science database (excluding patents). (b,c) topic-based distribution of MXene literature according to the number of published articles in all fields (b), and in experimental research on membrane-based separations only (c) [119].*

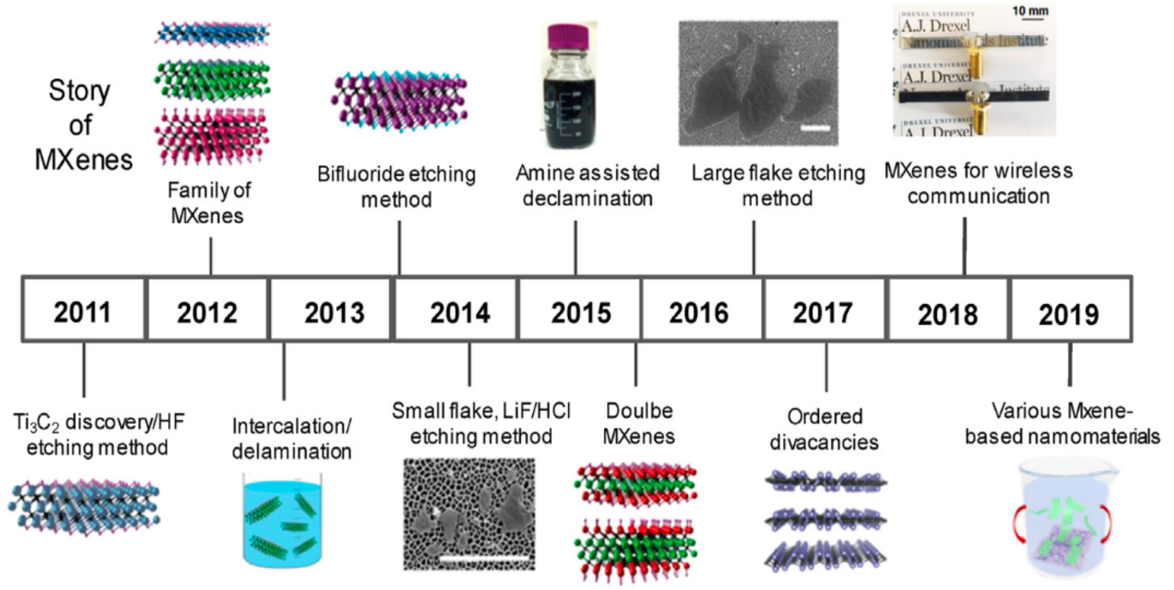

*Figure 15: Timeline of MXene [119].*

In figure 15 are summarized the evolution in fabrication of MXenes from discovery in 2011, until recent MXenes-based nanomaterial in late 2019, including the development of intercalations, Mxene clay, ordered divacancies and ordered double-M layers [116].

There are 792 possible existing combinations of MAX phases, combining 11 M, 12 A, 2 X and 3n values (excluding solid solutions and ordered-M layers). But only about 70 MAX phases appear to exist to date and among those only around 20 have been etched into a 2D material [118]. Moreover, among the 12 A elements forming the MAX forming MAX phases, only Al had been effectively etched until 2018, where Si was etched from $Ti_3SiC_2$ to produce $Ti_3C_2$ MXene [117]. Therefore, the discovery of new MAX phases and their corresponding 2D MXenes becomes a significant research path.

Many characterization methods such as X-ray diffraction (XRD), X-ray photoelectron spectroscopy (XPS) and energy-dispersive X-ray spectroscopy (EDS) have been employed, but still understanding and specific control of surface moieties has been unclear [118]. Non-terminated MXenes are yet to be produced and they can be synthesized by bottom-up fabrication methods such as physical vapor deposition (PVD) and CVD. Mainly, MXenes have been produced by top-down approaches, and only very few attempts have been made in growing ML and SL-MXene through bottom-up methods, thus, some work needed to be dedicated in this region [118].

MXene dispersions in aqueous medium are being stored in subzero temperatures to give longer life, but this solution is not feasible in practice and thus better techniques need to be explored for storing MXene solution and at the same time prevent them from being oxidized [118].

The use of MXenes in many applications such as hydrogen storage, supercapacitors, batteries and desalination are still in their initial stages. In the second part of this thesis are reported the techniques and design to produce advanced MXene membranes for multiple purpose such as desalination and water purification.
Finally, mainstream of recent works published on properties of MXenes, ie. electrical, electronic, mechanical etc. are on basis of theoretical studies such as DFT or MD, therefore an experimental coverage of these findings is required to verify those theoretical simulations [118].

# PART 2 – MXene-based membrane design

## 2.1 - Introduction to membranes with nanomaterials

Membrane design has been a direct application area of nanomaterials researcher [1]. The exploitation of nanoparticles as filters (nanofillers) or yielding nanocomposites structures for example, is a viable strategy of engineering the permeability, selectivity and/or stability of polymeric and ceramic membranes [2]. For selecting or producing the right filler for the right membrane applications, numerous studies focused on the particle size and shape, pore size and pore shape, surface chemistry and chemical stability of nanofillers as classical design parameters [3]. Several nanomaterials also proved to be useful as supported nanolaminate membranes (NLMs), having asymmetric structure similar to thin-film composite (TFC) membranes [4]. Among the nanomaterials used for membrane research, the family of graphene-like materials (GFMs) have attracted special and growing attention [5]. GFMs have successfully served as functional fillers of nanocomposites membranes as well as NLMs with tunable nanochannels [6]. Leading by graphene membranes, research has revealed the unique advantages of flat materials in membrane development, providing crucial insights into the role of particle morphology and surface chemistry [8]. Beyond graphene, a wide range of 2D inorganic, as well as organic nanomaterials, have been increasingly investigated for membrane applications [9].

On the top of the 2D nanomaterials used in membrane research, few of them like exfoliated hexagonal boron nitrides (h-BNs), graphitic carbon nitride (g-$C_3N_4$), transition metal dichalcogenides (TMDs) and metal carbide, nitride or carbonitrides (MXenes) are of special interest as graphene analogs [10]. Thanks to their strong structural, physical and/or chemical similarities, those materials can take advantages from the results achieved by research in developing graphene-based membranes. Nevertheless, different 2D material offer different properties that meet the need of different applications. In this respect, MXenes are of particular interest due to their rich surface chemistry and unique physicochemical properties [11]. Although, the majority of MXenes literature is currently based on a specific type of MXene, ie. $Ti_3C_2T_x$, the MXenes are highly customizable as a family of materials [12]. The precursor of MXene, MAX phases, offer an immense compositional vastness, as already said in the first part of this document, the precursor selection not only determines the chemical but also affects the physical properties of resulting MXenes considerably. Moreover, MXenes are post-functionalizable materials: during or after the etching from MAX phases and delamination, it is possible to introduce a variety of functional groups to MXenes, which provides another level of tunability [17,18]. Thus, MXenes constitute a highly versatile superfamily of nanomaterials and bring an unprecedented level of materials design capability at the disposal of advanced membrane research.

Several reviews also focused on the application potential of MXenes for a wide range of subjects, as mentioned before, however, only a couple of reviews [9,41,47] examined MXene-based separation membranes as a part of general discussions on the MXene applications or 2D membranes.

### 2.1.1 - MXene-based membrane materials

There are two main ways of synthesizing MXenes, as mentioned above, by CVD which is bottom-up approach, and by selectively etching the A element from the precursor MAX phase followed by exfoliation, which is the top-down approach.

The CVD method can potentially produce high-quality 2D MXene with large lateral size and few defect [53]. However, CVD is not suitable for fabrication of large-area membranes, and only few type of carbide MXene have been produced yet, thus more emphasis is being placed on the top-down synthesis method.

The vast majority of the MXene-based membranes available in the literature are based on the top-down route, starting with MAX phases as parent materials.

## 2.2 – PROPERTIES OF MXENE MEMBRANES

MXenes demonstrate several desirable properties that can be capitalized for designing high-performance membranes, exploiting the benefits of 2D morphology for membrane design, fabrication and stability, solution processability and chemical stability of MXenes in aqueous dispersions. Furthermore, MXenes have excellent electrical, mechanical, and antimicrobial properties, which are crucial roles in membrane performance for different applications.

### 2.2.1 – 2D Morphology

The 2D morphology of MXenes are similar to the 2D of graphene-like materials, the high aspect ratio of regular Mxene nanosheets endows the resulting membranes with nanochannels that resulted in lengthened the diffusion pathways for solute transport (figure 16a). These nanochannels are formed by pinholes, internal spacing between parallel and wrinkled nanosheets known as nanogalleries, and voids between nanosheets edge which can be considered as nanoslits.

The longer length of the permeation pathways allows the differentiation of solute transport rates, which serves as the basis of selectivity for the membranes formed by MXenes or any 2D materials [182]. Moreover, by engineering the interlayer spacing of MXene assemblies, one can create well-defined transport channels for enabling size-exclusion-based molecular separation membranes: $Ti_3C_2T_x$ nanosheets demonstrate an interlayer spacing of $\approx$0.64 nm in the wet state, which allows water transport but retains solute of size larger than this interlayer spacing [60]. This interlayer spacing can be further decreased to a range of 0.52-0.38 nm when dried and/or heated, making the resulting MXene-based membranes suitable for gas separation [70]. The lateral dimension, flake size, of MXene nanosheets can also be tailored from 6 to <1 $\mu m$ by varying the etching and exfoliation conditions. Thus, it becomes possible to modulate efficiently the key parameters of diffusion pathways and membranes thickness to engine the separation performance of the MXene-based membranes [71]. Besides, as with other 2D materials, MXenes are not perfectly flat and get wrinkled, which adds up to the microstructural properties of resulting nanolaminates (fig. 1b).

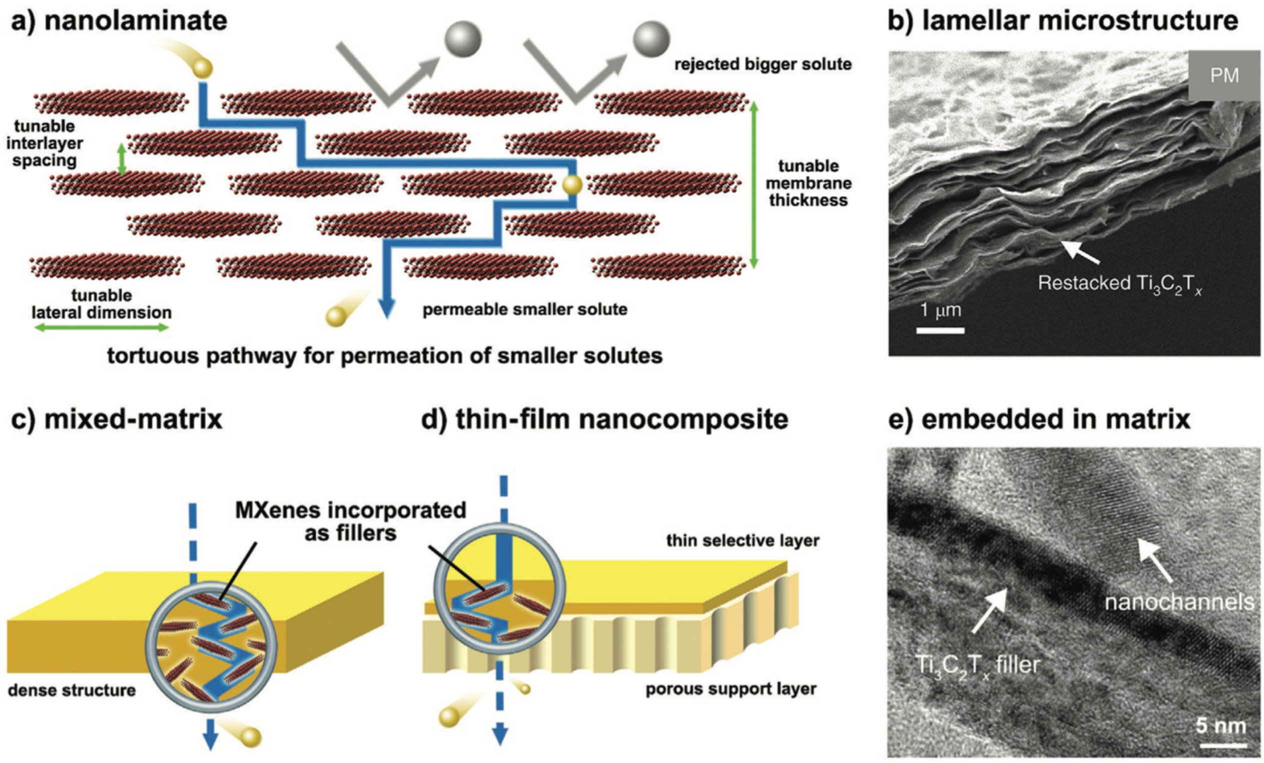

*Figure 16: (a) Solute transport through a MXene-based nanolaminate. (b) SEM image of a MXene-based nanolaminate. A Mixed-Matrix (c) and Thin-Film Nanocomposites (d) formed by MXene nanosheets as a filler material incorporated in bulk polymer matrices (c) or thin selective layers over a porous support (d). (e) HTEM image of a MXene nanosheet embedded in a polymer matrix.*

### 2.2.2 – Physicochemical properties

One of the most important physicochemical property of MXene-based materials is their hydrophilicity, which is the main reason behind their good water processability. The reason of MXene hydrophilicity comes from their surface terminal/functional groups, which replace the A atoms in the MAX phase precursors. These groups are typically based on oxygen and/or fluorine atoms, experimentally, $Ti_3C_2T_x$ nanosheets exhibit a higher O/F ratio when synthesized using HCl-LiF solutions instead of 50% HF [74]. The higher O/F ratio, along with the presence of -OH functional groups and intercalating cations such as $Li^+$ and $NH_4^+$, can provide MXene nanosheets with greater capacity to interact with water molecules: $Ti_3C_2T_x$-based sheets exhibit high water wettability (ie. high hydrophilicity) with water contact angles of ≈25-45° [60,71]. The presence of -OH functional groups and the associated negative charges, with high zeta potential values ranging between -30 and -80mV, also opens up the possibility of surface modifications via chemicals functionalization and electrostatic attractions [75]. To modify the surfaces of $Ti_3C_2T_x$ nanosheets, cationic surfactants or cationic/neutral polymers such as hexadecyltrimethylammonium bromide (CTAB), polyethyleneimine (PEI), poly-diallylmethylammonium chloride (PDDA), poly-dimethylsiloxane (PDMS), poly-ethylene oxide (PEO), and poly-vinyl alcohol (PVA) were utilized [76,77,78]. Beyond that, by using silanol chemistry on -OH groups, the $Ti_3C_2T_x$ nanosheets were also grafted with organosiloxanes to give a multitude of functional groups including $-NH_2$, -COOR, $-C_6H_6$ and $-C_{12}H_{26}$ [79]. These efforts not only confirm the feasibility of MXene-based materials, but also demonstrated the chemical versatility of MXenes, which is desirable for membrane development.

### 2.2.3 – Chemical stability

Another important aspect is the chemical stability of MXene, that play a crucial role for both solution processability and the performance of resulting membranes. Under an inert gas environment, $Ti_3C_2T_x$, with $T_x$= F or OH, are fairly stable until 800°C with a minimal level of oxidation at around 500°C [80]. As previously discussed, surface-exposed metal atoms of MXenes are easily oxidized [81]. One solution to prevent oxidization and improve durability for longer period, as said, is keeping colloidal MXenes in argon-filled containers at low temperatures. It is important to note that MXene are also considerably more stable in the dry form (as films) and as embedded in a polymeric matrix such as PVA [69,82]. On the other hand, the stability of $Ti_3C_2$ can be dramatically improved by annealing under hydrogen atmosphere [83].

### 2.2.4 – Electrical properties

The electrical conductivity of certain MXene-based materials is of particular interest to membrane applications: titanium carbide MXene have probably one of the most attractive conductivities among all solution-processable 2D materials, including graphene [32,68]. Reported $Ti_3C_2T_x$ films have a metallic conductivity around 10000 S/cm, allowing them to demonstrate potential in modulating ion transport under an externally applied potential [60]. A novel study in the field has successfully attested this concept by modulating the transport of NaCl and $MgSO_4$ salts through a $Ti_3C_2T_x$ membrane via switching between positive and negative voltages [84]. In the study, they attributed this voltage gating effect to the change in electrostatic interactions between $Ti_3C_2T_x$ nanosheets and cations, which led to ions intercalation and corresponding alterations in the interlayer spacing between $Ti_3C_2T_x$ nanosheets [84].

### 2.2.5 – Mechanical properties

Also the mechanical properties of MXene-based material are very interesting for membrane development. Single-layer $Ti_3C_2T_x$ MXene have very high Young's modulus of $\approx$0.33TPa possessing an even higher elasticity than graphene oxide and other solution-processed 2D materials [24]. More importantly, when combined with polymeric materials such as PDMS or PVA, the $Ti_3C_2T_x$ nanosheets enhance the overall mechanical properties of the resulting nanocomposites films [75]. Notice that PDMS (hydrophobic) and PVA (hydrophilic) are common membrane materials with different wettability behaviors.

### 2.2.6 – Antimicrobial properties

In addition to the chemical and physical properties introduced above, the antimicrobial behavior of MXenes is also important for certain membrane applications. Colloidal dispersions of $Ti_3C_2T_x$ nanosheets exhibit strong antibacterial activity against both Gram-negative and Gram-positive bacteria, overcoming that of GO [22]. Potent antibacterial activity of MXenes is also revealed in surface-deposited or polymeric-embedded forms as observed by different research [85,86,87].

Further discussion on these properties will be done in section 2.5.2 of this thesis, focusing on the MXene-based separation membranes.

## 2.3 – FABRICATION OF MXENE MEMBRANES

The discuss will focus on 3 types of membranes, as already shown in figure 16, which have been commonly utilized for preparing MXene-based membranes: 1) nanolaminate membranes (NLMs), 2) thin-film nanocomposites (TFNs) and 3) mixed-matrix membranes (MMMs).

### 2.3.1 – Nanolaminates membranes

The NLMs prepared by vacuum or pressure assisted filtration represent, in academic research, the most extensively studied membrane format for MXene-based membranes (illustration in figure 16a). The first step to fabricate NLMs is to disperse MXenes in solvents, usually water at an appropriate pH, forming a homogeneous and stable colloidal [70,71].

First two important parameters to take into account for preparing such membranes are the lateral dimension of the flakes and choice of support membranes. Moreover, several parameters such as the concentration and volume of colloidal dispersions, as well as the pressure applied will directly impact the compactness, thickness and integrity of the resulting membranes [90,91].

It should be appointed that there are alternative methods of preparing NLMs resembling the ones prepared by filtration methods, for example, Xu et al. has reported a preparation via spin coating of a MXene membrane on a flat-sheet polyacrylonitrile (PAN) supports. Similarly, dip coating of MXene materials on a four-channel ceramic $\alpha$-$Al_2O_3$ hollow fiber support was demonstrated [92].

Another important aspect in NLM fabrication lies in the solution processability of MXene-based materials, which is also linked to the rheological properties of dispersion. It has been shown that the colloidal dispersion of $Ti_3C_2T_x$ may exhibit viscoelastic behaviors at different concentrations depending on the rate of exfoliation [93]. Single-layer $Ti_3C_2T_x$ dispersions denote a noticeable viscoelastic behavior at a concentration as low as <0.36 mg/mL, while multilayer $Ti_3C_2T_x$ dispersion can reach high viscoelasticity with increasing elastic moduli at higher loadings [93]. These observation demonstrate that the rheological versatility of $Ti_3C_2T_x$ dispersions is an important factor for membrane fabrications even beyond the preparation of NLMs. Apart from the ease of fabrication, NLMs also constitute a practical platform to showcase the effects brought by chemical functionalization and intercalation. For this reason, PEI, borate ions and silver, titania ($TiO_2$) and ferric hydroxide nanoparticles, as well as GO nanosheets had been employed to improve the performance of MXene-based NLMs [70,71,93].

### 2.3.2 – Thin-Film Nanocomposites

The idea of TFN membrane is a modified version of TFCs (see figure 16d,e). Actually, the most commercially successful membranes for wastewater treatment and desalination are TFCs membranes, while TFNs are interesting for performance-driven research [182]. In fact, TFNs have demonstrated a great promise for a wide range of applications including nanofiltration (NF) and osmotically driven processes including forward osmosis (FO), reverse osmosis (RO) and pressure-retarded osmosis (PRO). Like to the conventional TFCs, the TFN membranes usually comprise an ultrathin polyamide (PA) selective layer over a porous substrate, that act as a support layer, to afford an asymmetric structure. To do so, the interfacial polymerization (IP) techniques serves as the core method of preparing such membranes, which has not been systematically studied so far for MXene-filled membranes [182]

### 2.3.3 – Mixed-Matrix Membranes

A common opinion to MXene-based membranes is that while NLMs are useful for academic research, TFNs and MMMs are still the more realistic membrane designs for practical applications [182]. The idea of MMMs revolves around the goal of engineering the transport properties of membranes, continuous matrix phase, by integrating of filler particles (illustration in figure 16c) [5].

The production of such membranes generally involves dispersing the filler material into the polymer dope solution before casting the membrane and inducing phase inversion either through solvent evaporation or nonsolvent-induced coagulation. A correct design of MMM have to take in consideration the following aspects: 1) uniformity and state of aggregation of the filler material in the prepared membrane, 2) dispersion stability of the filler material in the organic solvent system adopted by the polymer dope solution and 3) chemical compatibility of the filler material with the polymer matrix, particularly at the filler/polymer interface [5].

Thanks to their hydrophilicity and polarity, MXene-based material are highly compelling to this scope, as well as their rich surface chemistry which allow considerable versatility for further functionalization as well as strong interactions with a range of solvents. Experimentally, $Ti_3C_2T_x$ nanosheets are found to possess long-term dispersion and chemical stability in polar solvent such as N,N-dimethylformamide (DMF) and N-methyl-2-pyrrolidone (NMP), that are important solvents for mixed-matrix membranes [95]. Moreover, the presence of hydroxyl (-OH) terminations offers the possibility of using classical silanol chemistry to functionalize the surface of the nanosheets and increase their chemical compatibility at the filler/polymer interfaces, since silanol chemistry is the most extensively utilized chemistries for mitigating nonideal interfacial morphologies, ie. membrane defect [5]. Therefore, successful fabrication of $Ti_3C_2T_x$-based MMMs using various polymers as matrix had been reported for effective purification of water and organic solvents [79,84,96,97]. The roles played by MXene fillers in MMMs varies in more than one effort, can range from leveraging the 2D morphology and narrow interlayer spacing for size exclusion, tuning surface chemistries for promoting facilitated transport to altering the packing of polymer chains for enhancing mechanical properties and separation performance and lengthening diffusion pathways for realizing selective solute transport. By the way, these roles are not distinctly different from those played by other 2D materials fillers [5]. The truly value apported for MXene-based MMMs should be find toward exploiting the unique advantages of MXene-based materials such as the high electrical conductivity. In this respect, a preliminary study had shown that $1.5 \mu m$ thick $Ti_3C_2T_x$/PVA MMM not only exhibited enhanced mechanical stability that was sufficiently robust to endure repeated performance evaluations but also continued to stay electrically conductive, allowing water fluxes and electrostatically manipulated rejection rates to remain tunable by applying different voltages [84].

## 2.4 – PHYSICS OF MXENE-BASED MEMBRANES

Before evaluating the separation/purification performance, is important to provide a brief discussion on the separation mechanism of MXene-based membranes. In both MMMs and TFNs, MXenes serve as filler material rather than directly acting as the selective component. Moreover, the main contribution of MXenes in MMMs and TFNs is to engineer the transport properties of the matrix and lower the membrane resistance. Thus, to understand separation mechanism we will focus on NLMs followed by a brief discussion on how MXenes improve the performance of MMMs and TFN membranes.

### 2.4.1 – Liquid Separation by Nanolaminates

NLMs for water and organic solvent purification typically separate via two main mechanisms: 1) size exclusion or 2) Donnan exclusion principle [94]. As previously discuss in section 2.2, the size of the interlayer spacing plays an instrumental role in the size exclusion mechanism: solutes which are larger than the interlayer spacing between MXene nanosheets are sieved out or rejected, while smaller solutes are allowed to permeate through the interlayer spacing (figure 16a) [105,107]. Furthermore, MXene nanosheets are highly negatively charged, therefore charged solutes, such as ions, polyelectrolytes and organic dyes, can be separated via Donnan exclusion principle.

In Donnan exclusion principle, ions with the same charge of the membranes are electrostatically repelled away from the membrane, which, in turn, drives the rejection of the counter-ions to maintain electroneutrality of the solution [108]. Thanks to this electrostatic repulsion of the charged solutes, the nanoslits and interlayer spacing can be larger than the size of the solutes to be separated.

The interlayer spacing in the nanometer to sub-nanometer regime is achieved and controlled in MXene-based nanolaminates, thus the NF process is best suited for nanolaminates for water and organic solvent purification [182].
The flux of the solvent permeating through the MXene-based NLMs can be defined by **Hagen-Poiseuille equation** (Equation 1) which is valid for NLMs of other 2D materials [109].

$$\mathrm{Flux} = \frac{h^4 \Delta p}{12L^2 \eta \Delta x} \quad (1)$$

Where $h$ is the *d*-spacing between the MXene nanosheets, $\Delta p$ is the transmembrane pressure, *L* is the average lateral dimension of MXene nanosheets, $\eta$ is the viscosity of the solvent and $\Delta x$ is the membrane thickness.

### 2.4.2 – Gas Separation by Nanolaminates

A common mechanism of gas separation in NLMs is Knudsen diffusion [102]. When the mean free path of a gas molecule is larger than the channel it travels, Knudsen diffusion acts as the dominant mechanism of transport [103]. In such conditions, the molecular weights of the gases determine the separation selectivity, or more precisely, the selectivity is inversely proportional to the square root of the molecular weight of the permeating gas components, as shown in Equation 2 and 3 [104].

$$J = \frac{\pi n r^2 D_k \Delta p}{RT\tau l} \quad (2)$$

Where *J* is the flux of the membrane, *n* is the molar concentration of the gas, *r* is the pore radius, $\Delta p$ is the transmembrane pressure, *R* is the gas constant, *T* is the temperature, $\tau$ is the tortuosity of the pores and *l* is the diffusion length. $D_k$ is the **Knudsen diffusion coefficient** which is defined as given in Equation 3:

$$D_k = 0.66r\sqrt{\frac{8RT}{\pi M_w}} \quad (3)$$

Where $M_w$ is the molecular weight of the permeating gas [105].

Furthermore, MXene-based NLMs have huge potential to separate via a facilitated, ie. carrier mediated, transport mechanism. Facilitated transport is enabled by chemical carriers that can react reversibly with one gas component but not the other, that allows the interacting gas to permeate through the nanolaminate more preferentially than the non-interacting one [106]. Thanks to the rich surface chemistry and physicochemical versatility of MXene materials, MXene-based NLMs can be chemically modified with a multitude of different functional groups to target specific gas components in feed mixture [182].

### 2.4.3 – Separation by Composite Membranes

Despite to the NLMs, MXenes do not have a direct influence on the separation mechanism of MMMs and TFN membranes. This happen because their main objective is to serve the role of filler materials for lowering mass transfer resistance and achieving performance enhancements. Thus, adding MXenes does not alter the separation mechanism that is already governing the transport behavior of the membranes [182]. For example, MMMs and the "skin-like" selective layers of TFN membranes possess nonporous (dense) structures where solutes permeate via a solution-diffusion mechanism. According to the solution-diffusion mechanism, solute permeability is a function of its solubility and diffusivity like $P = S\ D$ where *P* is the permeability of the membrane, *S* is the solubility and *D* is the diffusivity of the solute permeating through the membrane [5].

Solubility is a thermodynamic term that quantifies the amount of solutes sorbed by the membrane, while diffusivity is a kinetic term which accounts for how fast the solute diffuse through the membrane [104]. Incorporating MXene fillers into the polymer matrix of MMMs or the selective layer of TFN membranes, can provide supplementary pathways of lower transport resistance as compared to the dense polymer matrix (figure 16c-e), thanks to the nanochannels made up by interlayer spacing of layered MXenes and the nanogaps at the polymer/filler interface. Consequently, increases the diffusivity of the solutes, leading to an enhancement in solute permeability. Similar enhancement in solute permeability is achieved by incorporating chemically functionalized MXenes with enhanced affinity towards the solutes to strengthen the solubility of the solutes [182].

Finally, in the case of dense membrane structures where solute transport remains hinged on the solution-diffusion mechanism and the addition of MXene fillers can alter diffusivity and solubility of solutes to bring an engineering of the transport properties of the membranes.

## 2.5 – MXENE-BASED SEPARATION MEMBRANES

MXenes offer incredible and suitable material properties that are well-aligned with the efforts at realizing next-generation membranes. As mentioned before, MXenes are also capable for designing different types of membranes. In fact, MXenes have been so far utilized for a wide range of separation/purification membrane applications. In this section, the discussion focus on the progress made in MXene-based membranes according to gas, water and organic solvent separation/purification applications.

### 2.5.1 – Gas Separation

Even if is in infancy stage, MXenes have already demonstrated valuable scope in membrane-based gas separation. In 2018, Ding et al. fabricated MXene-based NLMs via vacuum-assisted filtration on anodic aluminum oxide (AAO) supports [89]. By simply peeling off the deposited film, the researchers could prepare freestanding MXene membranes showing high mechanical robustness (see figure 17a, b).

Gas permeation analysis showed that the freestanding MXene nanolaminates are highly permeable to small gas molecules, ie. He: 2164 barrer; $H_2$: 2402 barrer, at 25°C and 1bar. Since the permeation of larger gas molecules, including $CO_2$, $O_2$, $N_2$ and $CH_4$, were quite low, Ding et al. demonstrated high selectivity for several small/large gas pairs. For example, $H_2/CO_2$ gas pair reached a high ideal and mixed-gas selectivity of 238.4 and 166.6 respectively, despite a selectivity of only $\approx 4.7$ was predicted based on Knudsen diffusion. This result overcome the 2008 Robeson upper bound [103], a hypothetical boundary line that showcase a practical performance limit of conventional polymeric membranes, significantly (figure 17c).

However, the ideal $CO_2/N_2$ selectivity was very low since the permeability of $CO_2$ was lower than that of $N_2$ ($CO_2$: 10 barrer; $N_2$: 19 barrer) [89]. The authors attributed this observation to the restriction of $CO_2$ diffusion due to strong interaction of $CO_2$ molecules and MXenes: oxygen-containing functional groups on MXene surfaces might be exerting a "trapping effect" on the permeating $CO_2$ molecules. Ding et al. have verified this argument by measuring the interaction energies of $CO_2$ and $N_2$ with MXenes, which were -175.1 and -97.5 kJ $mol^{-1}$, respectively. Hence, MXene NLMs appear promising for applications that require the suppression of $CO_2$ permeation [89].

#### 2.5.1.1 – Carbon Capture

One way to increase the $CO_2$ permeation is to reduce the overall transport resistance by developing thinner NLMs with accurate interlayer spacings. Shen et al. [70] had successfully employed this strategy by manipulating the crosslinking of MXene nanosheets with borate ($B_4O_7^{2-}$) and PEI (figure 17d,e). They demonstrated that both borate and PEI/borate intercalation allowed the discrimination between $CO_2$ and $CH_4$ (or $N_2$) together with an increase in mechanical strength. This was further confirmed with a 43% increase in the equilibrium $CO_2$ adsorption of borate/PEI-intercalated MXene (13% for borate-modified MXene) as compared to pristine MXene as shown in figure 17f. With this result, the borate/PEI-intercalated MXene-based membranes transcended the separation performance of even MOF-based membranes. On the other hand, it had been reported that the composition of the feed gas, like the relative humidity, substantially affect the overall performance of MXene-based membranes. This effect had been demonstrated by Shan et al, where $H_2/CO_2$ selectivity fall for about 50% (from 19.7 to 9.8) when the relative humidity increased from 40% to 90% [70].

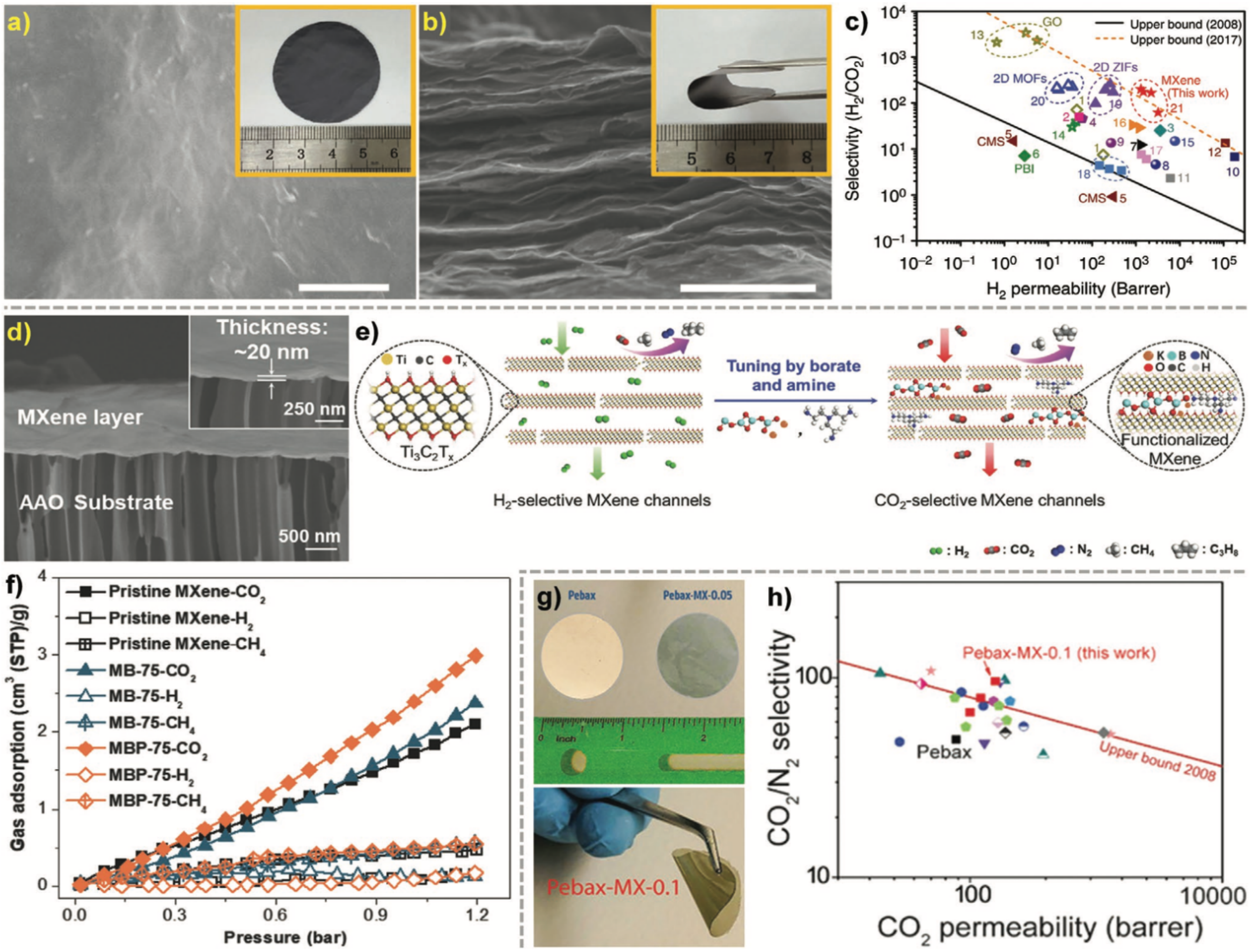

*Figure 17: Gas separation performance of MXene-based membranes. a) Top and b) cross-sectional SEM images of a freestanding MXene membrane. c) H2/CO2 separation performance of the MXene membrane in Robeson-type plot [89]. d) An MXene NLM deposited on AAO support. e) Depiction of the structure and gas transport behavior of $H_2$ and $CO_2$ selective MXene nanolaminates. f) gas adsorption properties of MXene-based nanolaminates at 25°C (MB: MXene crosslinked with borate; MBP: MXene crosslinked/intercalated with borate and PEI; "75" denotes the treatment temperature in °C) [70]. g) Unfilled and MXene-filled PEBA membranes prepared by solvent casting. h) Benchmarking of MMMs prepared by combining PEBAX 1657 and $Ti_3C_2T_x$ [114].*

The commonly accepted explanation for such evidence lies in the facilitated transport of $CO_2$ by $H_2O$ molecules that are intercalated between the nanogalleries. Considering the fact that moisture is typically present in the feed streams for $CO_2$-based separation processes [110,112], it could be beneficial to carry out a pre-treatment to dry feed gas streams, to overcome this problem. Besides to room-temperature operations, MXenes are also useful for gas separation at medium/high temperatures. In 2019, Fan et al. [113] have shown that MXene-based NLMs give high selectivity of 41 for $H_2/N_2$ separation at 320°C. Moreover, their AAO-support of the MXene membrane showed no sign of degradation up to 200h of operation [113], this could be relevant for industrial purpose on $H_2$ separation processes.

In another promising demonstration, Liu et al. [73] employed a MXenes as the filler of a poly(ether-block-amide) (PEBA) MMM for $CO_2$ capture. Using $Ti_3C_2T_x$ nanosheets at a filler loading as low as 0.15 wt%, the researchers have prepared high-performance composite membranes on PAN supports by spin coating. Due to the preferential affinity of polar $CO_2$ to polar $Ti_3C_2T_x$ particles and PEO blocks in PEBA used, the resulting MMM reached a remarkable $CO_2/N_2$ selectivity of 72.5 with the $CO_2$ permeance of 21.6 GPU, also here the resulting membrane showed good stability in a 120h long continuous operation [73]. Another recent study, conducted by Shamsabadi et al. in 2020 [114], using two PEBA varieties and water-soluble polyurethane, developed MMMs (and TFCs) for $CO_2$ capture. With Pebax 1657, which contains PEO blocks, they shown MMMs (figure 17g) with high permeability and selectivity, overcoming the 2008 Robeson upper bound for $CO_2/N_2$ (figure 17h). Surprisingly, they also observed that while the $Ti_3C_2T_x$ nanosheets exposed to open air degrades fast, MMMs are stable for 6 months as the polymer matrix serves as a protective layer [114].

### 2.5.1.2 – PAN-based filter

In 2019, Gao et al. [87] introduced a study concerning the filtration of a fine particulate matter (PM2.5: atmospheric particles with an effective aerodynamic diameter below 2.5 $\mu$m) from air using MXene-incorporated PAN-based filters.

The performance of particulate air filter, as considered in the very concept of effective aerodynamic diameter, is influenced not only by the mesh size of filters but also the attraction of particles to the filter surfaces [115]. Therefore, the authors added just 0.005-0.080 wt% of MXene into PAN, by combining MXene and PAN as the electrospinning precursor. The resulting electrospun composite filter exhibited superior PM2.5 removal performance in terms of both rate (4.2 vs 44 $\mu g\ cm^{-2} h^{-1}$ ) and filtering capacity (>2 times). Moreover, using a model Gram-positive species (Staphylococcus aureus), they have reported some preliminary observations on the inhibition of bacterial growth on the composite filters developed [87].

### 2.5.2 – Water Purification

One of the most attempt material properties of MXenes, for fabricating NLMs for gas separation, is likely their 2D morphology, which is properly possess by all 2D materials. Instead, for producing water separation membranes, MXenes offer much more: hydrophilicity, ion adsorption capacity, high surface charge, mechanical robustness, electrical conductivity, chemical tuneability, photothermal and photocatalytic as well as antibacterial properties are among the most interesting attributes of MXenes application in water separation [182]. There are two major topics where MXenes are involved in the wide range of water purification applications: 1) wastewater treatment, and 2) water desalination.

For wastewater treatment the studies focused on bacterial disinfection and solute removal. For water desalination, instead we cover molecular sieving and photothermal membrane distillation.

#### 2.5.2.1 – Wastewater Treatment

Looking for applications in wastewater treatment, Ding et al. [71] assembled $Ti_3C_2T_x$ MXene nanolaminates on AAO support via vacuum-assisted filtration. To create a high number of channels that facilitate water transport, they have utilized MXenes with lateral size of ≈ 100-400 nm. Moreover, they have intercalated MXenes with positively charged $Fe(OH)_3$ nanoparticles, which were removed later during the membrane fabrication, thus leaving a larger interlayer spacing between the MXene nanosheets (figure 18a-c). Thanks to this combined strategy, an outstanding high water permeability of >1000 L $m^{-2}$ $h^{-1}$ $bar^{-1}$ was reported (figure 18d). In addition, their MXene membranes achieved a rejection efficiency of >90% for organic molecules having average molecular sizes above 2.5nm.

To enable the rejection of small dye molecules with hydrated diameters in the range of 1.0-1.6nm, Kang et al. [94] incorporated 10-30 wt% of GO nanosheets into MXene nanolaminates (figure 18e). The overall thickness increases from ≈0.92 nm of the individual hydroxylated MXene nanosheets to ≈1.43 nm of the hybrid nanolaminates. Therefore, the effective nanochannel size of the hydrated MXene-GO composite membrane was ≈0.5nm, due to stacking effect. The MXene-GO composite membrane exhibited high rejection rates, during the pressure-driven filtration test, for charged dye molecules with hydrated radius of >0.5nm but performed worse for neutral and smaller dye molecules as shown in figure 18f. This result indicates that the nanogalleries formed in MXene nanolaminates provide size exclusion effect and the negative surface charge enhances the rejection of charged dyes by electrostatic repulsion [94].

In 2018, Wang et al. have employed double-layered MXene nanosheets for the preparation of supported membranes by vacuum-assisted filtration [109]. These membranes possessed rigid and highly ordered nanochannels, providing fast water transport and a water permeability of 2300 L m$^{-2}$ h$^{-1}$ bar$^{-1}$ as shown in figure 3g [109].

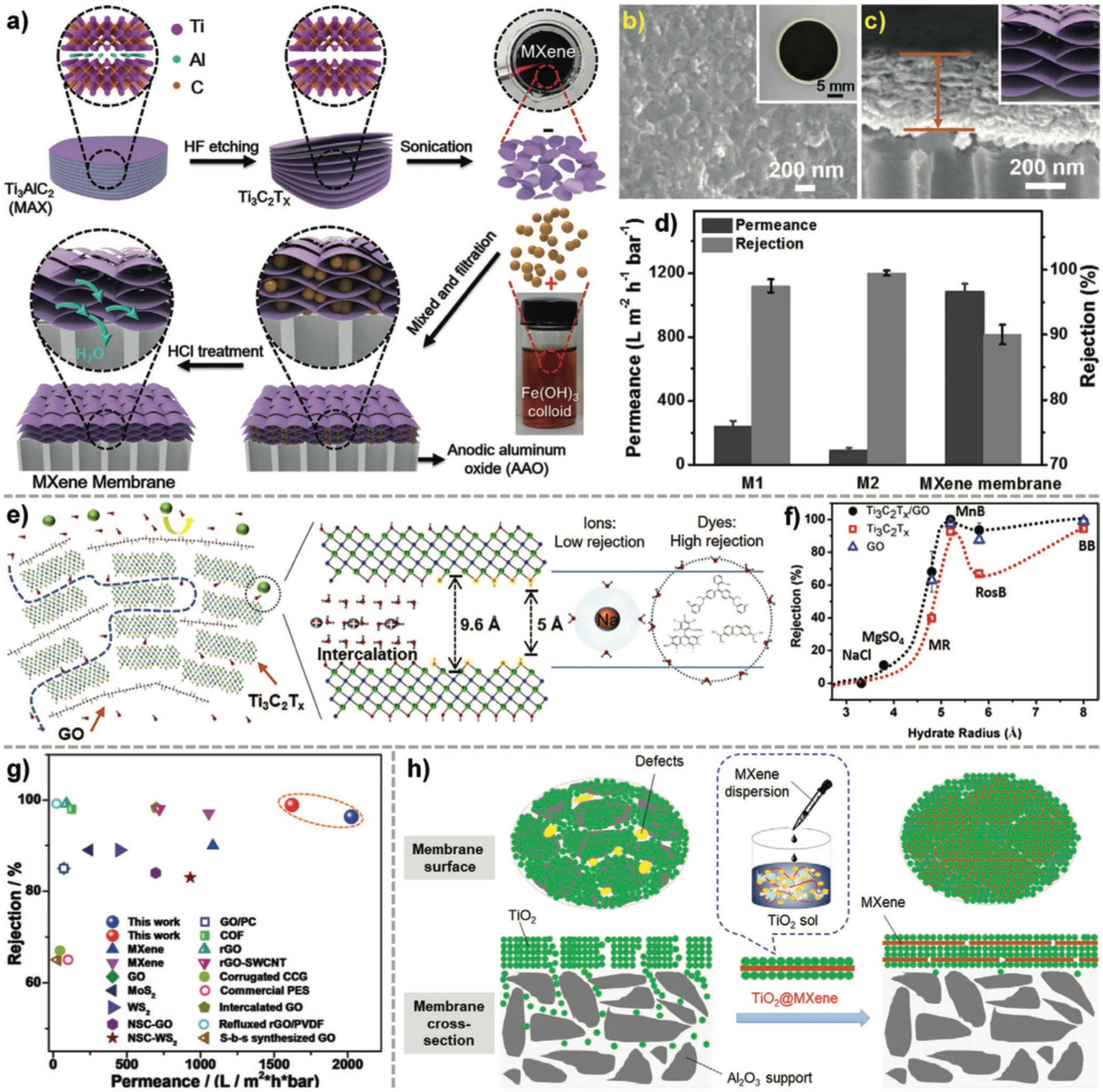

*Figure 18: Water purification by MXene-based membrane. a) Preparation. b) and c) characterization. d) performance of MXene-based NLMs with enlarged interlayer spacing achieved by the intercalation and subsequent removal of colloidal Fe(OH)$_3$ [71]. e) Conceptual diagram of size exclusion by GO-MXene hybrid membrane. f) Rejection efficiency comparison of GO-MXene hybrid membrane with respect to GO and MXene [94]. g) Performance comparison of MXene-based membrane and other 2D-based or commercial polymeric membranes for rejection of various dye molecules [109]. h) Effect of MXene nanosheets on defect prevention in TiO$_2$ mesoporous membranes [92].*

More recently, in 2020, Liu et al. [116] by combining again MXenes and GO, have reported hybrid NLMs reaching higher rejection rates for organic dyes: they have shown the rejection of humic acid and bovine serum albumin. However, MXene-GO hybrids exhibit lower water permeance than pure MXene NLMs in general. This could be possible because of the difference in lateral size between MXene and GO nanosheets used in these studied, therefore there is a need to pursue more systematic investigations.

In another interesting work, Xu et al. [92] have prepared MXene-incorporated mesoporous $TiO_2$ membranes for testing dextran rejection, see figure 18h. Notice that they used only 1.0 wt% MXene nanosheets. Xu and others coated disc-shaped and hollow fiber $\alpha$-$Al_2O_3$ supports with MXene dispersion by spin coating and dip coating respectively. After drying they calcined the hybrid membranes composed of $TiO_2$ hydrosols and MXenes at 400°C and developed a durable membrane, which reached superior dextran rejections. The researcher attributed the enhanced performance of $TiO_2$-MXene membranes to the prevention of structural defects by MXenes (figure 18h): MXenes limited the infiltration of hydrosol particles through the support during membrane fabrication and sealed large defects, thus providing better dextran rejection without sacrificing the water flux dramatically [92]. In a parallel work, Sun et al. [117] varied different parameters, such as the dip-coating duration, the loading ratio of MXenes, the duration and temperature of the calcination process. They observed only <20% and <40% decline in water flux, for 1 and 5 wt% MXene incorporations, respectively. Interesting, they could manipulate the molecular cut-off and pore size of $TiO_2$-MXene membranes by playing with the rest of the parameters effectively [117]. However, talking about the practicality of water treatment membranes, the resistance of membranes to fouling is equally critical. Thinking that a fast-fouling membrane has a limited chance for practical applications, if there are any. Also in this case, MXenes appear promising as a new material platform [182].

In 2017, Rasool et al. [85] demonstrated the antibacterial properties of MXene NLMs, inhibiting the growth of both Gram-positive and Gram-negative bacteria, as shown in figure 19a. They also observed that their MXene membrane exhibit antibacterial activity when oxidized in open air naturally (figure 19b). Later, Pandey et al. [86] developed a composite NLM composed of silver nanoparticles (AgNPs) and MXenes, that shown high-performance antibacterial activity by adding 21% AgNPs to the MXene membrane (figure 19c). This effect is presumably due to the synergistic antibacterial activity of AgNPs and MXenes [86]. In figure 19d, hybrid AgNP-MXene membranes (Ag@MXene) demonstrated virtually complete inhibition of *Escherichia coli* (*E. coli*) cells. Moreover, the bacterial cells grown on Ag@MXene membranes lost their envelope integrity as it shown comparing figure 19e and 19f. In addition, the inclusion of AgNPs also improved the water permeance (figure 19g), while no significant drop happened in the rejection of Rhodamine B, methyl green, and BSA (figure 19f) [118].

Another important aspect for separation membranes, parallel to biofouling, it comes from suffering the fouling of oily substances, particularly for wastewater treatment processes. Thus, oil-water separation is an important subject on its own: Saththasivam et al. [119] and Li et al. [120], in 2019, had developed oil-water separating nanolaminates by depositing MXenes on print paper and polyethersulfone (PESf) substrates, respectively. In both studies were shown promising results with low fouling and high resistance to oils, including oily solvents [119,120]. Further discussion on the solvent resistance of MXene-based membranes are provided forward in section 2.5.3 of this thesis.

### 2.5.2.2 – Water Desalination

Nanoenabled ion sieving membranes have gained increasing attention in the last couple of years, thanks to an urgent needing to increase the efficiency of desalination processes. The mechanism behind ion sieving membranes is mainly size exclusion and Donnan principles [182]. The most efficient way to achieve this, for MXene-based NLMs, is to engineer the interlayer spacing, allowing water molecules to pass through while excluding hydrated ions. With this attempt, several studies have evaluated the ion and water transport through MXene-based membranes.

Early in 2015, Ren et al. [60] compared the water and positively-charged ions transport behavior of $Ti_3C_2T_x$ MXene and GO based NLMs. The researcher observed that $1.5\mu m$ thick MXene nanolaminate (shown in figure 20a,b) provided around 6 times higher water permeability than GO membrane of same thicknesses, precisely 37.4 vs 6.5 L $m^{-2}$ $h^{-1}$ $bar^{-1}$ respectively. The MXene nanolaminates allowed the transport of about 3 layers of water molecules, thanks to its average nanochannel size of 0.64nm. This thick MXene membrane can reject any ions with hydration radius larger than 0.64nm, but ions with hydration radius smaller than this value permeate through.

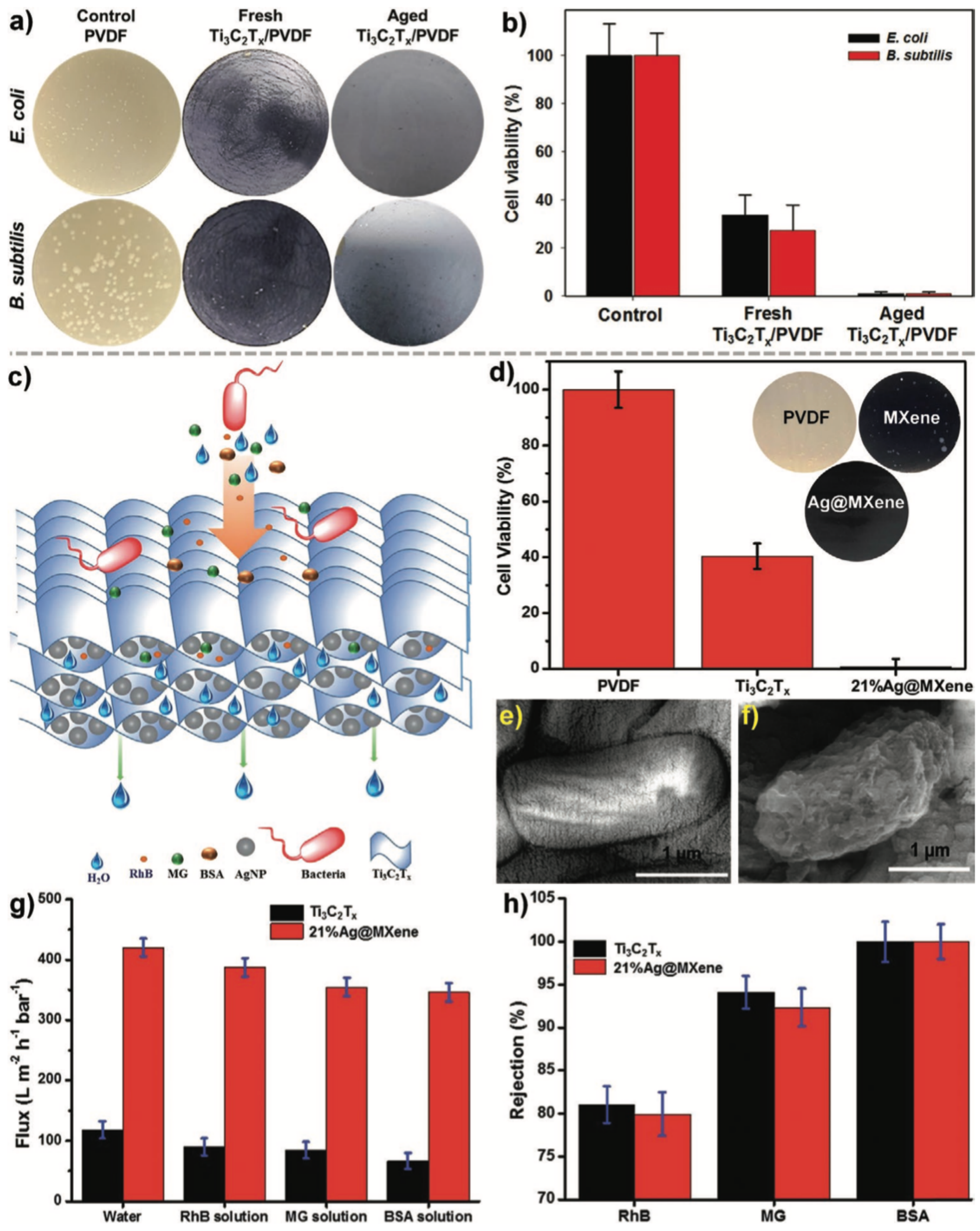

*Figure 19:MXene-based antibacterial membranes for water purification. a) Colonies and b) viable counts comparison of Gram-negative and -positive bacteria on a PVDF support and MXene membranes [85]. c) Illustration of the hybrid AgNP-MXene membrane. d) Survival of bacterial cells exposed to PVDF, MXene and Ag@MXene membranes. Bacterial cell before e) and after f) Ag@MXene exposure. g) Water flux, and h) solute rejection of MXene and Ag@MXene membranes [86].*

Also, the charge of ions plays a crucial role in MXene-based membranes: due to the strong negative charge of MXenes, multivalent cations such as $Mg^{2+}$, $Al^{3+}$ and $Ca^{2+}$, have shown slower permeation rates than monovalent ones (ie. $Na^+$, $K^+$ and $Li^+$) given that their high charges have the capacity to narrow nanochannels in the MXene nanolaminates via electrostatic attraction (figure 20c). Contrary, small-sized monovalent cations such as $Na^+$ can expand nanochannels forming an electric double-layer (see figure 20d). The resulted provided by Han et al. [121] supported these conclusions. In their experiment, a MXene NLMs supported with PESf ultrafiltration membranes was used, they observed a 23% rejection for $Mg^{2+}$ ($MgCl_2$) while $Na^+$ rejection remained at 13.8% (NaCl) despite a slightly higher flux was achieved for $MgCl_2$ solution than for NaCl solution, 460 and 435 L $m^{-2}$ $h^{-1}$ $bar^{-1}$ respectively [121]. In their overall work, Kang et al. [94] also studied the transport of salt ions across the MXene-GO composite membrane (figure 20e), and recorded a small ion rejection below 11% for both NaCl and $MgCl_2$ under pressure-driven conditions. As well as in a pure GO or MXene nanolaminates, the nanochannels of hydrated MXene-GO hybrid membranes were too large to exclude small ions with hydrated diameters less than 0.5nm [122]. To overcome this issue, Sun et al. [123], in 2019, explored the utility of sintering temperature (60, 200, 300, 400, 450, 500 °C) on engineering interlayer spacing of MXene ($Ti_3C_2T_x$) layers coated on tubular $\alpha$-$Al_2O_3$ substrates. They showed interesting results, MXene membranes dried at 60°C had an interlayer spacing of 3.71 Å, which dropped to 2.68 Å at 400°C sintering. Partial oxidation of the MXene layer occurred when the sintering temperature was 450°C and above (in air), manifested by the color change of the membrane, from dark green/gray to reflective white. Notably, the sintering of MXenes membranes at 400°C gave the best rejection rates for all salts tested ($Na_2SO_4$, $MgSO_4$, NaCl and $MgCl_2$) [123]. What merge from all these studies is that the interlayers spacing of MXene nanolaminates is the key parameter for desalination applications. Thus, it is clear the importance of preventing swelling of MXene during operation. To overcome this issue Lu et al. [124], in 2019, proposed a strategy to develop antiswelling MXene membranes by temperature-induced self-crosslinking of hydroxylated $Ti_3C_2T_x$ via $H_2O$ condensation. As results, the salt rejection performances of the membranes improved as the degree of crosslinking increase but at the expense of decrease in permeability [124]. Reducing further the thickness of such membranes might be promising for a wide range of applications.

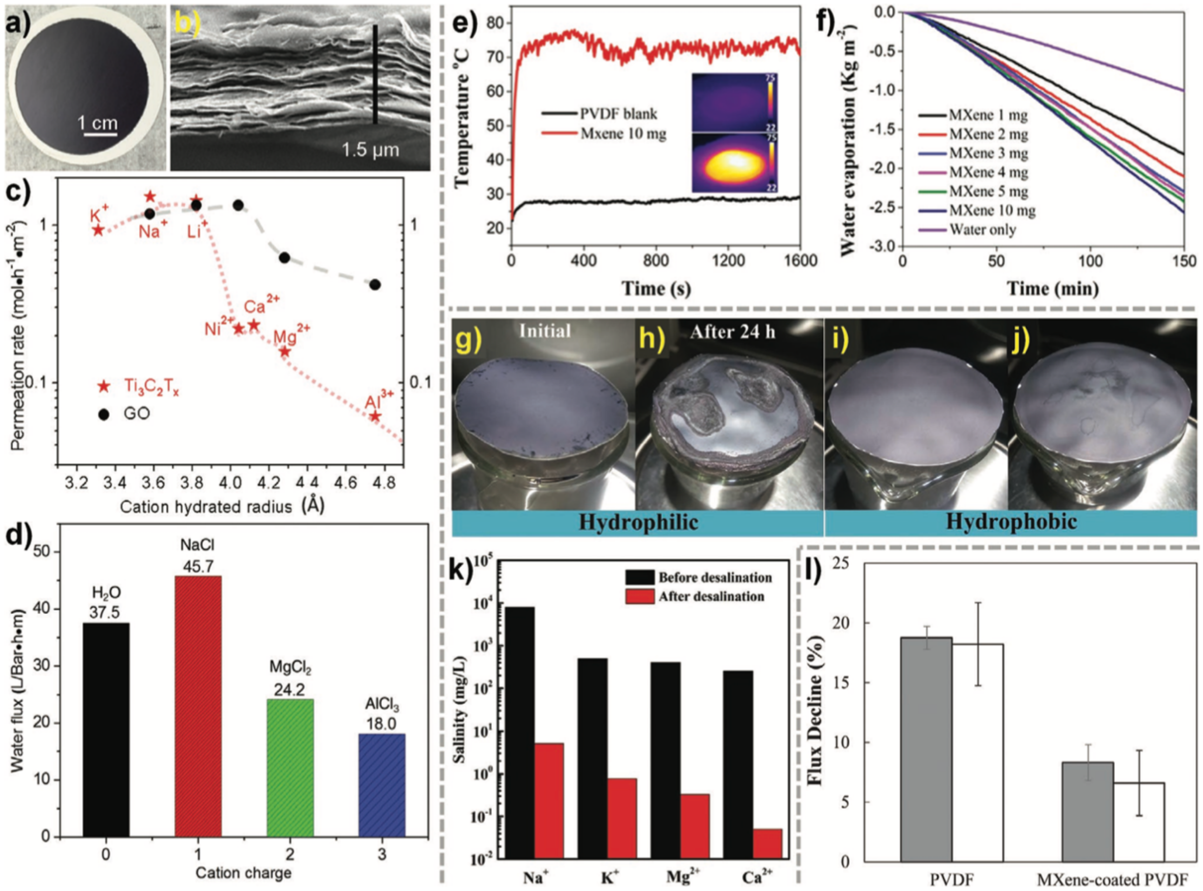

*Figure 20: MXene-based membranes developed for desalination application. a) Top-wide and b) magnified cross-sectional views of a nanolaminate MXene ($Ti_3C_2T_x$) membrane for ion sieving. c) Permeation rates of different cations through MXene and GO NLM membranes. d) Water flux of $Ti_3C_2T_x$ membrane for deionized water and salt solutions with cations of different valencies [60]. e) Time-dependent heating profiles of PDMS-modified PVDF-supported MXene NLMs under one sun illumination in the open-air atmosphere (inset: membranes under infrared camera). f) Water evaporation rates of MXene-PVDF membranes with different $Ti_3C_2T_x$ loadings under one sun illumination [125]. MXene-based hydrophilic (g,h) and hydrophobic (i,j) membranes, before (g,i) and after (h,j) 24h solar desalination. k) Photothermal desalination performance of MXene-based hydrophobic nanolaminate for different cations [126]. l) Flux decline of PVDF and PVDF-supported MXene nanolaminate membranes after 21h photothermal membrane distillation with a feed composition of 10 g L$^{-1}$ NaCl and 200 BSA as foulant [127].*

In general, 2D materials, including MXenes, offer a new eligible ways of supplying freshwater out of seawater thanks to their photothermal properties. The conversion of the sunlight (solar) energy into heat is useful for evaporating water, giving rise to solar distillation.

Combine the idea of solar distillation with membrane technologies to yield photothermal desalination/distillation. For this purpose, Wang et al. [125] had made the first demonstration of MXenes $Ti_3C_2$ utility in photothermal desalination with an extraordinary high light-to-heat conversion efficiency. Wang and coworkers deposited MXenes on poly(vinylidene difluoride) (PVDF) supports and surface modifying with PDMS, achieving a membrane that could self-float on the water surface. They could achieve ≈84% conversion efficiency, between 60 to 150 min, using this membrane platform, under one sun irradiation with a pretty fast heating rate (figure 20e,f)[125]. In a successive study, Que et al. [126] prepared a similar self-floating membrane by modifying the MXene layer deposited on PVDF with a fluorinated silane coupling agent, trimethoxy(1H,1H,2H,2H-per-fluorodecyl)silane. Thanks to the antiwetting behavior of the surface modifying agent, the resulting membrane could handle real seawater with organics and heavy metal, without the accumulation of salt crystals on top of the membrane, see figure 20g-j. Accordingly, they could achieve an energy conversion efficiency (solar to steam) of 71% with a high level of stability (>200h operation). Moreover, the hydrophobic MXene membrane showed a remarkable desalination performance for different cations, as shown in figure 20k [126]. Proceeding further, Tan et al. [127] have tested the feasibility of direct contact membrane distillation with MXene-incorporated membranes. Taking up the material designs for self-floating membranes, Tan and coworker coated the MXene-deposited PVDF supports with PDMS, using these hydrophobic membranes, they reached a photothermal conversion of 5.8 $kW/m^2$ in a solar-assisted membrane distillation. They also reported the antifouling properties of their membranes with feeds containing 200 ppm of bovine serum albumin and 10 g/L of NaCl, results reported in figure 20l [127]. Moving forward, Zha et al. [128] reported on antibiofouling filters for photothermal distillation prepared by dip coating highly porous cellulose supports with pore size of 30-50$\mu$m with $Ti_3C_2T_x$. Comparing the $Ti_3C_2T_x$-based filters with GO-coated filters, the former showed superior performance for steam generation and bacterial disinfection [128].

## 2.5.3 – Organic Solvent Purification

Due to their high solvent resistance, MXenes are promising for the purification of organics solvents [75,79]. MXenes are useful for obtaining highly robust membranes thanks to their elastic modulus at around 260-240 GPa, which is comparable to that of GO ($\approx$110-420 GPa) [129]. Moreover, functionalizing the surfaces is possible to limit the solvent uptake and swelling of MXene-filled membranes for different solvents. For example, $Ti_3C_2T_x$-$NH_2$ and $Ti_3C_2T_x$-COOR derivatives (of PEI- and PDMS-based membranes) have inhibited solvent uptake and swelling more efficiently against nonpolar solvents (e.g. toluene or n-heptane), while alklyl-modified derivatives ($Ti_3C_2T_x$-$C_6H_6$ and $Ti_3C_2T_x$-$C_{12}H_{26}$) performed better with polar solvents (eg. Isopropanol or athyl acetate) [79]. Thus, MXenes attracted growing attention for organic solvent nanofiltration (OSN) as well as pervaporation of solvent mixtures, both of which demand highly stable membranes under long-term exposure to organics solvents.

#### 2.5.3.1 – Organic Solvent Nanofiltration (OSN)

In later 2016, Wu et al. [75] studied the rejection to oligomeric (200-1000 Da) poly(ethylene glycol) (PEG) molecules in isopropanol, preparing a PAN-supported TFN membranes by incorporating different amounts of hydroxyl-rich $Ti_3C_2T_x$ into PEI or PDMS matrix (figure 21a). Indifferently of the loading ratio of MXenes and type of polymer matrix, all membranes provided a superior rejection to the oligomeric molecules, as shown in figure 21b,c. Interestingly, PAN/PEI- $Ti_3C_2T_x$-4 (with 4 wt% MXene loading) showed ≈99.4% rejection to PEG-800 at 10 bar [75].

In order to explore the role of chemical functionalization of MXenes on PEG rejection, Hao et al. [79] proceeded in similar way, fixing the ratio of MXene loading at 3 wt%, they found that different functionalities are useful for different solvents. As previously mentioned, the swelling or uptake behavior of resulting membranes is crucial for this outcome.

Trying a different approach, Han et al. [133] prepared MMMs by incorporating $Ti_3C_2T_x$ into a polyimide (P84) matrix via phase inversion (PI) followed by crosslinking with triethylenetetramine (TETA). By optimizing the filling ratio, Han and coworkers achieved a virtually complete rejection of gentian violet (named also crystal violet, 408 g/mol) at a high flux of 268 L/(m$^2$h) under 0.1 MPa and ambient temperature. This membrane also exhibit an excellent solvent resistance to DMF, acetone and methanol after crosslinking [133].

MXene-based NLMs are useful not only for dye removal from aqueous samples, as outlined before, but are also useful for rejecting dyes from organic solvents. Wang et al. [109] developed a nylon-supported MXene-only nanolaminate that achieved a rejection rate of over 96% for the organic dye molecules larger than >2.0 nm from isopropanol, as shown in figure 21d. Recently, Wei et al. [130] reported a nylon-supported GO/MXene hybrid NLM that can also reach over 90% dye rejection rates (figure 21e). Their hybrid membranes showed a high stability for long-term operations, demonstrated while testing the membranes with different organic solvents such as acetone, methanol, ethanol and isopropanol [130].

The flux of MXene-based OSN membrane is also interesting, considering that it depends on the type of solvents used.

It is known that the flux of the incompressible and Newtonian fluids passing through channels made up of 2D materials can be described well by Hagen-Poiseuille law (Equation 1). The utility of Hagen-Poiseuille law for MXene-based membranes have been shown by Wang et al. [109] and Wu et al. [18] for NLMs, and by Wei et al. [130] for TFNs.

Accordingly, the permeance values obtained in both cases were inversely proportional to the viscosity of the organic solvents tested. One step forward, Wang et al. also showed that the permeance through nanolaminates exhibit a further inversely proportionate relationship to both molecular diameter and solubility of the organic solvents [109]. So far, this suggest that the geometry as well as physicochemical nature of the nanochannels formed in MXene-based NLMs directly influence the permeation behavior of solvents during OSN process.

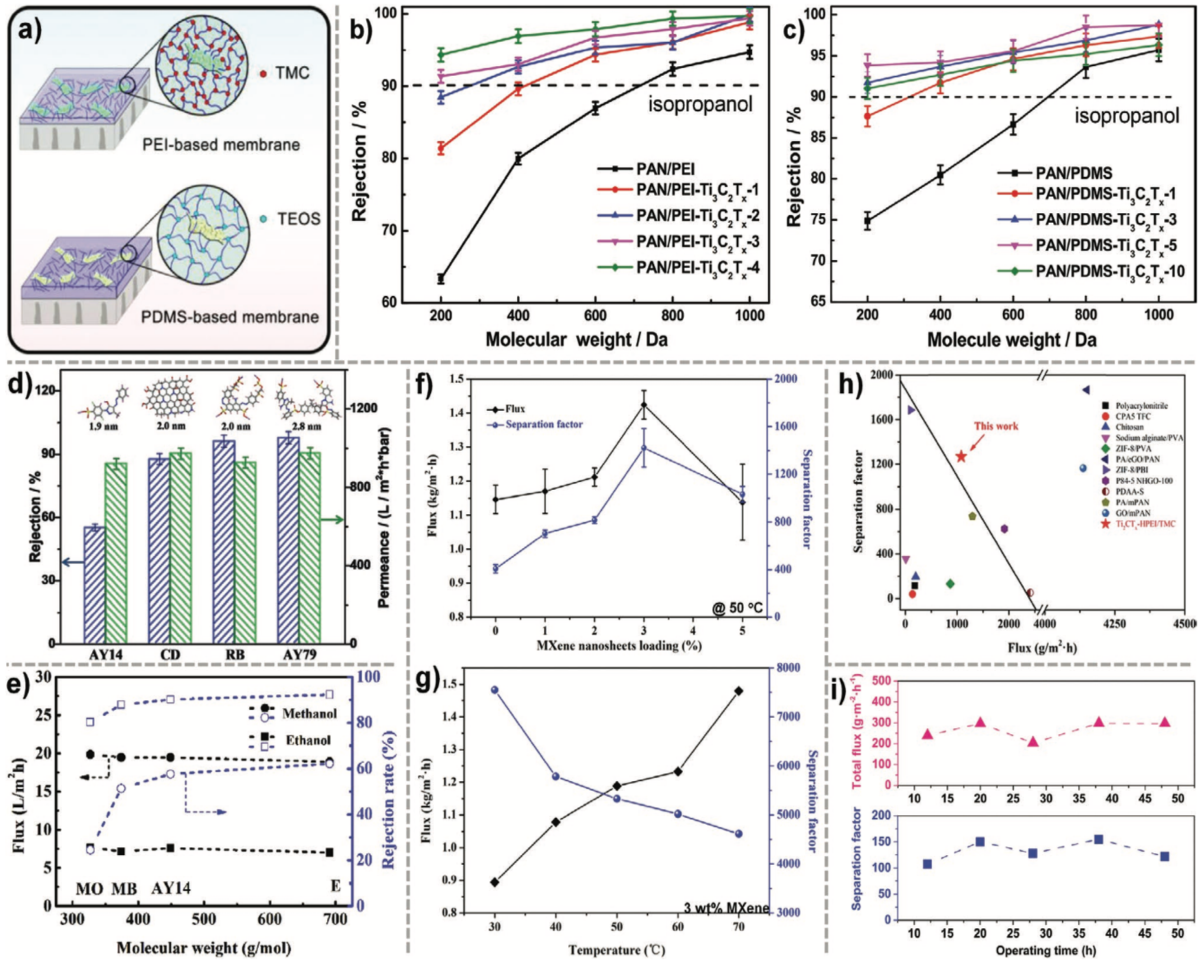

*Figure 21: MXene-based membranes developed for solvent purification applications. a) Schematic of the preparation of MXene-filled TFN membranes prepared by using PAN as support and PEI or PDMS as the selective layer matrix [79]. b,c) PEG rejection performances of PAN/PEI-MXene (b) and PAN/PDMS-MXene (c) membranes from isopropyl alcohol [75]. d) Removal of different dyes from isopropanol using nylon-supported MXene nanolaminates [109]. e) Removal of various dyes from methanol and ethanol using GO/MXene nanolaminates (with 70 wt% MXene) [130]. f,g) Dehydration of ethanol (10 wt% water) (f) and ethyl acetate (2 wt% water) (g) using chitosan-MXene MMMs [96]. h) Performance comparison of PAN/PEI-MXene TFN membrane for the dehydration of isopropanol (90 wt% water) [131]. i) Long-term dehydration of ethanol (95 wt%) using MXene nanolaminates at room temperature [132].*

### 2.5.3.2 – Solvent Dehydration by Pervaporation

In addition to OSN, MXene-based membranes have been effectively employed for the pervaporation-based dehydration of various solvents by different research [96, 131,132]. Analogous to OSN membranes, organic solvent pervaporation membranes have to be stable under long-term exposure to organic solvents. Thus, Xu et al. [96] have prepared a stable MMM composed of chitosan and 1-5 wt% $Ti_3C_2T_x$. For ethanol dehydration, chitosan-MXene MMM with 3 wt% loading remarkably exhibited high improvement in both flux and separation factor by almost 25% and 250% respectively, as shown in figure 6f. Xu and coworkers also tested the role of operation temperature for dehydration of ethyl acetate, as it known, higher temperatures increase the swelling and hence the free volume of such membranes, causing high flux at the expense of lowered selectivity, and they found 50°C as an optimum value (figure 21g)[96].

Recently, in 2019, Liu et al. [131] developed a PAN-supported TFN membrane by incorporating MXenes into hyperbranched PEI based on a membrane design approach similar to two earlier studies [75,79]. In the next section we further investigate these studies. Liu et al., with their highly uniform PAN/PEI-$Ti_2CT_x$ membranes, could reduce the water content in the isopropanol/water mixture from 10 to <1 wt% with a flux, at 50°C, that overcome values available in literature for various tipes of membranes, as it shown in figure 21h. Interestingly, they found that $Ti_3C_2T_x$ exhibit poorer results in terms of selectivity, which might be due to their lower hydrophilicity or higher layer thickness [131].

In another recent work, Wu et al. [132] tested the utility of nylon-supported $Ti_3C_2T_x$ membranes for the dehydration of alcohols. They used 2$\mu$m thick MXene membranes and reported not very high fluxes or separation factors, as clearly show in figure 21i. Anyway, their membrane exhibit quite an appealing performance at room temperature compared to 50°C, with more than 30% higher separation factor at only nearly 10% lower flux. Furthermore, Wu et al. observe small fluctuations of both flux and selectivity for long-term operation, meaning high stability and low deterioration of the membrane (figure 21i) [132].

## 2.6 – FUTURE DIRECTIONS

The studies on MXene-based membranes are growing rapidly particularly in 2019 and 2020. Besides that, most of these works are focused on applications that can also be met by graphene materials or other 2D materials. Moreover, the majority of published studies are on NLMs prepared by vacuum-filtration of MXene only. Thus, it would be more effective to conduct research in the following directions:

1- Focusing on applications that MXenes can offer more than other 2D materials;
2- Exploring MXene-polymer composites deeply by visiting more established and scalable methodologies used in designing polymer-based membranes.

Last but not least, simulation and modeling techniques might help identify areas and membrane designs in which MXenes might show superior performance [182].

## 2.6.1 – Rising Membrane Operations

### 2.6.1.1 – Electroresponsive Membranes

Preceding studies on various material systems have shown that electroresponsive membranes are promising for water treatment applications [134-136]. MXenes are promising for designing electroresponsive membranes, thanks to the outstanding electrical, electrochemical and mechanical characteristics. In 2018, Ren et al. [84] in a pioneering study, have reported the utility of MXenes for fabricating electroresponsive membranes. Ren and coworker, first deposited MXene-based NLMs ($Ti_3C_2T_x$) on PVDF supports with vacuum-assisted filtration. Then, they tuned the interlayer spacing as well as surface charge of the MXene nanolaminates by modulating the external voltage applied, for improved rejection towards metal ions and a charged organic dye (figure 22a). Ren et al. showed that under an osmotically driven condition, ie. concentration gradient, a negative potential of -0.6 V restrains the permeation of both monovalent ($Na^+$, NaCl) and divalent ($Mg^{2+}$, $MgCl_2$) cations through the MXene membranes. Moreover, a positive potential of +0.4 V increases the permeation rates of ions. Furthermore, under vacuum, they could improve the rejection of a positively charged dye, methylene blue, by applying a negative potential to MXene membrane, as shown in figure 22b. In addition, Ren and coworkers have also demonstrated that larger MXenes flakes, prepared via less intense exfoliation method, provide better electrical conductivity and mechanical stability, leading an improved performance for solute rejection [84].

As further studies, it would be interesting to address the deterioration of the electroresponsive performance of such MXene-based NLMs upon repeated cycles of use. Thus, in necessary to understand deeply the key role of electrochemical reactions taking place during such operations. In fact, there is a growing interest to better control the electrochemical behavior of MXene to exploit the as electrocatalyst for a wide range of applications [33,137,138]. Providing a better understanding of the interactions between ions and MXenes on top of this will broaden the horizons of MXene-based membranes for application areas beyond separations [182]. Among those application areas, interesting ones can be membrane capacitive deionization [139], light-controlled nanofluidics [140], osmotic energy harvesting [141], membrane fuel cells [142-145] and lithium-sulfur batteries [146-148] just to name a few. Consequentially, the progress to be made in these areas might help accelerate the development of MXene-based membranes for separation application. Therefore, a suggestion to researcher in these fields is to consider these applications enabled by MXenes and other 2D materials, with a more holistic approach through the lens of nanoionics [149].

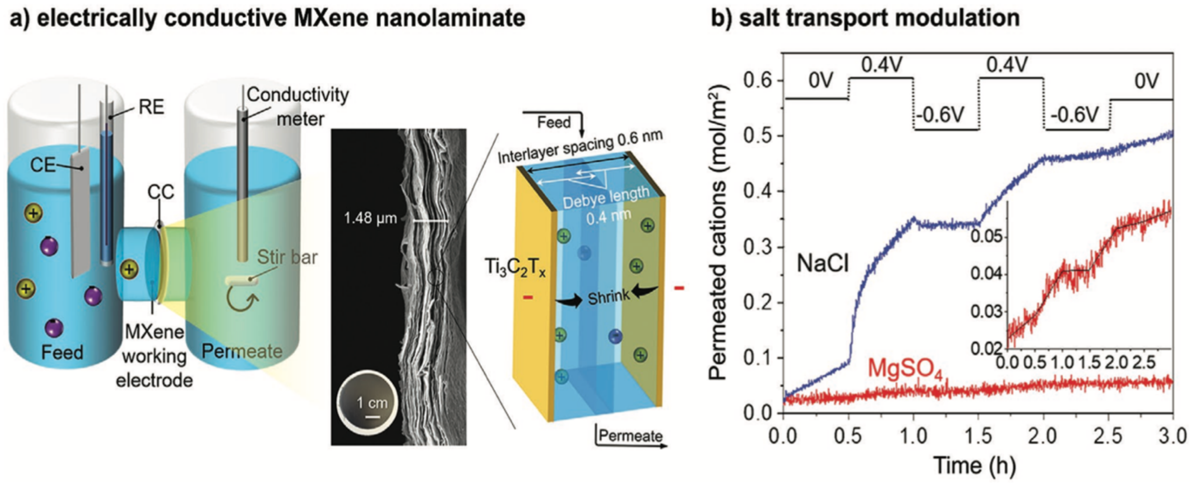

*Figure 22: a) Schematic illustration showing a U-shaped device, where a PVDF-supported MXene membrane was placed in the center as a working electrode with an annular Ti foil as a current collector (CC); CE and RE stand for counter electrode and reference electrode, respectively. b) Salt transport through the MXene membrane can be modulated as exemplified by the ability to control the permeation of cations by tuning the applied voltage [84].*

### 2.6.1.2 – Reactive Membranes

Nanomaterial-enabled reactive membranes provide promising prospect of wastewater treatment based on the in-situ removal of organic or ionic contaminants, via reductive and/or oxidative reactions [150-152]. Contrary to the inert ones, the reactive membranes might help avoid the need for additional steps of separation processes or the consumption of expensive chemicals. A key feature is that the catalytic performance of the nanomaterials should be high and durable. Pandey et al. [153] have demonstrated, in 2018, high performance reactive membranes capable of converting carcinogenic bromate ($BrO_3^-$) ions into less toxic bromide ($Br^-$) ions, without the use of an additional catalyst or energy input. They have achieved an incredible reduction capacity of 321.8 mg $BrO_3^-$ per gram of $Ti_3C_2T_x$ with a virtually complete reduction at pH 7. They observed that in presence of co-ions such as $SO_4^{2-}$, $NO_3^-$, and $PO_4^{3-}$, the conversion rate showed a minor drop to 92% only. On the other hand, one drawback of this system was the partial oxidation of MXenes, which limits its reusability as a reactive membrane. Thus, it is essential to enhance the stability of MXenes for long-term performance [153]. As another future direction, can be wise to target applications beyond the detoxification of bromate. In a previously important study, Ying et al. [154] showed that $Ti_3C_2T_x$ nanosheets exhibit a unique reductive removal performance for the conversion of toxic chromium(IV) ions ($Cr^{4+}$) into less toxic chromium(III) ($Cr^{3+}$) ions. Afterwards, the $Cr^{3+}$ ions, at pH 5, were easily removed without any further treatment to reach the drinking water standard [154]. More recently, in 2019, Xie et al. [72] have demonstrated the feasibility of such an approach by removing chromate ($HCrO^{4-}$, the dominant form od chromium(IV) at neutral pH) using hybrid NLM composed of GO and $Ti_3C_2T_x$ nanosheets. In another study, Liu et al. [155] have used a MXene-based catalyst, containing 20% cobalt oxide, $Co_3O_4$) that demonstrated a surprising performance for the degradation of bisphenol A, an endocrine-disruptive compound. These results, open a field of research in which MXene-based membranes are worth investigating for the detoxification of a wide range of contaminants. In fact, as demonstrated for energy applications, MXenes and their hybrids are effective and versatile electrocatalyst, often with extraordinary performance [156,157]. In this prospect, it should be interesting to investigate the potential of MXenes for building electroreactive membranes, as well.

## 2.6.2 – Unexplored Membrane Formats

Neither PI (phase inversion), nor IP (interfacial polymerization) has yet to be widely for developing MXene-based membranes so far. To encourage the exploration of PI and IP for MXene-based membrane research we can start from the knowledge learnt from graphene-based membranes, providing also a brief perspective on the potential utility of layer-by-layer (LbL) assembly for producing MXene-based membranes.

### 2.6.2.1 – Phase Inversion

As already mentioned in section 2.3, polymer-MXene composites prepared either as MMMs or TFNs are more promising for realistic applications. For both preparation PI is a crucial method. Nevertheless, there are only very few studies on this topic, recently in 2019, Han et al. [133] reported the utility of PI for preparation of MXene-polymer composite membranes (PA-based MMM). In their application-driven study, Han and coworkers, briefly discussed the advantages of using PI. Thus, there is more room for advanced research on this topic, as well as the impact of MXenes on PI process itself. During phase inversion, the MXenes (as other nanofillers) inevitably influence the phase separation behavior and hence packing of polymer chains. It had been previously shown that hydrophilic additives could facilitate the demixing process, where a solvent and coagulant counter-diffuse in the polymer-solvent-coagulant tertiary systems [158,159]. During the PI of graphene-polymer systems, the polymer chains solidify fast with limited rearrangement capacity, resulting in membranes having a high surface pore density and size as well as overall porosity [158, 160]. So far, given their high hydrophilicity and topogical similarity to graphene, MXenes should expect to exhibit high capacity to develop highly permeable membranes with a wide range of polymers. Interestingly, should keep in mind that, upon phase separation, MXenes will naturally be exposed to the membrane surface, which might be an interesting way to develop antibiofouling membranes, as already mentioned the antibiofouling properties of MXenes in section 2.5.2.1. On the other hand, the concentration of MXenes should be precisely tuned in such systems, since the phase separation process is dictated by not only the thermodynamic but also rheological factors [161]. Should be noticed that excessive use of MXenes, like other nanofillers, could also delay demixing, resulting in the densification of membrane structures due to increase in viscosity of the polymer dope solutions. Hence, it is important to balance these parameters to make full use of MXenes in the design of PI-based MMMs [182].

#### 2.6.2.2 – Interfacial Polymerization

IP refers to the reaction of two very reactive monomers, usually acid chloride and an amine, at the interface of two immiscible solvents to form a dense polymeric layer, usually polyamide-based [105]. PA-based TFC membranes prepared via IP are of particular interest for a wide range of industrial separation processes. The goal is to fabricate IP-based PA membranes with reduced surface roughness, increased hydrophilicity, antifouling properties and enhanced chorine resistance. In graphene counterparts, the incorporation of GO into PA membranes during IP has shown good results in all these four interrelated aspects [162]. GO nanosheets are providing smoother PA layers likely by retarding the diffusion of aqueous monomers into the organic phase, thus MXenes can exhibit a similar effect with their 2D morphology [163,163]. However, MXenes should also be useful in preventing chloride ions from replacing amidic hydrogen and interrupt chlorination, thanks to the capacity of MXenes to form strong hydrogen bonds [95]. Moreover, as previously discussed in section 2.2, MXenes are also antibacterial and hydrophilic like GO, which is useful for biofouling control. Hence, MXenes can offer a good potential for designing IP-based membranes: by crosslinking MXene-incorporated PEI (hyperbranched PEI) with TMC (in n-hexane), Liu et al. [133], in 2019, and previously other research group [75,79], had created PA-based selective layers on various support membranes. From a chemical point of view, this is a straightforward method of IP for fabricating TFN membranes. On the other hand, the designing of IP-based TFN membranes, starting by monomers, needs more precisely optimization of several parameters, like the choice of monomers and their concentrations, filler loading ratio and crosslinking reaction time [182].

### 2.6.2.3 – Layer-by-Layer Assembly

Even if is less emphasized than PI and IP, layer by layer assembly appears to be a refined way of designing membranes. In the last years, various compositions of LbL-assembled films demonstrated promising performance as separation membranes, as well as barrier [164]. LbL-based separation membranes usually consist of polymeric building blocks, but also the nanosheet-based or nanosheets incorporated LbL membrane designs, which combine the advantages of LbL material design and 2D materials, are also trending, especially for graphene-based LbL membranes [165,166]. Also MXene-incorporated LbL films have been prepared so far, for applications such as electromagnetic interference shielding and supercapacitive energy storage [167,168]. Hence, MXene-based LbL membranes for separation/purification applications could be developed in future. Besides, it should keep in mind that the LbL technique can be performed in different fashions like dipping, spinning, spraying or a combination of those, and the properties of the resulting films usually differ drastically. Straightforward, by playing with the deposition conditions, the properties of such films can be precisely tuned at a molecular level. Thanks to these features, LbL method can be promising for designing advanced separation membranes using MXenes [182].

### 2.6.3 – Simulation and Modelling Approaches

Since flat materials toolbox is expanding very rapidly, experimentalist have difficulties in matching the right material for the right applications, which also applied to MXenes. So far, computer-aided materials design holds a huge promise for boosting the research outcome. For both MXenes and their parents materials, MAX phases, computational/theoretical investigations reveal fine details of structure-property relationship that are often inaccessible or hard to study experimentally. At this point, the majority of the computational studies are based on *ab initio* calculations using density functional theory (DFT) [21,169,170,171].

In the fundamental domain, those calculations covered mechanical, structural, magnetic, electrical and electrochemical properties, as well as the nature of chemical bonding and relative stability of MXenes, as already mentioned in part 1 of this thesis [21,169,170]. However, on the applications side, the main focus was on energy storage [169,171]. Even though, as already discussed in section 2.2, the electrical and electrochemical behavior of certain MXenes, ie. $Ti_3C_2T_x$, is also very interesting for membrane applications. In this regard is useful to summarize some key points of those investigations first, followed by a couple of pioneering modeling/simulation studies directly focused on MXene-based separation membranes. Tang et al. [169] investigated the electronic properties of MXene $Ti_3C_2$ monolayers with pristine, hydroxylated and fluorinated surfaces, they revealed clear changes in narrow band-gap semiconducting or metallic characteristics. Earlier, Kurtoglu et al. [21] have exposed the high metallicity and stiffness of a wide range of MXenes, like $Ta_2C$, $Ta_3C_2$, $Ta_4C_3$, $Cr_2C$, $Zr_2C$, $V_2C$, $Ti_2C$, $Ti_3C_2$ and $Ti_4C_3$. Inside this context, Anasori et al. [170] have investigated MXenes containing two different transition metal (ie. Ta, Cr, Ti, Nb, Mo or V). These double-transition-metal MXenes were present in the form of $M_2'M''C_2$ and $M_2'M_2''C_3$ (as shown in figure 8a), where M' and M'' are the outer and inner layer metals, respectively. This study has revealed the uniquely different electrochemical behavior of $Mo_2TiC_2$ compared to $Ti_3C_2T_x$. Going forward, Anasori and coworkers, have supported their evaluations with experimental results, as well. More recently, Berdiyorov et al. [171] have employed DFT simulations for exploring the water desalination potential of MXenes.

In this study, Berdiyorov et al. studied ionic transport through $Ti_3C_2(OH)_2$ to understand mechanism behind charge-selectivity. They also showed that depending on the charge of intercalating ions, the spacing between the MXene layers expand or contracts dynamically, which also alters the ionic transport behavior. As consequence, for improving membrane design, the author suggested the possibility that the performance of MXene-based ion sieving membranes could be improved by manipulating the surface terminations, which in turn, alter the surface charges [171].

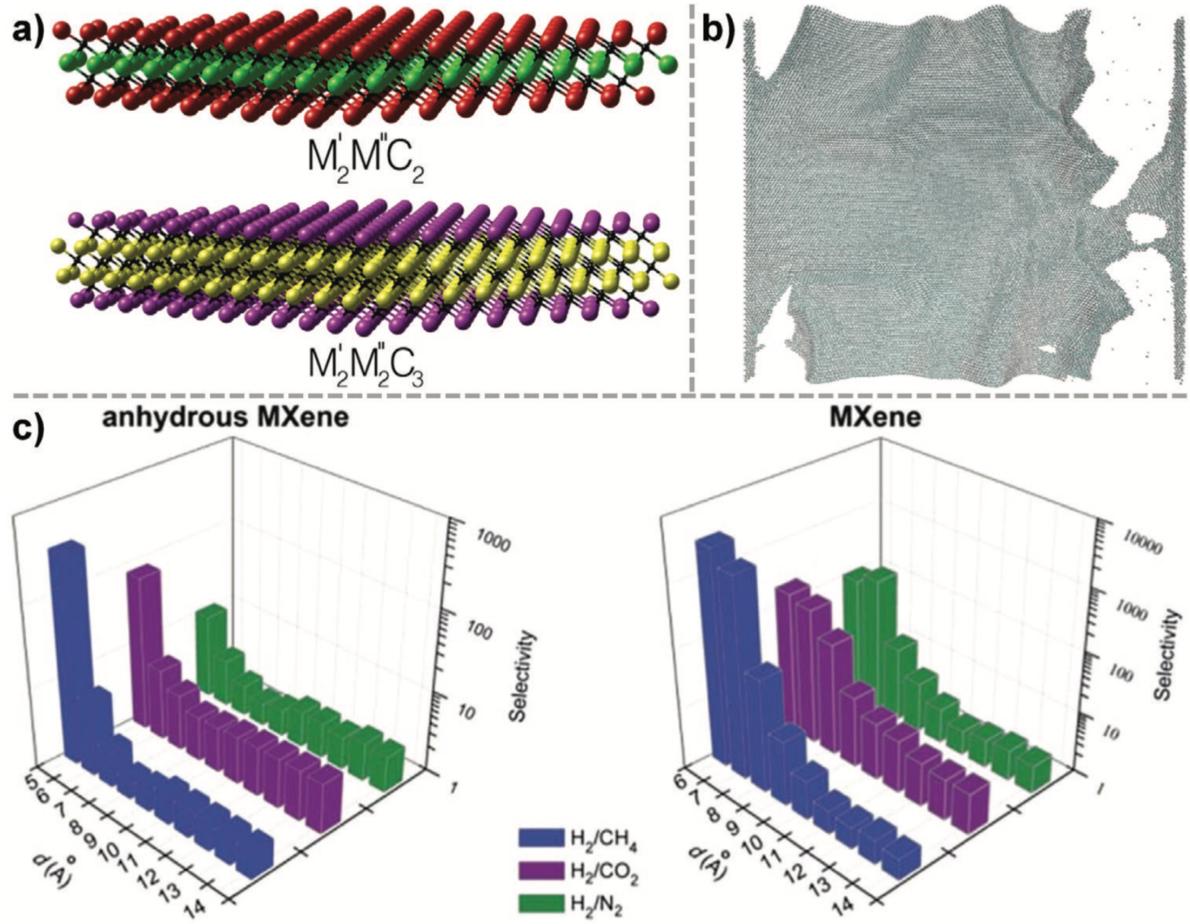

*Figure 23: Simulation-aided materials design in MXenes. a) Double-transition-metal $M_2'M''C_2$ and $M_2'M_2''C_3$ MXenes [170]. b) Atomistic configuration of the $Ti_2C$ MXene under strain [172]. c) Diffusion selectivity of $H_2$ with respect to $CH_4$ (blue), $CO_2$ (purple) and $N_2$ (green) for anhydrous MXene and hydrous MXene membranes [173].*

The classical molecular simulation strategies like molecular dynamics (MD) remained relatively less explored for MXenes. In 2015, Borysiuk et al. [172] studied the mechanical properties of $Ti_{n+1}C_n$ under tensile loading using large-scale classical molecular dynamics simulations (figure 23b). The calculated strain-stress curves showed a linear trend at a small strain ($\leq 1\%$) and the resulting Young's moduli were close to the data obtained by DFT simulations in previous study [21]. More recently, Li et al. [173] reported on the selective diffusion of small gas molecules (He, $H_2$, $CO_2$, $N_2$ and $CH_4$) passing through two adjacent MXenes, the results showed that the intercalated water molecules may increase the selectivity toward $H_2$ considerably, as clearly shown in figure 23c. On the other hand, when water intercalation exceeded a certain concentration, the diffusion of large gas molecules dropped dramatically [173]. It should be possible in the future to understand deeply the transport mechanism of MXene-based membranes thanks to simulation/computational study.

To this aim, in 2020, Shamsabadi et al. [114] and Wu et al. [21] contribute to this direction on gas and liquid separations, respectively. In fact, using MD

simulations, Shamsabadi and coworkers revealed the crucial role of interfacial interactions between PA blocks of Pebax 1657 and $Ti_3C_2T_x$ for achieving high $CO_2$ permeability of resulting MMMs. In addition, MD simulations also showed great utility for confirming and explaining the solvent transport in neat as well as chemically modified MXenes (ie. $Ti_3C_2T_x$, $Ti_3C_2T_x$-$NH_2$ and $Ti_3C_2T_x$-$C_{12}H_{25}$) [114,21].
Proceeding further, molecular dynamics simulations might also be helpful for evaluating the potential of porous MXenes for membrane fabrications. MXenes are intrinsically layered nanosheets, even in the thinnest form: a monolayer of $M_2X$ MXene, for example, has a quasi-trilayered structure. This feature results in possible point surface defects that might occur in MXene nanosheets during etching and exfoliation, leading to not always in-plane porosity, which, for example in not the case of truly monolayered GO. However, porous MXenes are achievable and already successfully exploited for different applications [174,175], as mentioned in part 1 of this thesis. Therefore, to better understand the transport behavior of MXene-based membranes and possibly developing superior membranes that utilize porous MXenes, MD simulations can be a crucial element for further explorations.

### 2.6.4 – Scale-Up Potential

Leaving their performance merits aside, MXenes and thus MXene-based membranes, are in their infancy for securely foreseeing their commercialization potential. Even most MAX phases are far from being commercially available at an affordable price at the moment, as already discussed in part 1, however there are significant efforts for producing common MAX phases in bulk quantities [176,177]. Nevertheless, the scalable production of MXenes is even more challenging as there are safety issues associated with fluorine-based etching chemistries [17]. One possible safer solution to this problem could be the use of strong bases, ie. sodium hydroxide or tetrabutylammonium hydroxide, as etchants and so potentially easier to scale [178,179]. In any case, the yield and/or product quality of non-fluorinated-based method need further improvement. On the other hand, alternative etching processes inevitably provide MXene products with significantly different surface chemical compositions. From the point of view of membrane design, this might be an opportunity to engineer the properties of membranes. However, it is important to investigate scalable techniques for the processing of MXene into membranes. Industrially acceptable methods, such as blade-casting variations, are likely among the first options for NLMs and MMMs [114,180].
Nevertheless, it still be a challenge to prepare large-scale freestanding MXene membranes, but there are already examples of small-scale freestanding MXene

membranes prepared by vacuum filtration [89,181]. Now, the most realistic and potentially more scalable choice are the composite membranes. Noting that, as discussed previously in section 2.6.2, phase inversion (PI) and interfacial polymerization (IP) methods are also worth a closer look within this context.

# PART 3 – CONCLUSIONS

MXenes is an emerging material for the design of high-performance membranes for gas separation, solvent purification and water purification. Between these three broad areas of separation/purification applications, gas separation is quite less studied. Anyhow, MXenes still promising for designing gas separation membranes that operate at high temperature. Differently, MXenes have shown more results and success for solvent purification, as NLMs, as well as fillers of polymer-based composite membranes. Moreover, thanks to their unique properties, MXenes offer a multitude of opportunities for water purification application, exploiting their antibacterial, photothermal and catalytic activities [182].

It should be notice that the major of the studies reported so far dealt with different material systems, experimental conditions and separation tasks. Hence, there is still large room for confirming and improving results obtained for MXene-based membranes so far. In addition, except for a couple of studies that provide the comparison between MXenes and graphene-based materials, most of research focused on MXenes alone without benchmarking against other materials under identical conditions. Consequently, it is hard to compare the performance of MXenes with respect to other 2D materials without supposing too many assumptions. Thus, is not so clear if MXenes are superior to other 2D materials or not for many application areas. Further comparative studies are needed in the future to answer correctly to this question. In this regard, in Table 1, are reported studies on membrane applications of non-MXene 2D materials, including graphene-based materials and exfoliated g-$C_3N_4$ (graphitic carbon nitride), h-BN (hexagonal boron nitride), TMDs (transition metal dichalcogenide), MOFs (metal organic frameworks) and COFs (covalent organic frameworks).

| **Membrane materials** | **Membrane format** | **Separation applications** | **Critical remarks and selected indicators of membrane performance** | **Ref** |
|---|---|---|---|---|
| GO in ODPA-TMPDA | MMM (solvent-casting) | Gas separation ($CO_2/CH_4$) | • fillers improved $CO_2/CH_4$ selectivity at <10 wt% filling ratio<br>• fillers improved the mechanical strength of resulting MMM | [C1] |
| GO, on PEI-modified hollow fiber PAI | NLM (dip-coating) | Water desalination | • GO layer improved salt rejection (NaCl and $MgCl_2$)<br>• GO layer reduced overall water permeability | [C2] |

| | | | | |
|---|---|---|---|---|
| GO in PA, on PSf | TFN (IP) | Water desalination | • interlayer spacings of nanosheets serve as channels for water transport (as suggested by an increase in overall flux)<br>• salt rejection (NaCl and $Na_2SO_4$) dropped marginally | [C3] |
| rGO, on nylon | NLM (vacuum filtration) | OSN | • hyperbranched PEI improved dye rejection<br>• membrane survived basic/acidic/and oxidative environments | [C4] |
| h-BN, on PVDF | MMM (solvent-cast) | Gas separation ($CO_2$/$CH_4$) | • permeability increased with the increased loading of h-BN<br>• mechanical stability increased with the loading of h-BN | [C5] |
| h-BN, on PES | TFN (IP) | OSN & water treatment | • 0.05 wt% h-BN provided 4-fold improvement in water flux<br>• addition of h-BN decreased dye rejection by 10% | [C6] |
| Modified-h-BN in PPA on PES | TFN (IP) | OSN & water treatment | • pure water flux increased by 59% with h-BN addition<br>• addition of modified-h-BN lowered organic matter rejection | [C7] |
| g-$C_3N_4$ in PIM-1 | MMM (solvent-casting) | Gas separation (various pairs) | • selectivity enhancement was higher than permeability enhancement<br>• fillers improved the overall mechanical performance | [C8] |
| g-$C_3N_4$, on AAO | NLM (vacuum-filtration) | Water treatment | • artificial nanopores in g-C3N4 contributed to fast transport<br>• an inverse linear relationship observed between film thickness (70 to 190 nm) and dye rejection (90 to 63 %) | [C9] |
| g-$C_3N_4$ in sodium alginate | MMM (spin-coating) | Pervaporation (ethanol dehydration) | • permeation flux and separation factors improved with the increase in loading up to 3 wt%<br>• PDA-modified g-C3N4 blocked water transport effectively | [C10] |
| TMD ($MoS_2$ intercalated with $Li^+$ ions), on AAO | NLM (vacuum-filtration) | Gas separation ($H_2$/$CO_2$) | • high permeability to small gas molecules (He, H2) | [C11] |

| | | | | |
|---|---|---|---|---|
| | | | • low permeability to large gas molecules ($CO_2$, $O_2$, $N_2$, $CH_4$) • $H_2/CO_2$ selectivity is closed to Knudsen selectivity<br>• membranes were thermally stable up to 160 °C | |
| TMD ($MoS_2$), in polyamide, on PFs | TFN (IP) | Water desalination | • improvements observed in both salt rejection and water flux<br>• nanosheets reduced membrane fouling (BSA)<br>• nanosheet loss observed during operation until the compaction of the selective layer | [C12] |
| TMD ($MoS_2$), on PFs | NLM (pressure-filtration) | Water treatment | • hydrated TMDs enables high water permeability<br>• completely dried TMDs yields low permeability by a severe reduction of interlayer spacings (restacking process) | [C13] |
| TMD ($MoS_2$), on PFs | NLM (pressure-filtration) | OSN | • drying processes affected membrane stability substantially<br>• stable membranes afforded long-term (7 days) operation for dye removal (from isopropanol) | [C14] |
| MOF (CuBDC) in 6FDA-DAM & PIM-1 | MMM (solvent-casting) | Gas separation ($CO_2/CH_4$) | • low filler loading (<5 wt%) improved performance<br>• high filler loading sacrifices $CO_2$ permeability severely | [C15] |
| MOF (CuBDC) in PIM-1, on AAO | TFN (spin-coating) | Gas separation ($CO_2/CH_4$) | • selectivity improved as compared to the neat polymer<br>• high filler loading decreases gas permeabilities substantially | [C16] |
| MOF ($Zn_2(bim)_4$), on $\alpha$-$Al_2O_3$ | NLM (hot-drop-coating) | Gas separation ($H_2/CO_2$) | • highest $H_2/CO_2$ selectivity (261) was achieved when the substrate was preheated at 120 °C<br>• $Zn_2(bim)_4$ nanosheets possess low accessible surface area | [C17] |

| | | | | |
|---|---|---|---|---|
| COF (COF-1), on $\alpha$-$Al_2O_3$ substrate | NLM (drop-coating) | Gas separation ($H_2/N_2$) | • Gas permeance decreased with increasing temperature<br>• $H_2/N_2$ selectivity observed to be close to Knudsen selectivity<br>• membrane porosity decreased when COF-1 is exfoliated | [C18] |
| COF (NUS-2 and NUS-3) in Ultem or PBI | MMM (solvent-casting) | Gas separation ($H_2/CO_2$ & $H_2/CH_4$) | • a high level of non-ideality observed at a low filling ratio<br>• 20 wt% filling ratio surpassed the upper bound for $H_2/CO_2$<br>• polymer choice influenced $H_2/CO_2$ separation performance (Ultem-based MMMs remained below Knudsen selectivity) | [C19] |
| COF (COF 9), on AAO | NLM (vacuum-filtration) | Water treatment | • nanopores of COF 9 help retaining high water flux at high transmembrane pressure (when the membrane is fouled)<br>• inner-wall carboxyl groups (of COF 9) aided cation transport | [C20] |

An uncleared question regard to the oxidation issue of MXenes, and if this will limit the prospects of MXenes considerably [182].

Another aspect to consider is that the current literature on MXene-based membranes is clearly dominated by nanolaminates prepared via filtration-assisted film deposition methods, and the quasi-total article on experimental MXenes talk about titanium carbide only, and most of this are on $Ti_3C_2T_x$ as clearly seen in table 2, which summarize the works reported in this thesis, with type of MXene used, application area and type of membrane. Clearly, more work in the recent future should be done to explore new type of MXene and not only titanium carbide family, but also nitride carbide ones with different type of membrane with a particular attention to mixed composite membrane.

| **MXene / application** | **Type of membrane** | **Performance parameters / Major data** | **Key finding** | **Pub. Date / Ref** |
|---|---|---|---|---|
| $Ti_3C_2T_x$ / Gas separation (He, $H_2$, $CO_2$, $O_2$, $N_2$, $CH_4$, $C_3H_6$, $C_3H_8$) | NLM (vacuum-filtration) on AAO disc | Selectivity<br>- $H_2/CO_2$ ~238,4<br>- $H_2$/He ~1,10<br>- He/$CO_2$~216,4<br>- $CO_2/N_2$ ~0,49 | - High selectivity for small/large gas pairs.<br>- $H_2/CO_2$ results overcome the 2008 Robeson upper bound.<br>- Suppression of $CO_2$ permeation | 2018 [89] |
| $Ti_3C_2T_x$-borate and PEI intercalated / Gas separation ($H_2$, $CO_2$, $N_2$, $CH_4$, $C_3H_8$) | NLM (vacuum-filtration) on Dopamine-modified AAO disc | - 43% increase in equilibrium $CO_2$ absorption of borate/PEI MXene<br>- 13% increase for borate-modified MXene (wrt pristine MXene) | - Increase $CO_2/CH_4/N_2$ permeation (increase interlayer spacing)<br>- Result overcome MOF-based membranes<br>- Relative humidity affect performance badly | 2018 [70] |
| $Ti_3C_2T_x$ / Gas separation ($H_2$, $N_2$) @ high temp. | NLM (vacuum-filtration) on AAO disc | - high selectivity of ~41 for $H_2/N_2$ at 320°C<br>- no degradation up to 200h operation | - High selectivity for $H_2/N_2$ at high T<br>- Long time stability membrane<br>- Relevant for industrial purpose on $H_2$ separation process | 2019 [113] |
| $Ti_3C_2T_x$ / PAN-based filter for PM2.5 filter | Composite MXene 0.005/0.080 wt% with PAN electrospinned | - removal rate of PM2.5 of $\sim 44 \mu g\ cm^{-2}\ h^{-1}$ (vs 4.2)<br>- filtering capacity > 2 times<br>- inhibition of Gram-positive (Staphylococcus aureus) bacteria species | - superior removal performance of PM2.5 in terms of rate and filtering capacity<br>- inhibition of bacterial growth | 2019 [87] |
| $Ti_3C_2T_x$ / Gas separation ($CO_2$, $N_2$) @ low/mid temp. | MMM PEBA (spin-coating) on flat-sheet PAN | - $CO_2/N_2$ selectivity of ~72.5<br>- $CO_2$ permeance of ~21,6 GPU<br>- Good stability over 120h | - low filler loading of 0.15 wt%<br>- high selectivity on $CO_2/N_2$<br>- high permeance of $CO_2$<br>- good stability in time | 2019 [73] |
| $Ti_3C_2T_x$ / Gas separation ($H_2$, $CO_2$ $N_2$, $CH_4$) | TFN and MMM PEBAX-1657 (rod-coating) on flat-sheet PTMSP-PVDF | - $CO_2/N_2$ selectivity above 100<br>- $CO_2$ permeability over 100 barrer<br>- stable for over 6 months in polymer matrix | - high permeability and selectivity and stability, overcoming 2008 Robeson upper bound for $CO_2/N_2$<br>- for $CO_2$ capture application | 2019 [114] |

| | | | | |
|---|---|---|---|---|
| $Ti_3C_2T_x$ / Water purification (desalination, dye removal) | NLM (vacuum-filtration) 1,5$\mu m$ thick on flat-sheet PVDF | - water flux ~6 times higher than GO (37.4 vs 6.5 L $m^{-2}h^{-1}$)<br>- average size of nanochannels ~ 0.64 nm particles with hydration radius smaller will permeate<br>- slower permeation for cations, proportional to their charges due to the strong negative charges of MXene surface | - compared water and cations transport of MXene and GO NLMs<br>- small-sized monovalent cations can expand nanochannels forming an EDL<br>- multivalent cations due to their higher charges have the capacity to narrow the nanochannels via electrostatic attraction | 2015 [60] |
| $Ti_3C_2T_x$-$Fe(OH)_3$ intercalated / Water purification (dye and nanoparticle removal) | NLM (vacuum-filtration) on AAO disc with MXene lateral size of ≈100-400 nm | - water permeability > 1000 L $m^{-2}h^{-1}$<br>- rejection efficiency > 90% for organic molecules with sizes > 2.5 nm | - outstanding water permeability and high removal rate for compounds larger than 2.5nm<br>- larger interlayer spacing thanks to $Fe(OH)_3$ NPs intercalated and removed after | 2017 [71] |
| $Ti_3C_2$ / Water purification (desalination by photothermal membrane distillation) | PDMS-coated NLM (vacuum-filtration) on flat-sheet PVDF | - achieve ≈84% conversion efficiency between 60 and 150 min, under 1 sun irradiation | - self-floating membrane with extraordinary high light-to-heat conversion efficiency with fast heating rate | 2017 [125] |
| $Ti_3C_2T_x$ / Water purification (dye removal) | NLM (vacuum-filtration) on flat-sheet PESf substrate | - water flux~405 L $m^{-2}h^{-1}$<br>- 92% dye removal C. Red<br>- 80% dye removal Gentian Violet<br>- 23% rejection for $Mg^{2+}$<br>- 13.8% rejection for $Na^+$ | - owing to the MXene composite loose lamellar structure, the composite membrane could exhibit effective permselectivity in the separation of dyes from salts | 2017 [121] |
| $Ti_3C_2T_x$-GO (10-30 wt%) hybrid / Water purification (desalination, dye removal) | NLM (vacuum-filtration) on flat-sheet cellulose acetate and Nylon, AAO disc | - water flux ~ 25 $Lm^{-2}h^{-1}$<br>- high rejection rates for charged dye molecules with hydrated radius >0.5 nm | - high rejection rates for smaller charged molecules and dyes with radius > 0.5 nm<br>- provide size exclusion effect plus electrostatic repulsion | 2017 [94] |
| $Ti_3C_2T_x$ (1.0 wt%)-$TiO_2$ / Water purification (dextran removal) | Inorganic composite $TiO_2$ (matrix) on AAO disc and 4-channel $\alpha$-$Al_2O_3$ tubes | - calcinating at 400°C to develop a durable membrane<br>- superior dextran rejection > 95% | - a crack-free $TiO_2$-MXene layer was well created on microporous disks by a single cycle of coating, drying and calcination, which could simplify the | 2018 [92] |

| | | | | |
|---|---|---|---|---|
| | (100nm) (spin-coating, dip-coating) | (molecular weight > 30 kDa)<br>- water flux 90 L $m^{-2}h^{-1}$ | process decreasing the cost of membrane fabrication | |
| $Ti_3C_2T_x$-Ag NPs / Water purification (dye removal, organic matter) | Composite NLM of MXene and Ag nanoparticles (21%) on Polyvinylidene difluoride | - dye removal $\sim$79,9% (Rhodamine B), $\sim$92,3% (methyl green)<br>- organic dye removal >99% (bovine serum albumin)<br>- bacteria inhibition >99.9% (E. coli)<br>- water flux $\sim$ 420 $Lm^{-2}h^{-1}$ | - Ultrahigh flux and fouling-resistance antibacterial membrane<br>- 99% of E. coli growth inhibition (vs 60% without Ag NPs)<br>- Ag NPs improved also water flux | 2018<br>[86] |
| Water purification (desalination by photothermal membrane distillation) | Surface-modified (fluorinated silane) NLM (vacuum-filtration) on flat-sheet PVDF | - conversion efficiency $\approx$ 71%<br>- high level of stability with > 200h operation<br>- coupling agent: trimethoxy(1H,1H,2H,2H-per-fluorodecyl)silane | - antiwetting self-floating membrane that could handle real seawater with heavy metals and organic with high stability<br>- remarkable desalination performance for different cations | 2018<br>[126] |
| $Ti_3C_2T_x$-$TiO_2$ / Water purification (dextran removal) | Inorganic composite $TiO_2$ (matrix) on 4-channel $\alpha$-$Al_2O_3$ tubes (300nm) dip-coating | - water permeance 100-140 L $m^{-2}h^{-1}$<br>- dextran removal >90% (molecular weight >20 kDa | - dextran molecules find ideal pathways (longitudinal-lateral transport nano-channel) between $TiO_2$ NPs and MXene<br>- they could manipulate molecular cut-off and pore size of $TiO_2$-MXene playing on duration and temp. of calcination process | 2018<br>[117] |
| $Ti_3C_2T_x$ / Water purification (desalination by photothermal membrane distillation) | PDMS-coated NLM (vacuum-filtration) on flat-sheet PVDF | - photothermal conversion efficiency of 5.8 $kW/m^2$<br>- antifouling properties tested with BSA and NaCl | - solar-assisted membrane distillation with high photothermal efficiency and antifouling properties | 2018<br>[127] |
| $Ti_3C_2T_x$ / Water purification (oil removal) | NLM (vacuum-filtration) on print paper | - water flux $\sim$ 472 $Lm^{-2}h^{-1}$<br>With oil content >99% (total organic carbon) | - the print paper was employed as a substrate mechanical flexibility and strength<br>- hydrophilic MXene layer serve as functions as a selective layer to effectively separate emulsified oil from water | 2019<br>[119] |

| | | | | |
|---|---|---|---|---|
| $Ti_3C_2T_x$ / Water purification (desalination) | Inorganic composite (pressure filtration) on 1-channel $\alpha$-$Al_2O_3$ tubes (120 nm) | -water flux$\sim$5/25 $Lm^2h^{-1}$<br>- salts rejection 50-99% ($Na_2SO_4$ > $Mg_2SO_4$ > NaCl > $MgCl_2$)<br>- sintering temperature from 60 to 500 °C<br>- over 450°C in air partial oxidation of MXene, changing color from dark grey to reflection white | - The interlayer spacing of MXene-derived membranes lessened from 0.371 nm at 60 °C to 0.265 nm at 450 °C (optimal for salt rejection is 400°C). This resulted from the moisture loss and de-functionalization (-OH) occurring within MXene film at elevated temp. | 2019 [123] |
| $Ti_3C_2T_x$-GO hybrid / Water purification (dye, organic matter removal) | GO hybrid NLM (vacuum-filtration) on flat-sheet mixed cellulose ester (450 nm) | - lower water permeance wrt pure MXene ($\sim$71.9)<br>- higher rejection rates for organic dyes (>99%) for humic acid and bovine serum albumin | - low water permeance could be because of difference in lateral size of MXene and GO<br>- this outstanding was attributed to combined effect of molecular sieving, mainly, and electrostatic interaction | 2020 [116] |
| $Ti_3C_2T_x$ / Water purification (oil removal) | NLM (vacuum-filtration) on flat-sheet PESf substrate | - low fouling<br>- high resistance to oil, including oily solvents | - oil-separating nanolaminates | 2019 [120] |
| $Ti_3C_2T_x$ / Water purification (desalination) | Thick laminate (vacuum-filtration) on flat-sheet PA | - salt rejection performance increase as the degree of crosslinking increase but at the expense of decrease in permeance | - antiswelling MXene membrane by temperature-induced self-crosslinking of hydroxylated $Ti_3C_2T_x$ via $H_2O$ condensation | 2019 [124] |
| $Ti_3C_2T_x$-GO hybrid / Water and solvent purification (dye removal) | NLM (vacuum-filtration) on flat-sheet Nylon 220nm | - water flux $\sim$8.5-11 $Lm^2h^{-1}$<br>- rejection over 90%<br>- high stability for long-term operations | - the resultant GO/MXene membranes showed very high flux for pure solvents and outstanding dyes molecular separation performance (>90%) | 2019 [130] |
| Hydroxyl-rich $Ti_3C_2T_x$ / Solvent purification (PEG removal) | TFN (drop-casting, dip-coating) on PEI or PDMS (as matrix) on flat-sheet PAN | - PAN/PEI-$Ti_3C_2T_x$ (with 4wt% MXene loading) showed $\approx$99.4% rejection to PEG-800 at 10 bar<br>- studied rejection to oligomeric PEG molecules (200-1000 Da) | - indifferently of the loading ratio of MXene and type of polymer matrix, all membranes provided superior rejection to the oligomeric molecules | 2016 [75] |
| Hydroxyl-rich $Ti_3C_2T_x$ (fixed 3 wt%) / Solvent | TFN (drop-casting, dip-coating) on PEI or PDMS (as | - loading ratio of MXene fixed at 3 wt% | - exploring the role of chemical functionalization of MXene on PEG they | 2017 [79] |

| | | | | |
|---|---|---|---|---|
| purification (PEG removal) | matrix) on flat-sheet PAN | | found that different functionalities are useful for different solvents | |
| Double-layered MXene / Solvent purification (dye removal) | NLM (vacuum-filtration) on flat-sheet Nylon | - outstanding water permeability of $\sim 2300\ Lm^{-2}h^{-1}$<br>- rejection >96% for organic dyes larger than 2.0 nm | -the membrane possessed rigid and highly ordered nanochannels providing fast water transport and highest permeability | 2018 [109] |
| $Ti_3C_2T_x$ (1-5 wt%) / Solvent purification (dehydration by pervaporation) | MMM (spin-coating) Chitosan (matrix) on flat-sheet PAN | - with 3 wt% exhibit high improvement for both flux (25%) and separation factor (250%)<br>- T=50°C optimum value for flux/selectivity cutoff | - stable MMM composed of chitosan and 1-5 wt% $Ti_3C_2T_x$ for ethanol dehydration<br>- higher T increase the swelling causing high flux at the expense of selectivity | 2018 [96] |
| $Ti_3C_2T_x$ / Solvent purification (dye removal) | MMM (phase inversion & crosslinking) Crosslinked P84 (matrix) with TETA | - complete rejection of gentian violet<br>- high flux ~268 $Lm^2h^{-1}$ under 0.1 MPa<br>- excellent solvent resistance to DMF, acetone and methanol | - different approach for OSN membrane showed virtually complete rejection of gentian violet with high flux and high solvent resistance after crosslinking | 2018 [133] |
| PAN/PEI-$Ti_2CT_x$ / Solvent purification (dehydration by pervaporation) | Neat/hybrid NLM (vacuum-filtration) in Hyperbranched PEI on flat-sheet PAN | - reduce the water content in the isopropanol/water mixture from 10 to <1 wt% at 50°C<br>- water flux > 1000 $Lm^2h^{-1}$ | - flux values that overcome values available in literature for various type of membrane<br>- poor results in terms of selectivity (for $Ti_3C_2T_x$) | 2019 [131] |
| $Ti_3C_2T_x$ / Solvent purification (dehydration by pervaporation) | NLM (vacuum-filtration) on flat-sheet Nylon (2 $\mu m$ thick MXene) | - not very high flux (~200-300 $Lm^2h^{-1}$)<br>- not very high separation factor (~100-150)<br>- high stability and low deterioration of the membrane | - the membrane exhibit an appealing performance at room temperature compared to 50°C with more than 30% higher separation factor at only 10% lower flux<br>- small fluctuations of both flux and selectivity for long-term operation | 2019 [132] |

In addition, an overall evaluation is necessary to examine the effects of various emerging MXenes on membrane preparation and membrane properties in terms of charge, hydrophilicity, interlayer spacing and surface smoothness, since it is difficult to evaluate the interactions between contaminants and

MXene, the homogeneity of MXene dispersion in various solvents and the development of effective incorporation methods [183]. This information could enable measurement of large-scale and long-term membrane stability for promoting applications of MXene-based membranes. In figure 24, it is shown the area of future study of MXene-based membranes in terms of their properties, solute physicochemical properties, operation conditions and solvent/water quality conditions in liquid separation [183].

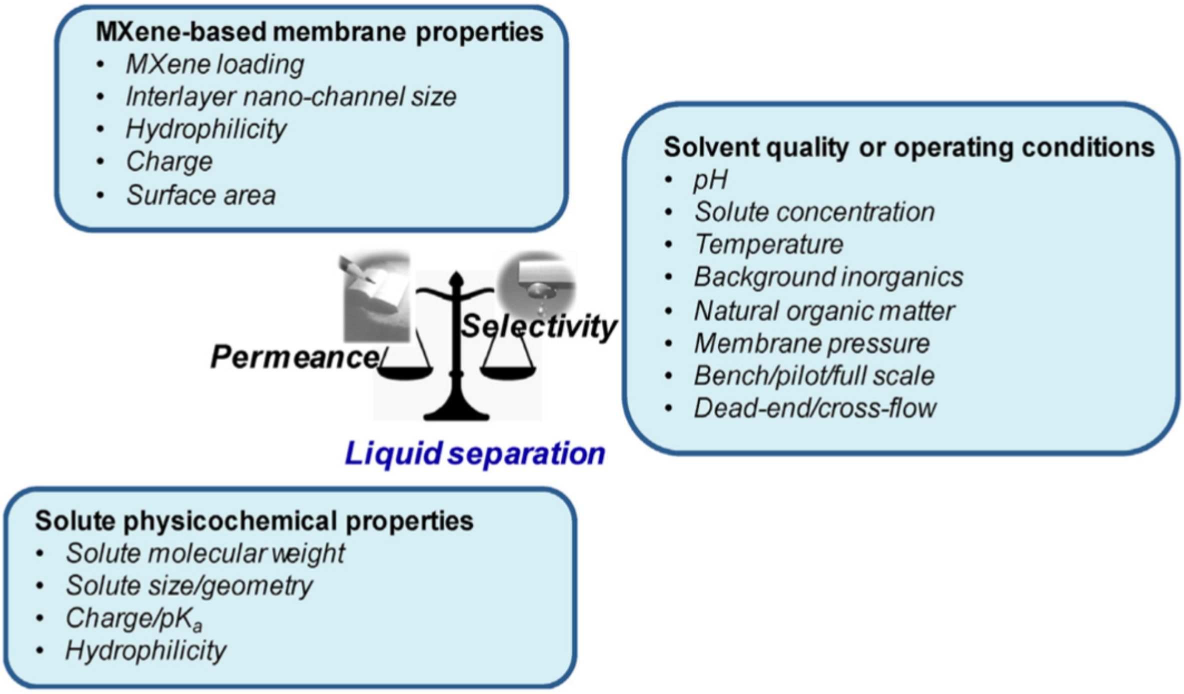

*Figure 24: Areas of future study of MXene-based membrane in liquid separation [183]*

In section 2.6 of part 2 are proposed several future directions concerning more realistic strategies for membrane preparation for future research.
Taking into account the rich chemistry of MXenes, we currently exploit a very small fraction of possible MXene structures. The most of existing reports on MXene-based structure membranes are experiment-driven focusing on titanium carbide MXene varieties, but yet still, there are attempts to involve simulation/modeling approaches to inform the designing of MXene-based membrane [183]. Intensifying these efforts should help identify uncommon MXenes suitable for membrane design. In general, the prospects are that MXene-based membranes will continue their fast progress made in less than 5 years in the future with growing speed. In table 3 are reported the reviews that contributed so far covering the membrane application of MXenes.

| 2DMs covered | Focused topics | Essential remarks | Pub. Date | Ref. |
|---|---|---|---|---|
| GFMs, MXenes | Fabrication/modification of water treatment and desalination membranes with various nanocarbons (including GFMs, MXenes) | Includes MXenes although only a few reports were available at that time | Feb 2016 | [4] |
| GFMs, MOFs, zeolites, TMDs, LDHs, h-BN, MXenes | Design and performance of evaluation of advanced membranes (NLMs and MMMs) prepared by 2DMs for water and gas separations | A detailed and profoundly insightful evaluation of NLMs (referred to as laminar membranes) | July 2016 | [10] |
| MXenes only | Synthesis, characterization, materials properties, composites preparation, applications (energy storage/conversion, environmental remediation including membrane separations, electromagnetic interference shielding) | A comprehensive evaluation of the preparation of MXene-based composites useful for membrane design purposes | Dec 2016 | [27] |
| GFMs, MOFs, TMDs, MXenes, zeolites, COFs, g-$C_3N_4$ | Examples of 2DM-based advanced membranes, principles, and methods of membrane design, separation mechanisms of membranes | An essential read for designing advanced membranes with 2DMs | Jan 2018 | [9] |
| GFMs, h-BN, TMDs, LDHs (layered double hydroxides), MOFs, MXenes | Composite membranes (MMMs), the possible role of 2DMs for preventing plasticization, synthesis and general properties of 2DMs, critical examples of membrane designs based on 2DMs | An insightful account of advanced membrane design for gas separation with a particular focus on 2DMs | Feb 2018 | [8] |
| MXenes only | Environmental applications (adsorption of heavy metals, dyes, radioactive pollutants, gaseous molecules), synthesis | Focuses on adsorbents but provides a brief introduction on MXene membranes | May 2018 | [41] |
| MXenes only | Applications (energy storage/conversion, contaminant adsorption, and water treatment including membranes), synthesis, materials properties | Provides well-organized tabulated information on synthesis and applications of MXenes | Oct 2018 | [42] |
| GFMs, MXenes, TMDs | Preparation and GFM-based gas separation membranes (both MMMs and NLMs), the progress of other 2DMs | A quick introduction for tailoring the permeability/selectivity of gas separation membranes | Oct 2018 | [43] |
| GFMs, MOFs, COF, TMDs, h-BN, | Membrane fabrications with 2DMs (including MMMs and NLMs), performance evaluation of 2DM- | Provides useful tips and insights on designing 2DM-based advanced membranes | Feb 2019 | [44] |

| | | | | |
|---|---|---|---|---|
| g-$C_3N_4$, MXenes | based membranes in gas, water, and ion separations | | | |
| GFMs, h-BN, TMDs, MXenes | Membrane applications including water purification, desalination, ion extraction, and energy storage and conversion | Discusses a wide range of potential applications of 2DM-based NLMs | May 2019 | [45] |
| GFMs, MXenes, h-BN, TMDs, COF, MOF | Membrane design and applications of 2DMs including water, gas, and solvent | Provides a quick introduction to the broad field of 2DM-based membranes | May 2019 | [46] |
| MXenes only | Applications (energy storage/conversion, composites, lubrication, sensors, and membranes), materials properties, synthesis, structure, and stability | A succinct account of MXene membranes with critical comments on polymer-MXene composites | June 2019 | [31] |
| MXenes only | Environmental remediation (adsorbents, water treatment, desalination, sensors), stability, synthesis | A balanced and critical evaluation of adsorbents and water separation membranes | June 2019 | [47] |
| Various type of material system including 2DMs | Ion-NLM interactions, membrane design, regulation of ion transport through NLMs, applications concerning energy and beyond | A helpful read on the relations of membrane separations and certain energy-related applications | Dec 2019 | [149] |
| MXenes only | Membrane design and preparation, liquid separation, water purification, organic solvent filtration, membrane properties, area of future studies | A review on MXene-based membrane for water purification application | April 2020 | [183] |
| MXenes only | Membrane design and preparation, water separation, gas separation, organosolvent separation, antibacterial/antibiofouling membranes, electroresponsive membranes | The first dedicated report on the evaluation of MXene-based membranes | June 2020 | [182] |

The listed reports are focused om the applications of MXenes including membranes or reviews dedicated to the membrane applications of 2D materials in general. Reviews that are included on this table contain a notable amount of information on MXene-based membranes (> 100 words) and sorted the content based on the online publication dates of examined reviews.

# BIBLIOGRAPHY

## PART 1

[1] X. Duan, C. Wang, A. Pan, R. Yu, X. Duan, Two-dimensional transition metal dichalcogenides as atomically thin semiconductors: opportunities and challenges, Chem. Soc. Rev. 44 (2015) 8859e8876, https://doi.org/10.1039/C5CS00507H.

[2] P. Chen, Z. Zhang, X. Duan, X. Duan, Chemical synthesis of two-dimensional atomic crystals, heterostructures and superlattices, Chem. Soc. Rev. 47 (2018) 3129e3151, https://doi.org/10.1039/C7CS00887B.

[3] K.S. Novoselov, A.K. Geim, S. V Morozov, D. Jiang, Y. Zhang, S. V Dubonos, I. V Grigorieva, A.A. Firsov, Electric field effect in atomically thin carbon films, Science (80-) 306 (2004) 666e669.

[4] C. Ataca, H. S¸ ahin, S. Ciraci, Stable, single-layer MX 2 transition-metal oxides and dichalcogenides in a honeycomb-like structure, J. Phys. Chem. C 116 (2012) 8983e8999, https://doi.org/10.1021/jp212558p.

[5] D. Pacile, J.C. Meyer, Ç.O. Girit, A. Zettl, The two-dimensional phase of boron nitride: few-atomic-layer sheets and suspended membranes, Appl. Phys. Lett. 92 (2008) 133107, https://doi.org/10.1063/1.2903702.

[6] B. Lalmi, H. Oughaddou, H. Enriquez, A. Kara, S. Vizzini, B. Ealet, B. Aufray, Epitaxial growth of a silicene sheet, Appl. Phys. Lett. 97 (2010), 223109, https://doi.org/10.1063/1.3524215.

[7] A.J. Mannix, X.-F. Zhou, B. Kiraly, J.D. Wood, D. Alducin, B.D. Myers, X. Liu, B.L. Fisher, U. Santiago, J.R. Guest, M.J. Yacaman, A. Ponce, A.R. Oganov, M.C. Hersam, N.P. Guisinger, Synthesis of borophenes: anisotropic, two- dimensional boron polymorphs, Science 350 (2015) 1513e1516, https://doi.org/10.1126/science.aad1080.

[8] H. Liu, A.T. Neal, Z. Zhu, Z. Luo, X. Xu, D. Tomanek, P.D. Ye, Phosphorene: an unexplored 2D semiconductor with a high hole mobility, ACS Nano 8 (2014) 4033e4041, https://doi.org/10.1021/nn501226z.

[9] L. Banszerus, M. Schmitz, S. Engels, M. Goldsche, K. Watanabe, T. Taniguchi, B. Beschoten, C. Stampfer, Ballistic transport exceeding 28 mm in CVD grown graphene, Nano Lett. 16 (2016) 1387e1391, https://doi.org/10.1021/ acs.nanolett.5b04840.

[10] C. Lee, X. Wei, J.W. Kysar, J. Hone, Measurement of the elastic properties and intrinsic strength of monolayer graphene, Science 321 (2008) 385e388, https://doi.org/10.1126/science.1157996.

[11] Y. Zhu, S. Murali, M.D. Stoller, K.J. Ganesh, W. Cai, P.J. Ferreira, A. Pirkle, R.M. Wallace, K.A. Cychosz, M. Thommes, D. Su, E.A. Stach, R.S. Ruoff, Carbon-based supercapacitors produced by activation of graphene, Science 332 (2011) 1537e1541, https://doi.org/10.1126/science.1200770.

[12] A.A. Balandin, Thermal properties of graphene and nanostructured carbon materials, Nat. Mater. 10 (2011) 569e581, https://doi.org/10.1038/ nmat3064.

[13] Gunture, A. Singh, A. Bhati, P. Khare, K.M. Tripathi, S.K. Sonkar, Soluble graphene nanosheets for the sunlight-induced photodegradation of the mixture of dyes and its environmental assessment, Sci. Rep. 9 (2019) 2522, https://doi.org/10.1038/s41598-019-38717-1.

[14] K.M. Tripathi, T. Kim, D. Losic, T.T. Tung, Recent advances in engineered graphene and composites for detection of volatile organic compounds (VOCs) and non-invasive diseases diagnosis, Carbon N. Y. 110 (2016) 97e129, https://doi.org/10.1016/J.CARBON.2016.08.040.

[15] J. Lyu, M. Mayyas, O. Salim, H. Zhu, D. Chu, R.K. Joshi, Electrochemical performance of hydrothermally synthesized rGO based electrodes, Mater. Today Energy. 13 (2019) 277e284, https://doi.org/10.1016/J.MTENER.2019.06.006.

[16] Y. You, X.H. Jin, X.Y. Wen, V. Sahajwalla, V. Chen, H. Bustamante, R.K. Joshi, Application of graphene oxide membranes for removal of natural organic matter from water, Carbon N. Y. 129 (2018), https://doi.org/10.1016/j.carbon.2017.12.032.

[17] Y. Myung, S. Jung, T.T. Tung, K.M. Tripathi, T. Kim, Graphene-based aerogels derived from biomass for energy storage and environmental remediation, ACS

Sustain. Chem. Eng. 7 (2019) 3772e3782, https://doi.org/10.1021/ acssuschemeng.8b04202.

[18] Q.H. Wang, K. Kalantar-Zadeh, A. Kis, J.N. Coleman, M.S. Strano, Electronics and optoelectronics of two-dimensional transition metal dichalcogenides, Nat. Nanotechnol. 7 (2012) 699e712, https://doi.org/10.1038/ nnano.2012.193.

[19] L. Cao, Two-dimensional transition-metal dichalcogenide materials: toward an age of atomic-scale photonics, MRS Bull. 40 (2015) 592e599, https:// doi.org/10.1557/mrs.2015.144.

[20] R. M. Ronchi, J. T. Arantes, S. F. Santos, Synthesis, structure, properties and applications of MXenes:current status and perspectives, Ceramics International 45 (2019) 18167-18188, https://doi.org/10.1016/j.ceramint.2019.06.114 .

[21] M. Naguib, M. Kurtoglu, V. Presser, J. Lu, J. Niu, M. Heon, L. Hultman, Y. Gogotsi, M.W. Barsoum, Two-dimensional nanocrystals produced by exfoliation of Ti3AlC2, Adv. Mater. 23 (2011) 4248e4253, https://doi.org/ 10.1002/adma.201102306.

[22] M. Naguib, Y. Gogotsi, Synthesis of two-dimensional materials by selective extraction, Acc. Chem. Res. 48 (2015) 128e135, https://doi.org/10.1021/ ar500346b.

[23] M. Naguib, V.N. Mochalin, M.W. Barsoum, Y. Gogotsi, 25th anniversary article: MXenes: a new family of two-dimensional materials, Adv. Mater. 26 (2014) 992e1005, https://doi.org/10.1002/adma.201304138.

[24] M.W. Barsoum, The MNþ1AXN phases: a new class of solids: thermodynamically stable nanolaminates, Prog. Solid State Chem. 28 (2000) 201e281, https://doi.org/10.1016/S0079-6786(00)00006-6.

[25] Z. Sun, D. Music, R. Ahuja, S. Li, J.M. Schneider, Bonding and classification of nanolayered ternary carbides, Phys. Rev. B. 70 (2004), 092102, https:// doi.org/10.1103/PhysRevB.70.092102.

[26] M.W. Barsoum, The Mn+1AXn phases and their properties, in: Ceram. Sci. Technol, Wiley-VCH Verlag GmbH & Co. KGaA, Weinheim, Germany, 2010, pp. 299e347, https://doi.org/10.1002/9783527631735.ch7.

[27] T. Ouisse, M.W. Barsoum, Magnetotransport in the MAX phases and their 2D derivatives: MXenes, Mater. Res. Lett. 5 (2017) 365e378, https://doi.org/ 10.1080/21663831.2017.1333537.

[28] B. Anasori, M.R. Lukatskaya, Y. Gogotsi, 2D metal carbides and nitrides (MXenes) for energy storage, Nat. Rev. Mater. 2 (2017) 16098, https:// doi.org/10.1038/natrevmats.2016.98.

[29] B. Anasori, Y. Xie, M. Beidaghi, J. Lu, B.C. Hosler, L. Hultman, P.R.C. Kent, Y. Gogotsi, M.W. Barsoum, Two-dimensional, ordered, double transition metals carbides (MXenes), ACS Nano 9 (2015) 9507e9516, https://doi.org/ 10.1021/acsnano.5b03591.

[30] O. Mashtalir, M. Naguib, V.N. Mochalin, Y. Dall'Agnese, M. Heon, M.W. Barsoum, Y. Gogotsi, Intercalation and delamination of layered carbides and carbonitrides, Nat. Commun. 4 (2013) 1716, https://doi.org/ 10.1038/ncomms2664.

[31] H.W.Hugosson,O.Eriksson,L.Nordstro€m,U.Jansson,L.Fast,A.Delin, J.M. Wills, B. Johansson, Theory of phase stabilities and bonding mechanisms in stoichiometric and substoichiometric molybdenum carbide, J. Appl. Phys. 86 (1999) 3758, https://doi.org/10.1063/1.371284.

[32] J. Halim, S. Kota, M.R. Lukatskaya, M. Naguib, M.-Q. Zhao, E.J. Moon, J. Pitock, J. Nanda, S.J. May, Y. Gogotsi, M.W. Barsoum, Synthesis and characterization of 2D molybdenum carbide (MXene), Adv. Funct. Mater. 26 (2016) 3118e3127, https://doi.org/10.1002/adfm.201505328.

[33] R. Meshkian, L.-Å. N€aslund, J. Halim, J. Lu, M.W. Barsoum, J. Rosen, Synthesis of two-dimensional molybdenum carbide, $Mo_2C$, from the gallium based atomic laminate $Mo_2Ga_2C$, Scr. Mater. 108 (2015) 147e150, https://doi.org/ 10.1016/J.SCRIPTAMAT.2015.07.003.

[34] A.N. Enyashin, A.L. Ivanovskii, Atomic structure, comparative stability and electronic properties of hydroxylated $Ti_2C$ and $Ti_3C_2$ nanotubes, Comput. Theor. Chem. 989 (2012) 27e32, https://doi.org/10.1016/ J.COMPTC.2012.02.034.

[35] Q. Tang, Z. Zhou, P. Shen, Are MXenes promising anode materials for Li-ion batteries? Computational studies on electronic properties and Li storage capability of $Ti_3C_2$ and $Ti_3C_2X_2$(X 1⁄4 F, OH) monolayer, J. Am. Chem. Soc. 134 (2012) 16909e16916, https://doi.org/10.1021/ja308463r.

[36] A.N. Enyashin, A.L. Ivanovskii, Structural and electronic properties and stability of MX enes Ti2C and Ti3C2 functionalized by methoxy groups, J. Phys. Chem. C 117 (2013) 13637e13643, https://doi.org/10.1021/jp401820b.

[37] M. Naguib, O. Mashtalir, J. Carle, V. Presser, J. Lu, L. Hultman, Y. Gogotsi, M.W. Barsoum, Two-dimensional transition metal carbides, ACS Nano 6 (2012) 1322e1331, https://doi.org/10.1021/nn204153h.

[38] V. Natu, M. Clites, E. Pomerantseva, M.W. Barsoum, Mesoporous MXene powders synthesized by acid induced crumpling and their use as Na-ion battery anodes, Mater. Res. Lett. 6 (2018) 230e235, https://doi.org/10.1080/21663831.2018.1434249.

[39] J. Zhou, X. Zha, F.Y. Chen, Q. Ye, P. Eklund, S. Du, Q. Huang, A two-dimensional zirconium carbide by selective etching of Al3C3 from nanolaminated Zr3Al3C5, Angew. Chem. Int. Ed. 55 (2016) 5008e5013, https://doi.org/ 10.1002/anie.201510432.

[40] P. Urbankowski, B. Anasori, T. Makaryan, D. Er, S. Kota, P.L. Walsh, M. Zhao, V.B. Shenoy, M.W. Barsoum, Y. Gogotsi, Synthesis of two-dimensional tita- nium nitride Ti4N3 (MXene), Nanoscale 8 (2016) 11385e11391, https://doi.org/10.1039/C6NR02253G.

[41] M.W. Barsoum, J. Golczewski, H.J. Seifert, F. Aldinger, Fabrication and electrical and thermal properties of Ti2InC, Hf2InC and (Ti,Hf)2InC, J. Alloy. Comp. 340 (2002) 173e179, https://doi.org/10.1016/S0925-8388(02)00107-X.

[42] M.W. Barsoum, T. El-Raghy, L. Farber, M. Amer, R. Christini, A. Adams, The topotactic transformation of Ti3SiC2 into a partially ordered cubic Ti(C[sub 0.67]Si[sub 0.06]) phase by the diffusion of Si into molten cryolite, J. Electrochem. Soc. 146 (1999) 3919, https://doi.org/10.1149/1.1392573.

[43] A.I. Gusev, A.A. Rempel, Atomic ordering and phase equilibria in strongly nonstoichiometric carbides and nitrides, in: Mater. Sci. Carbides, Nitrides Borides, Springer Netherlands, Dordrecht, 1999, pp. 47e64, https://doi.org/10.1007/978-94-011-4562-6_4.

[44] Z.Y. Al Balushi, K. Wang, R.K. Ghosh, R.A. Vila, S.M. Eichfeld, J.D. Caldwell, X. Qin, Y.-C. Lin, P.A. DeSario, G. Stone, S. Subramanian, D.F. Paul, R.M. Wallace, S. Datta, J.M. Redwing, J.A. Robinson, Two-dimensional gallium nitride realized via

graphene encapsulation, Nat. Mater. 15 (2016) 1166e1171, https://doi.org/10.1038/nmat4742.

[45] X. Xiao, H. Yu, H. Jin, M. Wu, Y. Fang, J. Sun, Z. Hu, T. Li, J. Wu, L. Huang, Y. Gogotsi, J. Zhou, Salt-templated synthesis of 2D metallic Mon and other nitrides, ACS Nano 11 (2017) 2180e2186, https://doi.org/10.1021/ acsnano.6b08534.

[46] Xiao, X.; Song, H. B.; Lin, S. Z.; Zhou, Y.; Zhan, X. J.; Hu, Z. M.; Zhang, Q.; Sun, J. Y.; Yang, B.; Li, T. Q.; Jiao, L. Y.; Zhou, J.; Tang, J.; Gogotsi, Y. Scalable Salt-Templated Synthesis of Two- Dimensional Transition Metal Oxides. Nat. Commun. 2016, 7, 11296.

[47] Li, N.; Yang, G. Z.; Sun, Y.; Song, H. W.; Cui, H.; Yang, G. W.; Wang, C. X. Free-Standing and Transparent Graphene Membrane of Polyhedron Box-Shaped Basic Building Units Directly Grown Using A NaCl Template for Flexible Transparent and Stretchable Solid-State Supercapacitors. Nano Lett. 2015, 15, 3195−3203.

[48] Heising, J.; Kanatzidis, M. G. Exfoliated and Restacked $MoS_2$ and $WS_2$: Ionic or Neutral Species? Encapsulation and Ordering of Hard Electropositive Cations. J. Am. Chem. Soc. 1999, 121, 11720− 11732.

[49] P. Urbankowski, B. Anasori, K. Hantanasirisakul, L. Yang, L. Zhang, B. Haines, S.J. May, S.J.L. Billinge, Y. Gogotsi, 2D molybdenum and vanadium nitrides synthesized by ammoniation of 2D transition metal carbides (MXenes), Nanoscale 9 (2017) 17722e17730, https://doi.org/10.1039/C7NR06721F.

[50] C. Xu, L. Wang, Z. Liu, L. Chen, J. Guo, N. Kang, X.L. Ma, H.M. Cheng, W. Ren, Large-area high-quality 2D ultrathin $Mo_2C$ superconducting crystals, Nat. Mater. 14 (2015) 1135e1141, https://doi.org/10.1038/nmat4374.

[51] Y. Gogotsi, Chemical vapour deposition: transition metal carbides go 2D, Nat. Mater. 14 (2015) 1079e1080, https://doi.org/10.1038/nmat4386.

[52] H.H. Huang, R.K. Joshi, K.K.H. De Silva, R. Badam, M. Yoshimura, Fabrication of reduced graphene oxide membranes for water desalination, J. Membr. Sci. (2019), https://doi.org/10.1016/j.memsci.2018.10.085.

[53] F. Wang, Y. You, X. Jin, R. Joshi, On the role of driving force in water transport through nanochannels within graphene oxide laminates, Nanoscale (2018), https://doi.org/10.1039/c8nr08419j.

[54] B. Lian, S. De Luca, Y. You, S. Alwarappan, M. Yoshimura, V. Sahajwalla, S.C. Smith, G. Leslie, R.K. Joshi, Extraordinary water adsorption characteris- tics of graphene oxide, Chem. Sci. 9 (2018), https://doi.org/10.1039/ c8sc00545a.

[55] M.S. Whittingham, A.J. Jacobson, Intercalation Chemistry, Academic Press, 1982.

[56] W. Müller-Warmuth, R. Schollhorn, Progress in Intercalation Research, Springer, Netherlands, 1994.

[57] M.R. Lukatskaya, O. Mashtalir, C.E. Ren, Y. Dall'Agnese, P. Rozier, P.L. Taberna, M. Naguib, P. Simon, M.W. Barsoum, Y. Gogotsi, Cation intercalation and high volumetric capacitance of two-dimensional titanium carbide, Science 341 (2013) 1502e1505, https://doi.org/10.1126/science.1241488.

[58] D.G. Ladha, A review on density functional theoryebased study on two-dimensional materials used in batteries, Mater. Today Chem. 11 (2019) 94e111, https://doi.org/10.1016/J.MTCHEM.2018.10.006.

[59] U. Kumar, V. Gaikwad, M. Mayyas, V. Sahajwalla, R.K. Joshi, Extraordinary supercapacitance in activated carbon produced via a sustainable approach, J. Power Sources 394 (2018), https://doi.org/10.1016/ j.jpowsour.2018.05.054.

[60] M. Ghidiu, M.R. Lukatskaya, M.-Q. Zhao, Y. Gogotsi, M.W. Barsoum, Conductive two-dimensional titanium carbide 'clay' with high volumetric capacitance, Nature 516 (2014) 78, https://doi.org/10.1038/nature13970.

[61] J. Li, X. Yuan, C. Lin, Y. Yang, L. Xu, X. Du, J. Xie, J. Lin, J. Sun, Achieving high pseudocapacitance of 2D titanium carbide (MXene) by cation intercalation and surface modification, Adv. Energy Mater. 7 (2017) 1602725, https:// doi.org/10.1002/aenm.201602725.

[62] J. Xu, J. Shim, J.-H. Park, S. Lee, MXene electrode for the integration of WSe 2 and MoS 2 field effect transistors, Adv. Funct. Mater. 26 (2016) 5328e5334, https://doi.org/10.1002/adfm.201600771.

[63] X.-H. Zha, Q. Huang, J. He, H. He, J. Zhai, J.S. Francisco, S. Du, The thermal and electrical properties of the promising semiconductor MXene $Hf_2CO_2$, Sci. Rep. 6 (2016) 27971, https://doi.org/10.1038/srep27971.

[64] B. Anasori, C. Shi, E.J. Moon, Y. Xie, C.A. Voigt, P.R.C. Kent, S.J. May, S.J.L. Billinge, M.W. Barsoum, Y. Gogotsi, Control of electronic properties of 2D

carbides (MXenes) by manipulating their transition metal layers, Nano- scale Horizons 1 (2016) 227e234, https://doi.org/10.1039/C5NH00125K.

[65] Y. Shao, F. Zhang, X. Shi, H. Pan, N-Functionalized MXenes: ultrahigh carrier mobility and multifunctional properties, Phys. Chem. Chem. Phys. 19 (2017) 28710e28717, https://doi.org/10.1039/C7CP05816K.

[66] Z. Ling, C.E. Ren, M.-Q. Zhao, J. Yang, J.M. Giammarco, J. Qiu, M.W. Barsoum, Y. Gogotsi, Flexible and conductive MXene films and nanocomposites with high capacitance, Proc. Natl. Acad. Sci. U.S.A. 111 (2014) 16676e16681, https://doi.org/10.1073/pnas.1414215111.

[67] A.D. Dillon, M.J. Ghidiu, A.L. Krick, J. Griggs, S.J. May, Y. Gogotsi, M.W. Barsoum, A.T. Fafarman, Highly conductive optical quality solution- processed films of 2D titanium carbide, Adv. Funct. Mater. 26 (2016) 4162e4168, https://doi.org/10.1002/adfm.201600357.

[68] X. Wen, X. Jin, F. Wang, Y. You, D. Chu, P.B. Zetterlund, R.K. Joshi, Cation-induced coagulation in graphene oxide suspensions, Mater, Today Chem. 13 (2019) 139e146, https://doi.org/10.1016/j.mtchem.2019.06.003.

[69] V.N. Borysiuk, V.N. Mochalin, Y. Gogotsi, Bending rigidity of two-dimensional titanium carbide (MXene) nanoribbons: a molecular dynamics study, Com- put. Mater. Sci. 143 (2018) 418e424, https://doi.org/10.1016/J.COMMATSCI.2017.11.028.

[70] Q. Wang, Simulations of the bending rigidity of graphene, Phys. Lett. A 374 (2010) 1180e1183, https://doi.org/10.1016/J.PHYSLETA.2009.12.063.

[71] J.W. Kang, S. Lee, Molecular dynamics study on the bending rigidity of graphene nanoribbons, Comput. Mater. Sci. 74 (2013) 107e113, https://doi.org/10.1016/J.COMMATSCI.2013.03.009.

[72] J.-W. Jiang, Z. Qi, H.S. Park, T. Rabczuk, Elastic bending modulus of single-layer molybdenum disulfide ($MoS_2$): finite thickness effect, Nanotech- nology 24 (2013) 435705, https://doi.org/10.1088/0957-4484/24/43/435705.

[73] V.N. Borysiuk, V.N. Mochalin, Y. Gogotsi, Molecular dynamic study of the mechanical properties of two-dimensional titanium carbides $Ti_{nþ1}C_n$(M- Xenes), Nanotechnology 26 (2015) 265705, https://doi.org/10.1088/0957-4484/26/26/265705.

[74] A. Lipatov, H. Lu, M. Alhabeb, B. Anasori, A. Gruverman, Y. Gogotsi, A. Sinitskii, Elastic properties of 2D $Ti_3C_2T_x$MXene monolayers and bilayers, Sci. Adv. 4 (2018), https://doi.org/10.1126/sciadv.aat0491 eaat0491.

[75] J.W. Suk, R.D. Piner, J. An, R.S. Ruoff, Mechanical properties of monolayer graphene oxide, ACS Nano (2010), https://doi.org/10.1021/nn101781v.

[76] K. Liu, Q. Yan, M. Chen, W. Fan, Y. Sun, J. Suh, D. Fu, S. Lee, J. Zhou, S. Tongay, J. Ji, J.B. Neaton, J. Wu, Elastic properties of chemical-vapor-deposited monolayer $MoS_2$, $WS_2$, and their bilayer heterostructures, Nano Lett. 14 (2014) 5097e5103, https://doi.org/10.1021/nl501793a.

[77] K. Hantanasirisakul, M.-Q. Zhao, P. Urbankowski, J. Halim, B. Anasori, S. Kota, C.E. Ren, M.W. Barsoum, Y. Gogotsi, Fabrication of $Ti_3C_2T_x$ MXene transparent thin films with tunable optoelectronic properties, Adv. Electron. Mater. 2 (2016) 1600050, https://doi.org/10.1002/aelm.201600050.

[78] A. Miranda, J. Halim, A. Lorke, M.W. Barsoum, Rendering $Ti_3C_2T_x$(MXene) monolayers visible, Mater. Res. Lett. 5 (2017) 322e328, https://doi.org/10.1080/21663831.2017.1280707.

[79] P. Blake, E.W. Hill, A.H. Castro Neto, K.S. Novoselov, D. Jiang, R. Yang, T.J. Booth, A.K. Geim, Making graphene visible, Appl. Phys. Lett. 91 (2007), 063124, https://doi.org/10.1063/1.2768624.

[80] Y. Xia, T.S. Mathis, M.-Q. Zhao, B. Anasori, A. Dang, Z. Zhou, H. Cho, Y. Gogotsi, S. Yang, Thickness-independent capacitance of vertically aligned liquid-crystalline MXenes, Nature 557 (2018) 409e412, https://doi.org/10.1038/s41586-018-0109-z.

[81] T. Habib, X. Zhao, S.A. Shah, Y. Chen, W. Sun, H. An, J.L. Lutkenhaus, M. Radovic, M.J. Green, Oxidation stability of $Ti_3C_2T_x$ MXene nanosheets in solvents and composite films, Npj 2D Mater. Appl. 3 (2019) 8, https://doi.org/10.1038/s41699-019-0089-3.

[82] G. Deysher, S. Sin, Y. Gogotsi, B. Anasori, Oxidized 2D titanium carbide MXene: flash oxidized powders, Mater. Today 21 (2018) 1064e1065, https://doi.org/10.1016/J.MATTOD.2018.10.035.

[83] A. Lipatov, M. Alhabeb, M.R. Lukatskaya, A. Boson, Y. Gogotsi, A. Sinitskii, Effect of synthesis on quality, electronic properties and environmental sta- bility

of individual monolayer $Ti_3C_2$ MXene flakes, Adv. Electron. Mater. 2 (2016), 1600255, https://doi.org/10.1002/aelm.201600255.

[84] C.J. Zhang, S. Pinilla, N. McEvoy, C.P. Cullen, B. Anasori, E. Long, S.-H. Park, A. Seral-Ascaso, A. Shmeliov, D. Krishnan, C. Morant, X. Liu, G.S. Duesberg, Y. Gogotsi, V. Nicolosi, Oxidation stability of colloidal two-dimensional ti- tanium carbides (MXenes), Chem. Mater. 29 (2017) 4848e4856, https:// doi.org/10.1021/acs.chemmater.7b00745.

[85] S. Huang, V.N. Mochalin, Hydrolysis of 2D transition-metal carbides (MXenes) in colloidal solutions, Inorg. Chem. 58 (2019) 1958e1966, https:// doi.org/10.1021/acs.inorgchem.8b02890.

[86] J.H. Los, K.V. Zakharchenko, M.I. Katsnelson, A. Fasolino, Melting temperature of graphene, Phys. Rev. B. 91 (2015), 045415, https://doi.org/10.1103/ PhysRevB.91.045415.

[87] S.K. Singh, M. Neek-Amal, S. Costamagna, F.M. Peeters, Rippling, buckling, and melting of single- and multilayer $MoS_2$, Phys. Rev. B. 91 (2015), 014101, https://doi.org/10.1103/PhysRevB.91.014101.

[88] V. Borysiuk, V.N. Mochalin, Thermal stability of two-dimensional titanium carbides Tinþ1Cn (MXenes) from classical molecular dynamics simulations, MRS Commun 9 (2019) 203e208, https://doi.org/10.1557/mrc.2019.2.

[89] Q. Peng, J. Guo, Q. Zhang, J. Xiang, B. Liu, A. Zhou, R. Liu, Y. Tian, Unique lead adsorption behavior of activated hydroxyl group in two-dimensional tita- nium carbide, J. Am. Chem. Soc. 136 (2014) 4113e4116, https://doi.org/ 10.1021/ja500506k.

[90] Q. Zhang, J. Teng, G. Zou, Q. Peng, Q. Du, T. Jiao, J. Xiang, Efficient phosphate sequestration for water purification by unique sandwich-like MXene/ magnetic iron oxide nanocomposites, Nanoscale 8 (2016) 7085e7093, https://doi.org/10.1039/C5NR09303A.

[91] A. Shahzad, K. Rasool, W. Miran, M. Nawaz, J. Jang, K.A. Mahmoud, D.S. Lee, Two-dimensional $Ti_3C_2T_x$MXene nanosheets for efficient copper removal from water, ACS Sustain. Chem. Eng. 5 (2017) 11481e11488, https://doi.org/ 10.1021/acssuschemeng.7b02695.

[92] Y. Ying, Y. Liu, X. Wang, Y. Mao, W. Cao, P. Hu, X. Peng, Two-dimensional titanium carbide for efficiently reductive removal of highly toxic chro- mium(VI)

from water, ACS Appl. Mater. Interfaces 7 (2015) 1795e1803, https://doi.org/10.1021/am5074722.

[93] K. Rasool, M. Helal, A. Ali, C.E. Ren, Y. Gogotsi, K.A. Mahmoud, Antibacterial activity of $Ti_3C_2T_x$MXene, ACS Nano 10 (2016) 3674e3684, https://doi.org/10.1021/acsnano.6b00181.

[94] Jastrzębska, A.; Szuplewska, A.; Wojciechowski, T.; Chudy, M.; Ziemkowska, W.; Chlubny, L.; Rozmysłowska, A.; Olszyna, A. (2017). "In vitro studies on cytotoxicity of delaminated $Ti_3C_2$ MXene". *Journal of Hazardous Materials*. **339**: 1–8. doi:10.1016/j.jhazmat.2017.06.004. PMID 28601597.

[95] Lin, H.; Wang, X.; Yu, L.; Chen, Y.; Shi, J. (2017). "Two-Dimensional Ultrathin MXene Ceramic Nanosheets for Photothermal Conversion". *Nano Letters*. **17** (1): 384-391 doi:10.1021/acs.nanolett.6b04339. PMID 28026960.

[96] C.E. Ren, K.B. Hatzell, M. Alhabeb, Z. Ling, K.A. Mahmoud, Y. Gogotsi, Charge- and size-selective ion sieving through $Ti_3C_2T_x$MXene membranes, J. Phys. Chem. Lett. 6 (2015) 4026e4031, https://doi.org/10.1021/acs.jpclett.5b01895.

[97] R.P. Pandey, K. Rasool, V.E. Madhavan, B. Aïssa, Y. Gogotsi, K.A. Mahmoud, Ultrahigh-flux and fouling-resistant membranes based on layered silver/ MXene ($Ti_3C_2T_x$)nanosheets, J. Mater. Chem. A. 6 (2018) 3522e3533, https://doi.org/10.1039/C7TA10888E.

[98] L. Ding, Y. Wei, Y. Wang, H. Chen, J. Caro, H. Wang, A two-dimensional lamellar membrane: MXene nanosheet stacks, Angew. Chem. Int. Ed. 56 (2017) 1825e1829, https://doi.org/10.1002/anie.201609306.

[99] H. Liu, C. Duan, C. Yang, W. Shen, F. Wang, Z. Zhu, A novel nitrite biosensor based on the direct electrochemistry of hemoglobin immobilized on MXene-$Ti_3C_2$, Sens. Actuators B Chem. 218 (2015) 60e66, https://doi.org/10.1016/J.SNB.2015.04.090.

[100] F. Shahzad, M. Alhabeb, C.B. Hatter, B. Anasori, S. Man Hong, C.M. Koo, Y. Gogotsi, Electromagnetic interference shielding with 2D transition metal carbides (MXenes), Science 353 (2016) 1137e1140, https://doi.org/10.1126/science.aag2421.

[101] M. Han, X. Yin, H. Wu, Z. Hou, C. Song, X. Li, L. Zhang, L. Cheng, Ti3C2 MXenes with modified surface for high-performance electromagnetic absorption and shielding in the X-band, ACS Appl. Mater. Interfaces 8 (2016) 21011e21019, https://doi.org/10.1021/acsami.6b06455.

[102] Y. Qing, W. Zhou, F. Luo, D. Zhu, Titanium carbide (MXene) nanosheets as promising microwave absorbers, Ceram. Int. 42 (2016) 16412e16416, https://doi.org/10.1016/J.CERAMINT.2016.07.150.

[103] M. Han, X. Yin, X. Li, B. Anasori, L. Zhang, L. Cheng, Y. Gogotsi, Laminated and two-dimensional carbon-supported microwave absorbers derived from MXenes, ACS Appl. Mater. Interfaces 9 (2017) 20038e20045, https://doi.org/10.1021/acsami.7b04602.

[104] G. Choi, F. Shahzad, Y.-M. Bahk, Y.M. Jhon, H. Park, M. Alhabeb, B. Anasori, D.- S. Kim, C.M. Koo, Y. Gogotsi, M. Seo, Enhanced terahertz shielding of MXenes with nano-metamaterials, Adv. Opt. Mater. 6 (2018) 1701076, https:// doi.org/10.1002/adom.201701076.

[105] G.-M. Weng, J. Li, M. Alhabeb, C. Karpovich, H. Wang, J. Lipton, K. Maleski, J. Kong, E. Shaulsky, M. Elimelech, Y. Gogotsi, A.D. Taylor, Layer-by-Layer assembly of cross-functional semi-transparent MXene-carbon nanotubes composite films for next-generation electromagnetic interference shielding, Adv. Funct. Mater. (2018) 1803360, https://doi.org/10.1002/ adfm.201803360.

[106] H. Zhang, L. Wang, Q. Chen, P. Li, A. Zhou, X. Cao, Q. Hu, Preparation, mechanical and anti-friction performance of MXene/polymer composites, Mater. Des. 92 (2016) 682e689, https://doi.org/10.1016/ J.MATDES.2015.12.084.

[107] L. Ding, Y. Wei, L. Li, T. Zhang, H. Wang, J. Xue, L.-X. Ding, S. Wang, J. Caro, Y. Gogotsi, MXene molecular sieving membranes for highly efficient gas separation, Nat. Commun. 9 (2018) 155, https://doi.org/10.1038/s41467- 017-02529-6.

[108] Z.W. Seh, K.D. Fredrickson, B. Anasori, J. Kibsgaard, A.L. Strickler, M.R. Lukatskaya, Y. Gogotsi, T.F. Jaramillo, A. Vojvodic, Two-dimensional molybdenum carbide (MXene) as an efficient electrocatalyst for hydrogen evolution, ACS Energy Lett 1 (2016) 589e594, https://doi.org/10.1021/ acsenergylett.6b00247.

[109] H. An, T. Habib, S. Shah, H. Gao, M. Radovic, M.J. Green, J.L. Lutkenhaus, Surface-agnostic highly stretchable and bendable conductive MXene multi-layers, Sci. Adv. 4 (2018), https://doi.org/10.1126/sciadv.aaq0118 eaaq0118.

[110] G. Ying, A.D. Dillon, A.T. Fafarman, M.W. Barsoum, Transparent, conductive solution processed spincast 2D $Ti_2CTx$(MXene) films, Mater. Res. Lett. 5 (2017) 391e398, https://doi.org/10.1080/21663831.2017.1296043.

[111] C.J. Zhang, B. Anasori, A. Seral-Ascaso, S.-H. Park, N. McEvoy, A. Shmeliov, G.S. Duesberg, J.N. Coleman, Y. Gogotsi, V. Nicolosi, Transparent, flexible, and conductive 2D titanium carbide (MXene) films with high volumetric capacitance, Adv. Mater. 29 (2017) 1702678, https://doi.org/10.1002/ adma.201702678.

[112] J. Halim, M.R. Lukatskaya, K.M. Cook, J. Lu, C.R. Smith, L.-Å. Na€slund, S.J. May, L. Hultman, Y. Gogotsi, P. Eklund, M.W. Barsoum, Transparent conductive two-dimensional titanium carbide epitaxial thin films, Chem. Mater. 26 (2014) 2374e2381, https://doi.org/10.1021/cm500641a.

[113] X. Wu, Z. Wang, M. Yu, L. Xiu, J. Qiu, Stabilizing the MXenes by carbon nanoplating for developing hierarchical nanohybrids with efficient lithium storage and hydrogen evolution capability, Adv. Mater. 29 (2017), 1607017, https://doi.org/10.1002/adma.201607017.

[114] K. Rasool, K.A. Mahmoud, D.J. Johnson, M. Helal, G.R. Berdiyorov, Y. Gogotsi, Efficient antibacterial membrane based on two-dimensional Ti3C2Tx (MXene) nanosheets, Sci. Rep. 7 (2017) 1598, https://doi.org/10.1038/ s41598-017-01714-3.

[115] K. Rasool, R.P. Pandey, P.A. Rasheed, S. Buczek, Y. Gogotsi, K.A. Mahmoud, Water treatment and environmental remediation applications of two-dimensional metal carbides (MXenes), Mater. Today (2019), https://doi.org/10.1016/J.MATTOD.2019.05.017.

[116] M. Alhabeb, K. Maleski, B. Anasori, P. Lelyukh, L. Clark, S. Sin, Y. Gogotsi, Guidelines for synthesis and processing of two-dimensional titanium carbide ($Ti_3C_2T_x$ MXene), Chem. Mater. 29 (2017) 7633e7644, https://doi.org/10.1021/acs.chemmater.7b02847.

[117] M. Alhabeb, K. Maleski, T.S. Mathis, A. Sarycheva, C.B. Hatter, S. Uzun, A. Levitt, Y. Gogotsi, Selective etching of silicon from $Ti_3SiC_2$ (MAX) to obtain 2D titanium carbide (MXene), Angew. Chem. 130 (2018) 5542e5546, https://doi.org/10.1002/ange.201802232.

[118] O. Salim, K.A. Mahmoud, K.K. Pant, R.K. Joshi; Introduction to MXenes: synthesis and characteristics; Materials Today Chemistry 14 (2019) 100191 https://doi.org/10.1016/j.mtchem.2019.08.010

[119] Karahan, Goh, Zhang, Yang, Yildrim, Chuah, Ahunbay, Lee, Ersolmaz, Chen, Bae, MXene Materials for Designing Advanced Separation Membranes, Adv. Mater. 2020, 32, 1906697, https://doi.org/10.1002/adma.201906697.

[120] Y. Al-Hamadani, B. Jun, M. Yoon, N. Taheri-Qazvini, S. A. Snyder, M. Jang, Y. Yoon, Applications of MXene-based membranes in water purification: a review, Chemosphere 254 (2020) 126821 https://doi.org/10.1016/j.chemosphere.2020.126821

## PART 2

[1] M. M. Pendergast, E. M. V. Hoek, A review of water treatment membrane nanotechnologies, Energy Environ. Sci. 2011, 4, 1946.

[2] X. Qu, J. Brame, Q. Li, P. J. J. Alvarez, Nanotechnology for a Safe and Sustainable Water Supply: Enabling Integrated Water Treatment and Reuse, Acc. Chem. Res. 2013, 46, 834.

[3] P. S. Goh, A. F. Ismail, N. Hilal, Nano-enabled membranes technology: Sustainable and revolutionary solutions for membrane desalination?, Desalination 2016, 380, 100.

[4] Y. Manawi, V. Kochkodan, M. A. Hussein, M. A. Khaleel, M. Khraisheh, N. Hilal, Can carbon-based nanomaterials revolutionize membrane fabrication for water treatment and desalination?, Desalination 2016, 391, 69.

[5] C. Y. Chuah, K. Goh, Y. Yang, H. Gong, W. Li, H. E. Karahan, M. D. Guiver, R. Wang, T.-H. Bae, Enhanced $O_2/N_2$ Separation of Mixed-Matrix Membrane Filled with Pluronic-Compatibilized Cobalt Phthalocyanine Particles, Chem. Rev. 2018, 118, 8655. doi: 10.1021/acs.chemrev.8b00091.

[6] G. Liu, W. Jin, N. Xu, Graphene-based membranes, Chem. Soc. Rev. 2015, 44, 5016.

[7] K. Goh, H. E. Karahan, L. Wei, T. Bae, A. G. Fane, R. Wang, Y. Chen, Carbon nanomaterials for advancing separation membranes: A strategic perspective, Carbon 2016, 109, 694.

[8] F. Moghadam, H. B. Park, Two-dimensional materials: an emerging platform for gas separation membranes, Curr. Opin. Chem. Eng. 2018, 20, 28.

[9] J. Zhu, J. Hou, A. Uliana, Y. Zhang, M. Tian, B. Van der Bruggen, The rapid emergence of two-dimensional nanomaterials for high-performance separation membranes, J. Mater. Chem. A 2018, 6, 3773.

[10] G. Liu, W. Jin, N. Xu, Two-Dimensional-Material Membranes: A New Family of High-Performance Separation Membranes, Angew. Chem., Int. Ed. 2016, 55, 13384.

[11] M. Alhabeb, K. Maleski, B. Anasori, P. Lelyukh, L. Clark, S. Sin, Y. Gogotsi, Guidelines for Synthesis and Processing of Two-Dimensional Titanium Carbide ($Ti_3C_2T_x$ MXene), Chem. Mater. 2017, 29, 7633.

[12] Y. Gogotsi, B. Anasori, The Rise of MXenes, ACS Nano 2019, 13, 8491.

[13] V. H. Nowotny, Strukturchemie einiger Verbindungen der Übergangsmetalle mit den elementen C, Si, Ge, Sn, Prog. Solid State Chem. 1971, 5, 27.

[14] M. W. Barsoum, The $M_{N+1}AX_N$ phases: A new class of solids: Thermodynamically stable nanolaminates, Prog. Solid State Chem. 2000, 28, 201.

[15] P. Eklund, M. Beckers, U. Jansson, H. Högberg, L. Hultman, The $M_{n+1}AX_n$ phases: Materials science and thin-film processing, Thin Solid Films 2010, 518, 1851.

[16] M. Sokol, V. Natu, S. Kota, M. W. Barsoum, On the Chemical Diversity of the MAX Phases, Trends Chem. 2019, 1, 210.

[17] L. Verger, V. Natu, M. Carey, M. W. Barsoum, MXenes: An Introduction of Their Synthesis, Select Properties, and Applications, Trends Chem. 2019, 1, 656.

[18] X. Wu, X. Cui, W. Wu, J. Wang, Y. Li, Z. Jiang, Elucidating Ultrafast Molecular Permeation through Well-Defined 2D Nanochannels of Lamellar Membranes, Angew. Chem., Int. Ed. 2019, 58, 18524.

[19] M. Naguib, M. Kurtoglu, V. Presser, J. Lu, J. Niu, M. Heon, L. Hultman, Y. Gogotsi, M. W. Barsoum, Two-Dimensional Nanocrystals Produced by Exfoliation of $Ti_3AlC_2$, Adv. Mater. 2011, 23, 4248.

[20] M. Naguib, O. Mashtalir, J. Carle, V. Presser, J. Lu, L. Hultman, Y. Gogotsi, M. W. Barsoum, ACS Nano 2012, 6, 1322.

[21] M. Kurtoglu, M. Naguib, Y. Gogotsi, M. W. Barsoum, Two-Dimensional Transition Metal Carbides, MRS Commun. 2012, 2, 133.

[22] K. Rasool, M. Helal, A. Ali, C. E. Ren, Y. Gogotsi, K. A. Mahmoud, Antibacterial Activity of $Ti_3C_2T_x$ MXene, ACS Nano 2016, 10, 3674.

[23] X.-H. Zha, J. Yin, Y. Zhou, Q. Huang, K. Luo, J. Lang, J. S. Francisco, J. He, S. Du, Intrinsic Structural, Electrical, Thermal, and Mechanical Properties of the Promising Conductor $Mo_2C$ MXene, J. Phys. Chem. C 2016, 120, 15082.

[24] A. Lipatov, H. Lu, M. Alhabeb, B. Anasori, A. Gruverman, Y. Gogotsi, A. Sinitskii, Elastic properties of 2D $Ti_3C_2T_x$ MXene monolayers and bilayers, Sci. Adv. 2018, 4, eaat0491.

[25] M. Naguib, V. N. Mochalin, M. W. Barsoum, Y. Gogotsi, 25th Anniversary Article: MXenes: A New Family of Two-Dimensional Materials, Adv. Mater. 2014, 26, 992.

[26] M. Naguib, Y. Gogotsi, Synthesis of Two-Dimensional Materials by Selective Extraction, Acc. Chem. Res. 2015, 48, 128.

[27] V. M. Hong Ng, H. Huang, K. Zhou, P. S. Lee, W. Que, J. Z. Xu, L. B. Kong, Recent progress in layered transition metal carbides and/or nitrides (MXenes) and their composites: synthesis and applications, J. Mater. Chem. A 2017, 5, 3039.

[28] M. Khazaei, A. Ranjbar, K. Esfarjani, D. Bogdanovski, R. Dronskowski, S. Yunoki, Phys. Chem. Chem. Phys. 2018, 20, 8579.

[29] X. Xiao, H. Wang, P. Urbankowski, Y. Gogotsi, Insights into exfoliation possibility of MAX phases to MXenes, Chem. Soc. Rev. 2018, 47, 8744.

[30] M. Khazaei, A. Mishra, N. S. Venkataramanan, A. K. Singh, S. Yunoki, Recent advances in MXenes: From fundamentals to applications, Curr. Opin. Solid State Mater. Sci. 2019, 23, 164.

[31] R. M. Ronchi, J. T. Arantes, S. F. Santos, Synthesis, structure, properties and applications of MXenes: Current status and perspectives, Ceram. Int. 2019, 45, 18167.

[32] B. Anasori, M. R. Lukatskaya, Y. Gogotsi, 2D metal carbides and nitrides (MXenes) for energy storage, Nat. Rev. Mater. 2017, 2, 16098.

[33] H. Wang, Y. Wu, X. Yuan, G. Zeng, J. Zhou, X. Wang, J. W. Chew, Formation of quasi-core-shell $In_2S_3$/anatase $TiO_2$@metallic $Ti_3C_2T_x$ hybrids with favorable charge transfer channels for excellent visible-light-photocatalytic performance, Adv. Mater. 2018, 30, 1704561.

[34] X. Li, C. Wang, Y. Cao, G. Wang, Functional MXene Materials: Progress of Their Applications, Chem. - Asian J. 2018, 13, 2742.

[35] J. Pang, R. G. Mendes, A. Bachmatiuk, L. Zhao, H. Q. Ta, T. Gemming, H. Liu, Z. Liu, M. H. Rummeli, Applications of 2D MXenes in energy conversion and storage systems, Chem. Soc. Rev. 2019, 48, 72.

[36] C. J. Zhang, Y. Ma, X. Zhang, S. Abdolhosseinzadeh, H. Sheng, W. Lan, A. Pakdel, J. Heier, F. Nüesch, Energy Environ. Mater. 2020, 3, 29.

[37] J. Zhu, E. Ha, G. Zhao, Y. Zhou, D. Huang, G. Yue, L. Hu, N. Sun, Y. Wang, L. Y. S. Lee, C. Xu, K.-Y. Wong, D. Astruc, P. Zhao, Recent advance in MXenes: A promising 2D material for catalysis, sensor and chemical adsorption, Coord. Chem. Rev. 2017, 352, 306.

[38] H. Lin, Y. Chen, J. Shi, Insights into 2D MXenes for Versatile Biomedical Applications: Current Advances and Challenges Ahead, Adv. Sci. 2018, 5, 1800518.

[39] K. Huang, Z. Li, J. Lin, G. Han, P. Huang, Two-dimensional transition metal carbides and nitrides (MXenes) for biomedical applications, Chem. Soc. Rev. 2018, 47, 5109.

[40] M. Soleymaniha, M.-A. Shahbazi, A. R. Rafieerad, A. Maleki, A. Amiri, A nontoxic biocompatible nanocomposite comprising black phosphorus with Au–γ-$Fe_2O_3$ nanoparticles, Adv. Healthcare Mater. 2019, 8, 1801137.

[41] Y. Zhang, L. Wang, N. Zhang, Z. Zhou, Adsorptive environmental applications of MXene nanomaterials: a review, RSC Adv. 2018, 8, 19895.

[42] B.-M. Jun, S. Kim, J. Heo, C. M. Park, N. Her, M. Jang, Y. Huang, J. Han, Y. Yoon, Review of MXenes as new nanomaterials for energy storage/delivery and selected environmental applications, Nano Res. 2019, 12, 471.

[43] L. Huang, H. Lin, Engineering Sub-Nanometer Channels in Two-Dimensional Materials for Membrane Gas Separation, Membranes 2018, 8, 100.

[44] S. Kim, H. Wang, Y. M. Lee, 2D Nanosheets and Their Composite Membranes for Water, Gas, and Ion Separation, Angew. Chem., Int. Ed. 2019, 58, 17512.

[45] Y. Kang, Y. Xia, H. Wang, X. Zhang, 2D Laminar Membranes for Selective Water and Ion Transport, Adv. Funct. Mater. 2019, 29, 1902014.

[46] T. Hyun, J. Jeong, A. Chae, Y. K. Kim, D.-Y. Koh, 2D-enabled membranes: materials and beyond, BMC Chem. Eng. 2019, 1, 12.

[47] K. Rasool, R. P. Pandey, P. A. Rasheed, S. Buczek, Y. Gogotsi, K. A. Mahmoud, Water treatment and environmental remediation applications of two-dimensional metal carbides (MXenes), Mater. Today 2019, 30, 80.

[48] P. Srimuk, F. Kaasik, B. Krüner, A. Tolosa, S. Fleischmann, N. Jäckel, M. C. Tekeli, M. Aslan, M. E. Suss, V. Presser, MXene as a novel intercalation-type pseudocapacitive cathode and anode for capacitive deionization, J. Mater. Chem. A 2016, 4, 18265.

[49] W. Bao, X. Tang, X. Guo, S. Choi, C. Wang, Y. Gogotsi, G. Wang, Porous Cryo-Dried MXene for Efficient Capacitive Deionization, Joule 2018, 2, 778.

[50] Q. Zhang, J. Teng, G. Zou, Q. Peng, Q. Du, T. Jiao, J. Xiang, Efficient phosphate sequestration for water purification by unique sandwich-like MXene/magnetic iron oxide nanocomposites, Nanoscale 2016, 8, 7085.

[51] A. Shahzad, K. Rasool, W. Miran, M. Nawaz, J. Jang, K. A. Mahmoud, D. S. Lee, Two-Dimensional $Ti_3C_2T_x$ MXene Nanosheets for Efficient Copper Removal from Water, ACS Sustainable Chem. Eng. 2017, 5, 11481.

[52] N.-N. Wang, H. Wang, Y. Wang, Y. Wei, J. Si, A. C. Y. Yuen, J. Xie, B. Yu, S. Zhu, H. Lu, W. Yang, Q. N. Chan, G. Yeoh, Robust, Lightweight, Hydrophobic, and Fire-Retarded Polyimide/MXene Aerogels for Effective Oil/Water Separation, ACS Appl. Mater. Interfaces 2019, 11, 40512.

[53] C. Xu, L. Wang, Z. Liu, L. Chen, J. Guo, N. Kang, X.-L. Ma, H.-M. Cheng, W. Ren, Large-area high-quality 2D ultrathin $Mo_2C$ superconducting crystals, Nat. Mater. 2015, 14, 1135.

[54] J. Zhou, X. Zha, F. Y. Chen, Q. Ye, P. Eklund, S. Du, Q. Huang, A Two-Dimensional Zirconium Carbide by Selective Etching of $Al_3C_3$ from Nanolaminated $Zr_3Al_3C_5$, Angew. Chem., Int. Ed. 2016, 55, 5008.

[55] J. Zhou, X. Zha, X. Zhou, F. Chen, G. Gao, S. Wang, C. Shen, T. Chen, C. Zhi, P. Eklund, S. Du, J. Xue, W. Shi, Z. Chai, Q. Huang, Synthesis and Electrochemical Properties of Two-Dimensional Hafnium Carbide, ACS Nano 2017, 11, 3841.

[56] M. Malaki, A. Maleki, R. S. Varma, MXenes and ultrasonication, J. Mater. Chem. A 2019, 7, 10843.

[57] M. Naguib, J. Come, B. Dyatkin, V. Presser, P. L. Taberna, P. Simon, M. W. Barsoum, Y. Gogotsi, MXene: a promising transition metal carbide anode for lithium-ion batteries, Electrochem. Commun. 2012, 16, 61.

[58] C. Li, S. Kota, C. Hu, M. W. Barsoum, On the Synthesis of Low-Cost, Titanium-Based MXenes, J. Ceram. Sci. Technol. 2016, 7, 301.

[59] M. Alhabeb, K. Maleski, T. S. Mathis, A. Sarycheva, C. B. Hatter, S. Uzun, A. Levitt, Y. Gogotsi, Selective Etching of Silicon from $Ti_3SiC_2$ (MAX) To Obtain 2D Titanium Carbide (MXene), Angew. Chem., Int. Ed. 2018, 57, 5444.

[60] C. E. Ren, K. B. Hatzell, M. Alhabeb, Z. Ling, K. A. Mahmoud, Y. Gogotsi, Charge- and Size-Selective Ion Sieving Through $Ti_3C_2T_x$ MXene Membranes, J. Phys. Chem. Lett. 2015, 6, 4026.

[61] J. Halim, M. R. Lukatskaya, K. M. Cook, J. Lu, C. R. Smith, L.-Å. Näslund, S. J. May, L. Hultman, Y. Gogotsi, P. Eklund, M. W. Barsoum, Transparent Conductive Two-Dimensional Titanium Carbide Epitaxial Thin Films, Chem. Mater. 2014, 26, 2374.

[62] L. H. Karlsson, J. Birch, J. Halim, M. W. Barsoum, P. O. Å. Persson, Atomically Resolved Structural and Chemical Investigation of Single MXene Sheets, Nano Lett. 2015, 15, 4955.

[63] L. Wang, H. Zhang, B. Wang, C. Shen, C. Zhang, Q. Hu, A. Zhou, B. Liu, Synthesis and electrochemical performance of $Ti_3C_2T_x$ with hydrothermal process, Electron. Mater. Lett. 2016, 12, 702.

[64] C. J. Zhang, M. P. Kremer, A. Seral-Ascaso, S.-H. Park, N. McEvoy, B. Anasori, Y. Gogotsi, V. Nicolosi, Adv. Funct. Mater. 2018, 28, 1705506.

[65] P. Lakhe, E. M. Prehn, T. Habib, J. L. Lutkenhaus, M. Radovic, M. S. Mannan, M. J. Green, Process Safety Analysis for $Ti_3C_2T_x$ MXene Synthesis and Processing, Ind. Eng. Chem. Res. 2019, 58, 1570.

[66] F. Du, H. Tang, L. Pan, T. Zhang, H. Lu, J. Xiong, J. Yang, C. J. Zhang, Environmental Friendly Scalable Production of Colloidal 2D Titanium Carbonitride MXene with Minimized Nanosheets Restacking for Excellent Cycle Life Lithium-Ion Batteries, Electrochim. Acta 2017, 235, 690.

[67] C. Zhang, S.-H. Park, A. Seral-Ascaso, S. Barwich, N. McEvoy, C. S. Boland, J. N. Coleman, Y. Gogotsi, V. Nicolosi, High capacity silicon anodes enabled by MXene viscous aqueous ink, Nat. Commun. 2019, 10, 849.

[68] C. J. Zhang, B. Anasori, A. Seral-Ascaso, S.-H. Park, N. McEvoy, Shmeliov, G. S. Duesberg, J. N. Coleman, Y. Gogotsi, V. Nicolosi, Transparent, Flexible, and Conductive 2D Titanium Carbide (MXene) Films with High Volumetric Capacitance, Adv. Mater. 2017, 29, 1702678.

[69] C. J. Zhang, S. Pinilla, N. McEvoy, C. P. Cullen, B. Anasori, E. Long, S.-H. Park, A. Seral-Ascaso, A. Shmeliov, D. Krishnan, C. Morant, X. Liu, G. S. Duesberg, Y. Gogotsi, V. Nicolosi, Oxidation Stability of Colloidal Two-Dimensional Titanium Carbides (MXenes), Chem. Mater. 2017, 29, 4848.

[70] J. Shen, G. Liu, Y. Ji, Q. Liu, L. Cheng, K. Guan, M. Zhang, G. Liu, J. Xiong, J. Yang, W. Jin, 2D MXene Nanofilms with Tunable Gas Transport Channels, Adv. Funct. Mater. 2018, 28, 1801511.

[71] L. Ding, Y. Wei, Y. Wang, H. Chen, J. Caro, H. Wang, A two-dimensional lamellar membrane: MXene nanosheet stacks, Angew. Chem., Int. Ed. 2017, 56, 1825.

[72] X. Xie, C. Chen, N. Zhang, Z.-R. Tang, J. Jiang, Y.-J. Xu, Microstructure and surface control of MXene films for water purification, Nat. Sustainability 2019, 2, 856.

[73] G. Liu, L. Cheng, G. Chen, F. Liang, G. Liu, W. Jin, Pebax-Based Membrane Filled with Two-Dimensional Mxene Nanosheets for Efficient $CO_2$ Capture, Chem. - Asian J. https://doi.org/10.1002/asia.201901433.

[74] M. A. Hope, A. C. Forse, K. J. Griffith, M. R. Lukatskaya, M. Ghidiu, Y. Gogotsi, C. P. Grey, NMR reveals the surface functionalisation of Ti 3 C 2 MXene, Phys. Chem. Chem. Phys. 2016, 18, 5099.

[75] X. Wu, L. Hao, J. Zhang, X. Zhang, J. Wang, J. Liu, Polymer-Ti3C2Tx composite membranes to overcome the trade-off in solvent resistant nanofiltration for alcohol-based system, J. Membr. Sci. 2016, 515, 175.

[76] J. Luo, W. Zhang, H. Yuan, C. Jin, L. Zhang, H. Huang, C. Liang, Y. Xia, J. Zhang, Y. Gan, X. Tao, Pillared structure design of MXene with ultralarge interlayer spacing for high-performance lithium-ion capacitors, ACS Nano 2017, 11, 2459.

[77] Z. Huang, S. Wang, S. Kota, Q. Pan, M. W. Barsoum, C. Y. Li, Structure and crystallization behavior of poly (ethylene oxide)/Ti3C2Tx MXene nanocomposites, Polymer 2016, 102, 119.

[78] Z. Ling, C. E. Ren, M.-Q. Zhao, J. Yang, J. M. Giammarco, J. Qiu, M. W. Barsoum, Y. Gogotsi, Flexible and conductive MXene films and nanocomposites with high capacitance, Proc. Natl. Acad. Sci. USA 2014, 111, 16676.

[79] L. Hao, H. Zhang, X. Wu, J. Zhang, J. Wang, Y. Li, Novel thin-film nanocomposite membranes filled with multi-functional Ti3C2Tx nanosheets for task-specific solvent transport, Composites, Part A 2017, 100, 139.

[80] K. Wang, Y. Zhou, W. Xu, D. Huang, Z. Wang, M. Hong, Fabrication and thermal stability of two-dimensional carbide Ti3C2 nanosheets, Ceram. Int. 2016, 42, 8419.

[81] D. Xiong, X. Li, Z. Bai, S. Lu, Recent Advances in Layered $Ti_3C_2T_x$ MXene for Electrochemical Energy Storage, Small 2018, 14, 1703419.

[82] T. Habib, X. Zhao, S. A. Shah, Y. Chen, W. Sun, H. An, J. L. Lutkenhaus, M. Radovic, M. J. Green, Oxidation stability of Ti 3 C 2 T x MXene nanosheets in solvents and composite films, npj 2D Mater. Appl. 2019, 3, 8.

[83] Y. Lee, S. J. Kim, Y.-J. Kim, Y. Lim, Y. Chae, B.-J. Lee, Y.-T. Kim, H. Han, Y. Gogotsi, A. C. Won, Oxidation-resistant titanium carbide MXene films, J. Mater. Chem. A 2019, 8, 573.

[84] C. E. Ren, M. Alhabeb, B. W. Byles, M.-Q. Zhao, B. Anasori, E. Pomerantseva, K. A. Mahmoud, Y. Gogotsi, Voltage-Gated Ions Sieving through 2D MXene $Ti_3C_2T_x$ Membranes, ACS Appl. Nano Mater. 2018, 1, 3644.

[85] K. Rasool, K. A. Mahmoud, D. J. Johnson, M. Helal, G. R. Berdiyorov, Y. Gogotsi, Efficient antibacterial membrane based on two-dimensional Ti 3 C 2 T x (MXene) nanosheets, Sci. Rep. 2017, 7, 1598.

[86] R. P. Pandey, K. Rasool, V. E. Madhavan, B. Aïssa, Y. Gogotsi, K. A. Mahmoud, Ultrahigh-flux and fouling-resistant membranes based on layered silver/MXene (Ti 3 C 2 T x) nanosheets, J. Mater. Chem. A 2018, 6, 3522.

[87] X. Gao, Z.-K. Li, J. Xue, Y. Qian, L.-Z. Zhang, J. Caro, H. Wang, Titanium carbide Ti3C2Tx (MXene) enhanced PAN nanofiber membrane for air purification, J. Membr. Sci. 2019, 586, 162.

[88] V. Natu, M. Sokol, L. Verger, M. W. Barsoum, Effect of Edge Charges on Stability and Aggregation of $Ti_3C_2T_z$ MXene Colloidal Suspensions, J. Phys. Chem. C 2018, 122, 27745.

[89] L. Ding, Y. Wei, L. Li, T. Zhang, H. Wang, J. Xue, L.-X. Ding, S. Wang, J. Caro, Y. Gogotsi, MXene molecular sieving membranes for highly efficient gas separation, Nat. Commun. 2018, 9, 155.

[90] W. L. Xu, C. Fang, F. Zhou, Z. Song, Q. Liu, R. Qiao, M. Yu, Self-assembly: a facile way of forming ultrathin, high-performance graphene oxide membranes for water purification, Nano Lett. 2017, 17, 2928.

[91] H. Zhou, Y. Wang, F. Wang, H. Deng, Y. Song, C. Li, Z. Ling, Water permeability in MXene membranes: Process matters, Chin. Chem. Lett. https://doi.org/10.1016/j.cclet.2019.10.037.

[92] Z. Xu, Y. Sun, Y. Zhuang, W. Jing, H. Ye, Z. Cui, Assembly of 2D MXene nanosheets and TiO2 nanoparticles for fabricating mesoporous TiO2-MXene membranes, J. Membr. Sci. 2018, 564, 35.

[93] B. Akuzum, K. Maleski, B. Anasori, P. Lelyukh, N. J. Alvarez, E. C. Kumbur, Y. Gogotsi, Rheological characteristics of 2D titanium carbide (MXene) dispersions: a guide for processing MXenes, ACS Nano 2018, 12, 2685.

[94] K. M. Kang, D. W. Kim, C. E. Ren, K. M. Cho, S. J. Kim, J. H. Choi, Y. T. Nam, Y. Gogotsi, H.-T. Jung, Selective Molecular Separation on $Ti_3C_2T_x$–Graphene Oxide Membranes during Pressure-Driven Filtration: Comparison with Graphene Oxide and MXenes, ACS Appl. Mater. Interfaces 2017, 9, 44687.

[95] K. Maleski, V. N. Mochalin, Y. Gogotsi, Dispersions of two-dimensional titanium carbide MXene in organic solvents, Chem. Mater. 2017, 29, 1632.

[96] Z. Xu, G. Liu, H. Ye, W. Jin, Z. Cui, Two-dimensional MXene incorporated chitosan mixed-matrix membranes for efficient solvent dehydration, J. Membr. Sci. 2018, 563, 625.

[97] Q. Luan, Y. Xie, D. Teng, R. Han, S. Zhang, Preparation of new 2D MXene/cellulose acetate mixed matrix membrane with excellent performance, Desalin. Water Treat. 2018, 108, 90.

[98] R. Mahajan, W. J. Koros, M. Thundyil, Membr. Technol. 1999, 1999, 6.

[99] T.-S. Chung, L. Y. Jiang, Y. Li, S. Kulprathipanja, Mixed matrix membranes (MMMs) comprising organic polymers with dispersed inorganic fillers for gas separation, Prog. Polym. Sci. 2007, 32, 483.

[100] M. A. Aroon, A. F. Ismail, T. Matsuura, M. M. Montazer-Rahmati, Performance studies of mixed matrix membranes for gas separation: A review, Sep. Purif. Technol. 2010, 75, 229.

[101] D. Qadir, H. Mukhtar, L. K. Keong, Mixed matrix membranes for water purification applications, Sep. Purif. Rev. 2017, 46, 62.

[102] Y. Jin, Y. Fan, X. Meng, W. Zhang, B. Meng, N. Yang, S. Liu, Theoretical and experimental insights into the mechanism for gas separation through nanochannels in 2D laminar MXene membranes, Processes 2019, 7, 751.

[103] L. M. Robeson, The upper bound revisited, J. Membr. Sci. 2008, 320, 390.

[104] J. G. Wijmans, R. W. Baker, The solution-diffusion model: a review, J. Membr. Sci. 1995, 107, 1.

[105] M. Mulder, Basic Principles of Membrane Technology, Springer, Dordrecht, Netherlands 1996.

[106] M. Galizia, W. S. Chi, Z. P. Smith, T. C. Merkel, R. W. Baker, B. D. Freeman, 50th Anniversary Perspective: Polymers and Mixed Matrix Membranes for Gas and Vapor Separation: A Review and Prospective Opportunities, Macromolecules 2017, 50, 7809.

[107] A. G. Fane, R. Wang, M. X. Hu, Synthetic membranes for water purification: status and future, Angew. Chem., Int. Ed. 2015, 54, 3368.

[108] J. M. Peeters, J. Boom, M. H. Mulder, H. Strathmann, Retention measurements of nanofiltration membranes with electrolyte solutions, J. Membr. Sci. 1998, 145, 199.

[109] J. Wang, P. Chen, B. Shi, W. Guo, M. Jaroniec, S.-Z. Z. Qiao, A regularly channeled lamellar membrane for unparalleled water and organics permeation, Angew. Chem., Int. Ed. 2018, 57, 6814.

[110] J. A. Mason, T. M. McDonald, T.-H. Bae, J. E. Bachman, K. Sumida, J. J. Dutton, S. S. Kaye, J. R. Long, Application of a High-Throughput Analyzer in Evaluating Solid Adsorbents for Post-Combustion Carbon Capture via Multicomponent Adsorption of $CO_2$, $N_2$, and $H_2O$, J. Am. Chem. Soc. 2015, 137, 4787.

[111] Y. Yang, C. Y. Chuah, H. Gong, T.-H. Bae, Robust microporous organic copolymers containing triphenylamine for high pressure CO2 capture application, J. CO2 Util. 2017, 19, 214.

[112] Y. Yang, C. Y. Chuah, T.-H. Bae, Polyamine-appended porous organic polymers for efficient post-combustion CO2 capture, Chem. Eng. J. 2019, 358, 1227.

[113] Y. Fan, L. Wei, X. Meng, W. Zhang, N. Yang, Y. Jin, X. Wang, M. Zhao, S. Liu, An unprecedented high-temperature-tolerance 2D laminar MXene membrane for ultrafast hydrogen sieving, J. Membr. Sci. 2019, 569, 117.

[114] A. A. Shamsabadi, A. Pournaghshband Isfahani, S. Khoshhal Salestan, A. Rahimpour, B. Ghalei, E. Sivaniah, M. Soroush, Pushing Rubbery Polymer Membranes To Be Economic for $CO_2$ Separation: Embedment with $Ti_3C_2T_x$ MXene Nanosheets, ACS Appl. Mater. Interfaces 2020, 12, 3984.

[115] Comparative Dosimetry of Radon in Mines and Homes, National Academies Press, Washington, D.C., USA 1991.

[116] T. Liu, X. Liu, N. Graham, W. Yu, K. Sun, Two-dimensional MXene incorporated graphene oxide composite membrane with enhanced water purification performance, J. Membr. Sci. 2020, 593, 117431.

[117] Y. Sun, Z. Xu, Y. Zhuang, G. Liu, W. Jin, G. Liu, W. Jing, Tunable dextran retention of MXene-TiO2 mesoporous membranes by adjusting the 2D MXene content, 2D Mater. 2018, 5, 045003.

[118] F. Alimohammadi, M. Sharifian, N. H. Attanayake, A. C. Thenuwara, Y. Gogotsi, B. Anasori, D. R. Strongin, Antimicrobial Properties of 2D $MnO_2$ and $MoS_2$ Nanomaterials Vertically Aligned on Graphene Materials and $Ti_3C_2$ MXene, Langmuir 2018, 34, 7192.

[119] J. Saththasivam, K. Wang, W. Yiming, Z. Liu, K. A. Mahmoud, A flexible Ti 3 C 2 T x (MXene)/paper membrane for efficient oil/water separation, RSC Adv. 2019, 9, 16296.

[120] Z.-K. Li, Y. Liu, L. Li, Y. Wei, J. Caro, H. Wang, Ultra-thin titanium carbide (MXene) sheet membranes for high-efficient oil/water emulsions separation, J. Membr. Sci. 2019, 592, 117361.

[121] R. Han, X. Ma, Y. Xie, D. Teng, S. Zhang, Preparation of a new 2D MXene/PES composite membrane with excellent hydrophilicity and high flux, RSC Adv. 2017, 7, 56204.

[122] B. Mi, Graphene oxide membranes for ionic and molecular sieving, Science 2014, 343, 740.

[123] Y. Sun, S. Li, Y. Zhuang, G. Liu, W. Xing, W. Jing, Adjustable interlayer spacing of ultrathin MXene-derived membranes for ion rejection, J. Membr. Sci. 2019, 591, 117350.

[124] Z. Lu, Y. Wei, J. Deng, L. Ding, Z. Li, H. Wang, Self-Crosslinked MXene ($Ti_3C_2T_x$) Membranes with Good Antiswelling Property for Monovalent Metal Ion Exclusion, ACS Nano 2019, 13, 10535.

[125] R. Li, L. Zhang, L. Shi, P. Wang, MXene $Ti_3C_2$: An Effective 2D Light-to-Heat Conversion Material, ACS Nano 2017, 11, 3752.

[126] J. Zhao, Y. Yang, C. Yang, Y. Tian, Y. Han, J. Liu, X. Yin, W. Que, A hydrophobic surface enabled salt-blocking 2D Ti 3 C 2 MXene membrane for efficient and stable solar desalination, J. Mater. Chem. A 2018, 6, 16196.

[127] Y. Z. Tan, H. Wang, L. Han, M. B. Tanis-Kanbur, M. V. Pranav, J. W. Chew, Photothermal-enhanced and fouling-resistant membrane for solar-assisted membrane distillation, J. Membr. Sci. 2018, 565, 254.

[128] X. Zha, X. Zhao, J. Pu, L. Tang, K. Ke, R. Bao, L. Bai, Z. Liu, M.-B. Yang, W. Yang, Flexible anti-biofouling MXene/cellulose fibrous membrane for sustainable solar-driven water purification, ACS Appl. Mater. Interfaces 2019, 11, 36589. A.

[129] Zandiatashbar, G. H. Lee, S. J. An, S. Lee, N. Mathew, M. Terrones, T. Hayashi, C. R. Picu, J. Hone, N. Koratkar, Effect of defects on the intrinsic strength and stiffness of graphene, Nat. Commun. 2014, 5, 3186.

[130] S. Wei, Y. Xie, Y. Xing, L. Wang, H. Ye, X. Xiong, S. Wang, K. Han, Two-dimensional graphene oxide/MXene composite lamellar membranes for efficient solvent permeation and molecular separation, J. Membr. Sci. 2019, 582, 414.

[131] G. Liu, J. Shen, Y. Ji, Q. Liu, G. Liu, J. Yang, W. Jin, Two-dimensional Ti 2 CT x MXene membranes with integrated and ordered nanochannels for efficient solvent dehydration, J. Mater. Chem. A 2019, 7, 12095.

[132] Y. Wu, L. Ding, Z. Lu, J. Deng, Y. Wei, Two-dimensional MXene membrane for ethanol dehydration, J. Membr. Sci. 2019, 590, 117300.

[133] R. Han, Y. Xie, X. Ma, Crosslinked P84 copolyimide/MXene mixed matrix membrane with excellent solvent resistance and permselectivity, Chin. J. Chem. Eng. 2019, 27, 877.

[134] A. Ronen, S. L. Walker, D. Jassby, Rev. Chem. Eng. 2016, 32, 533.

[135] P. Formoso, E. Pantuso, G. De Filpo, F. Nicoletta, Electro-conductive membranes for permeation enhancement and fouling mitigation: A short review, Membranes 2017, 7, 39.

[136] S.-C. Low, Q.-H. Ng, in Advanced Nanomaterials for Membrane Synthesis and Its Applications (Eds: W.-J. Lau, A. F. Ismail, A. Isloor, A. Al-Ahmed), Elsevier 2019, pp. 69–99.

[137] Y. Luo, G. Chen, X. Chen, H. Wang, Y. Luo, G. Chen, L. Ding, X. Chen, L. Ding, H. Wang, Efficient electrocatalytic N2 fixation with MXene under ambient conditions, Joule 2019, 3, 279.

[138] A. Sinopoli, Z. Othman, K. Rasool, K. A. Mahmoud, Electrocatalytic/photocatalytic properties and aqueous media applications of 2D transition metal carbides (MXenes), Curr. Opin. Solid. Mater. Sci. 2019, 23, 100760.

[139] L. Agartan, K. Hantanasirisakul, S. Buczek, B. Akuzum, K. A. Mahmoud, B. Anasori, Y. Gogotsi, E. C. Kumbur, Influence of operating conditions on the desalination performance of a symmetric pre-conditioned Ti3C2Tx-MXene membrane capacitive deionization system, Desalination 2020, 477, 114267.

[140] J. Lao, R. Lv, J. Gao, A. Wang, J. Wu, J. Luo, Aqueous Stable $Ti_3C_2$ MXene Membrane with Fast and Photoswitchable Nanofluidic Transport, ACS Nano 2018, 12, 12464.

[141] Z. Zhang, S. Yang, P. Zhang, J. Zhang, G. Chen, X. Feng, Mechanically strong MXene/Kevlar nanofiber composite membranes as high-performance nanofluidic osmotic power generators, Nat. Commun. 2019, 10, 2920.

[142] J. Zhang, Y. Liu, Z. Lv, T. Zhao, P. Li, Y. Sun, J. Wang, Sulfonated Ti3C2Tx to construct proton transfer pathways in polymer electrolyte membrane for enhanced conduction, Solid State Ionics 2017, 310, 100.

[143] M. Fei, R. Lin, Y. Deng, H. Xian, R. Bian, X. Zhang, J. Cheng, C. Xu, D. Cai, Polybenzimidazole/Mxene composite membranes for intermediate temperature polymer electrolyte membrane fuel cells, Nanotechnology 2018, 29, 035403.

[144] X. Zhang, C. Fan, N. Yao, P. Zhang, T. Hong, C. Xu, J. Cheng, Quaternary Ti3C2Tx enhanced ionic conduction in quaternized polysulfone membrane for alkaline anion exchange membrane fuel cells, J. Membr. Sci. 2018, 563, 882.

[145] C. Cheng, X. Zhang, Z. Yang, Low-temperature preferential oxidation of CO over Ag monolayer decorated Mo2C (MXene) for purifying H2, J. Phys.: Condens. Matter 2019, 31, 215201.

[146] C. Lin, W. Zhang, L. Wang, Z. Wang, W. Zhao, W. Duan, Z. Zhao, B. Liu, J. Jin, A few-layered Ti 3 C 2 nanosheet/glass fiber composite separator as a lithium polysulphide reservoir for high-performance lithium–sulfur batteries, J. Mater. Chem. A 2016, 4, 5993.

[147] L. Yin, G. Xu, P. Nie, H. Dou, X. Zhang, MXene debris modified eggshell membrane as separator for high-performance lithium-sulfur batteries, Chem. Eng. J. 2018, 352, 695.

[148] J. Wang, P. Zhai, T. Zhao, M. Li, Z. Yang, H. Zhang, J. Huang, Laminar MXene-Nafion-modified separator with highly inhibited shuttle effect for long-life lithium–sulfur batteries, Electrochim. Acta 2019, 320, 134558.

[149] H. Zhan, Z. Xiong, C. Cheng, Q. Liang, J. Z. Liu, D. Li, Solvation-Involved Nanoionics: New Opportunities from 2D Nanomaterial Laminar Membranes, Adv. Mater. 2020, 32, 1904562.

[150] J. Kim, B. Van der Bruggen, The use of nanoparticles in polymeric and ceramic membrane structures: review of manufacturing procedures and performance improvement for water treatment, Environ. Pollut. 2010, 158, 2335.

[151] S. R. Lewis, S. Datta, M. Gui, E. L. Coker, F. E. Huggins, S. Daunert, L. Bachas, D. Bhattacharyya, Reactive nanostructured membranes for water purification, Proc. Natl. Acad. Sci. USA 2011, 108, 8577.

[152] M. Gui, L. E. Ormsbee, D. Bhattacharyya, Reactive functionalized membranes for polychlorinated biphenyl degradation, Ind. Eng. Chem. Res. 2013, 52, 10430.

[153] R. P. Pandey, K. Rasool, P. Abdul Rasheed, K. A. Mahmoud, Reductive Sequestration of Toxic Bromate from Drinking Water using Lamellar Two-Dimensional $Ti_3C_2T_X$ (MXene), ACS Sustainable Chem. Eng. 2018, 6, 7910.

[154] Y. Ying, Y. Liu, X. Wang, Y. Mao, W. Cao, P. Hu, X. Peng, Two-dimensional titanium carbide for efficiently reductive removal of highly toxic chromium (VI) from water, ACS Appl. Mater. Interfaces 2015, 7, 1795.

[155] Y. Liu, R. Luo, Y. Li, J. Qi, C. Wang, J. Li, X. Sun, L. Wang, Sandwich-like Co3O4/MXene composite with enhanced catalytic performance for Bisphenol A degradation, Chem. Eng. J. 2018, 347, 731.

[156] Z. Zhang, H. Li, G. Zou, C. Fernandez, B. Liu, Q. Zhang, J. Hu, Q. Peng, Self-reduction synthesis of new MXene/Ag composites with unexpected electrocatalytic activity, ACS Sustainable Chem. Eng. 2016, 4, 6763.

[157] Q. Xue, Z. Pei, Y. Huang, M. Zhu, Z. Tang, H. Li, Y. Huang, N. Li, H. Zhang, C. Zhi, Mn 3 O 4 nanoparticles on layer-structured Ti 3 C 2 MXene towards the oxygen reduction reaction and zinc–air batteries, J. Mater. Chem. A 2017, 5, 20818.

[158] J. Lee, H. Chae, Y. J. Won, K. Lee, C.-H. Lee, H. H. Lee, I. Kim, J. Lee, Graphene oxide nanoplatelets composite membrane with hydrophilic and antifouling properties for wastewater treatment, J. Membr. Sci. 2013, 448, 223.

[159] J.-H. Choi, J. Jegal, W.-N. Kim, Fabrication and characterization of multi-walled carbon nanotubes/polymer blend membranes, J. Membr. Sci. 2006, 284, 406.

[160] S. Leaper, A. Abdel-Karim, B. Faki, J. M. Luque-Alled, M. Alberto, A. Vijayaraghavan, S. M. Holmes, G. Szekely, M. I. Badawy, N. Shokri, P. Gorgojo, Flux-enhanced PVDF mixed matrix membranes incorporating APTS-functionalized graphene oxide for membrane distillation, J. Membr. Sci. 2018, 554, 309.

[161] J. Lee, R. Wang, T.-H. Bae, High-performance reverse osmosis membranes fabricated on highly porous microstructured supports, Desalination 2018, 436, 48.

[162] H.-R. Chae, J. Lee, C.-H. Lee, I.-C. Kim, P.-K. Park, Graphene oxide-embedded thin-film composite reverse osmosis membrane with high flux, anti-biofouling, and chlorine resistance, J. Membr. Sci. 2015, 483, 128.

[163] A. K. Ghosh, E. M. V. Hoek, Impacts of support membrane structure and chemistry on polyamide–polysulfone interfacial composite membranes, J. Membr. Sci. 2009, 336, 140.

[164] N. Joseph, P. Ahmadiannamini, R. Hoogenboom, I. F. J. Vankelecom, Layer-by-layer preparation of polyelectrolyte multilayer membranes for separation, Polym. Chem. 2014, 5, 1817.

[165] W. Choi, J. Choi, J. Bang, J.-H. Lee, Layer-by-layer assembly of graphene oxide nanosheets on polyamide membranes for durable reverse-osmosis applications, ACS Appl. Mater. Interfaces 2013, 5, 12510.

[166] M. Hu, B. Mi, Enabling graphene oxide nanosheets as water separation membranes, Environ. Sci. Technol. 2013, 47, 3715.

[167] G.-M. Weng, J. Li, M. Alhabeb, C. Karpovich, H. Wang, J. Lipton, K. Maleski, J. Kong, E. Shaulsky, M. Elimelech, Y. Gogotsi, A. D. Taylor, Layer-by-Layer Assembly of Cross-Functional Semi-transparent MXene-Carbon Nanotubes Composite Films for Next-Generation Electromagnetic Interference Shielding, Adv. Funct. Mater. 2018, 28, 1803360.

[168] Z. Zhou, W. Panatdasirisuk, T. S. Mathis, B. Anasori, C. Lu, X. Zhang, Z. Liao, Y. Gogotsi, S. Yang, Layer-by-layer assembly of MXene and carbon nanotubes on electrospun polymer films for flexible energy storage, Nanoscale 2018, 10, 6005.

[169] Q. Tang, Z. Zhou, P. Shen, Are MXenes Promising Anode Materials for Li Ion Batteries? Computational Studies on Electronic Properties and Li Storage Capability of $Ti_3C_2$ and $Ti_3C_2X_2$ (X = F, OH) Monolayer, J. Am. Chem. Soc. 2012, 134, 16909.

[170] B. Anasori, Y. Xie, M. Beidaghi, J. Lu, B. C. Hosler, L. Hultman, P. R. C. Kent, Y. Gogotsi, M. W. Barsoum, Two-dimensional, ordered, double transition metals carbides (MXenes), ACS Nano 2015, 9, 9507. G. R.

[171] Berdiyorov, M. E. Madjet, K. A. Mahmoud, Ionic sieving through $Ti_3C_2(OH)_2$ MXene: First-principles calculations, Appl. Phys. Lett. 2016, 108, 113110.

[172] V. N. Borysiuk, V. N. Mochalin, Y. Gogotsi, Molecular dynamic study of the mechanical properties of two-dimensional titanium carbides Tin+ 1Cn (MXenes), Nanotechnology 2015, 26, 265705.

[173] L. Li, T. Zhang, Y. Duan, Y. Wei, C. Dong, L. Ding, Z. Qiao, H. Wang, Selective gas diffusion in two-dimensional MXene lamellar membranes: insights from molecular dynamics simulations, J. Mater. Chem. A 2018, 6, 11734.

[174] C. E. Ren, M.-Q. Zhao, T. Makaryan, J. Halim, M. Boota, S. Kota, B. Anasori, M. W. Barsoum, Y. Gogotsi, Porous two-dimensional transition metal carbide (MXene) flakes for high-performance Li-ion storage, ChemElectroChem 2016, 3, 689.

[175] M. Mojtabavi, A. VahidMohammadi, W. Liang, M. Beidaghi, M. Wanunu, Single-molecule sensing using nanopores in two-dimensional transition metal carbide (MXene) membranes, ACS Nano 2019, 13, 3042.

[176] M. Radovic, M. W. Barsoum, Am. Ceram. Soc. Bull. 2013, 92, 20.

[177] M. W. Barsoum, P. Eklund, in 2D Metal Carbides and Nitrides (MXenes) (Eds: B. Anasori, Y. Gogotsi), The $M_{n+1}AX_n$ Phases: The Precursors for MXenes, Springer International Publishing, Cham, Switzerland 2019, pp. 15–35.

[178] M. Naguib, R. R. Unocic, B. L. Armstrong, J. Nanda, Large-scale delamination of multi-layers transition metal carbides and carbonitrides “MXenes”, Dalton Trans. 2015, 44, 9353.

[179] T. Li, L. Yao, Q. Liu, J. Gu, R. Luo, J. Li, X. Yan, W. Wang, P. Liu, B. Chen, W. Zhang, W. Abbas, R. Naz, D. Zhang, Fluorine-Free Synthesis of High-Purity $Ti_3C_2T_x$ (T=OH, O) via Alkali Treatment, Angew. Chem., Int. Ed. 2018, 57, 6115.

[180] E. Yang, H. E. Karahan, K. Goh, C. Y. Chuah, R. Wang, T.-H. Bae, Scalable fabrication of graphene-based laminate membranes for liquid and gas separations by crosslinking-induced gelation and doctor-blade casting, Carbon 2019, 155, 129.

[181] G. Liu, J. Shen, Q. Liu, G. Liu, J. Xiong, J. Yang, W. Jin, Ultrathin two-dimensional MXene membrane for pervaporation desalination, J. Membr. Sci. 2018, 548, 548.

[182] H. E. Karahan, K. Goh, C. Zhang, E. Yang, C. Yildrim, C. Y. Chuah, M. G. Ahunbay, J. Lee, S. B. Tantekin-Ersolmaz, Y. Chen, T. H. Bae, MXene Materials for Designing Advanced Separation Membranes, Adv. Mater. 2020, 32, 1906697. DOI:10.1002/adma.201906697

[183] Y. A. J. Al-Hamadi, B.M. Jun, M. Yoon, N. Taheri-Qazvini, S. A. Snyder, M. Jang, Y. Yoon, Applications of MXene-based membranes in water purification: A review, Chemosphere 254, 2020, 126821. https://doi.org/10.1016/j.chemosphere.2020.126821

## PART 3

For the other references cited in this part, see bibliography Part 2.

[C1] W. Li, S. A. S. C. Samarasinghe, T.-H. Bae, Enhancing CO2/CH4 separation performance and mechanical strength of mixed-matrix membrane via combined use of graphene oxide and ZIF-8, J. Ind. Eng. Chem. 2018, 67, 156.

[C2] K. Goh, L. Setiawan, L. Wei, R. Si, A. G. Fane, R. Wang, Y. Chen, Graphene oxide as effective selective barriers on a hollow fiber membrane for water treatment process, J. Membr. Sci. 2015, 474, 244.

[C3] J. Yin, G. Zhu, B. Deng, Graphene oxide (GO) enhanced polyamide (PA) thin-film nanocomposite (TFN) membrane for water purification, Desalination 2016, 379, 93.

[C4] L. Huang, J. Chen, T. Gao, M. Zhang, Y. Li, L. Dai, L. Qu, G. Shi, Reduced Graphene Oxide Membranes for Ultrafast Organic Solvent Nanofiltration, Adv. Mater. 2016, 28, 8669.

[C5] A. R. Kamble, C. M. Patel, Z. V. P. Murthy, Modification of PVDF membrane by two-dimensional inorganic additive for improving gas permeation, Sep. Sci. Technol. 2019, 54, 311.

[C6] Z.-X. Low, J. Ji, D. Blumenstock, Y.-M. Chew, D. Wolverson, D. Mattia, Fouling resistant 2D boron nitride nanosheet – PES nanofiltration membranes, J. Membr. Sci. 2018, 563, 949.

[C7] C. Chen, J. Wang, D. Liu, C. Yang, Y. Liu, R. S. Ruoff, W. Lei, Functionalized boron nitride membranes with ultrafast solvent transport performance for molecular separation, Nat. Commun. 2018, 9, 1902.

[C8] Z. Tian, S. Wang, Y. Wang, X. Ma, K. Cao, D. Peng, X. Wu, H. Wu, Z. Jiang, Enhanced gas separation performance of mixed matrix membranes from graphitic carbon nitride nanosheets and polymers of intrinsic microporosity, J. Membr. Sci. 2016, 514, 15.

[C9] Y. Wang, L. Li, Y. Wei, J. Xue, H. Chen, L. Ding, J. Caro, H. Wang, Water Transport with Ultralow Friction through Partially Exfoliated g-$C_3N_4$ Nanosheet

Membranes with Self-Supporting Spacers, Angew. Chemie Int. Ed. 2017, 56, 8974.

[C10] K. Cao, Z. Jiang, X. Zhang, Y. Zhang, J. Zhao, R. Xing, S. Yang, C. Gao, F. Pan, Highly water-selective hybrid membrane by incorporating g-$C_3N_4$ nanosheets into polymer matrix, J. Membr. Sci. 2015, 490, 72.

[C11] A. Achari, S. Sahana, M. Eswaramoorthy, High performance $MoS_2$ membranes: effects of thermally driven phase transition on $CO_2$ separation efficiency, Energy Environ. Sci. 2016, 9, 1224.

[C12] Y. Li, S. Yang, K. Zhang, B. Van der Bruggen, Thin film nanocomposite reverse osmosis membrane modified by two dimensional laminar $MoS_2$ with improved desalination performance and fouling-resistant characteristics, Desalination 2019, 454, 48.

[C13] Z. Wang, Q. Tu, S. Zheng, J. J. Urban, S. Li, B. Mi, Understanding the Aqueous Stability and Filtration Capability of $MoS_2$ Membranes, Nano Lett. 2017, 17, 7289.

[C14] B.-Y. Guo, S.-D. Jiang, M.-J. Tang, K. Li, S. Sun, P.-Y. Chen, S. Zhang, $MoS_2$ Membranes for Organic Solvent Nanofiltration: Stability and Structural Control, J. Phys. Chem. Lett. 2019, 10, 4609.

[C15] Y. Yang, K. Goh, R. Wang, T.-H. Bae, High-performance nanocomposite membranes realized by efficient molecular sieving with CuBDC nanosheets, Chem. Commun. 2017, 53, 4254.

[C16] Y. Cheng, X. Wang, C. Jia, Y. Wang, L. Zhai, Q. Wang, D. Zhao, Ultrathin mixed matrix membranes containing two-dimensional metal-organic framework nanosheets for efficient $CO_2/CH_4$ separation, J. Membr. Sci. 2017, 539, 213.

[C17] Y. Peng, Y. Li, Y. Ban, H. Jin, W. Jiao, X. Liu, W. Yang, Metal-organic framework nanosheets as building blocks for molecular sieving membranes, Science 2014, 346, 1356.

[C18] G. Li, K. Zhang, T. Tsuru, Two-Dimensional Covalent Organic Framework (COF) Membranes Fabricated via the Assembly of Exfoliated COF Nanosheets, ACS Appl. Mater. Interfaces 2017, 9, 8433.

[C19] Z. Kang, Y. Peng, Y. Qian, D. Yuan, M. A. Addicoat, T. Heine, Z. Hu, L. Tee, Z. Guo, D. Zhao, Mixed Matrix Membranes (MMMs) Comprising Exfoliated 2D Covalent Organic Frameworks (COFs) for Efficient $CO_2$ Separation, Chem. Mater. 2016, 28, 1277.

[C20] V. A. Kuehl, J. Yin, P. H. H. Duong, B. Mastorovich, B. Newell, K. D. Li-Oakey, B. A. Parkinson, J. O. Hoberg, A Highly Ordered Nanoporous, Two-Dimensional Covalent Organic Framework with Modifiable Pores, and Its Application in Water Purification and Ion Sieving, J. Am. Chem. Soc. 2018, 140, 18200.